Corrosion behaviour of ferrous and non-ferrous alloys exposed to sulphate - reducing bacteria in industrial heat exchangers

Alicia Prithiraj

A dissertation submitted in fulfilment of the requirements for the degree of

Magister Technologiae: Engineering: Chemical

in the

FACULTY OF ENGINEERING AND TECHNOLOGY

DEPARTMENT OF CHEMICAL ENGINEERING

Supervisors: Professor PO Osifo and Professor IO Otunniyi

2018

Declaration

I, Alicia Prithiraj, hereby declare that the dissertation entitled: Corrosion behaviour of ferrous and non-ferrous alloys exposed to sulphate-reducing bacteria in industrial heat exchangers, which was done for the completion of a Masters degree in Chemical Engineering, is my own work.

Alicia Prithiraj

Date

Abstract

Corrosion responses of some carbon steels, stainless steel and copper alloys in the presence of a culture of bacteria (referred to as SRB-Sulphate-reducing bacteria) found in industrial heat exchangers, was studied to recommend best alloys under this service condition, with techno-economic consideration. Water from cooling towers in three plants in a petrochemical processing complex were analysed for SRB presence. Two of the water samples showed positive indication of SRB presence. The mixed cultures obtained from plant one were grown in prepared media and incubated at 35 °C for 18 days. Potentiodynamic polarisation studies in anaerobic conditions were done on the selected alloys in aqueous media with and without the grown SRB. Scanning electron microscopy (SEM) and energy dispersive X-ray spectroscopy (EDS) were then used to study the corrosion morphology and corrosion products formation. The voltamograms show higher i_{corr} for alloys under the SRB compared to the control media, indicating the SRB indeed increased the corrosion rates. The surface analysis showed pitting on steel alloy ASTM A106-B. Localised attack to the grain boundaries on a selective area, was seen on ASTM A516-70 dislodging the grains, and intergranular corrosion was seen throughout the exposed area of ASTM A179. Copper alloys showed pitting on ASTM B111 grade C71500 (70-30), and denickelification on ASTM B111 grade C70600 (90-10), and is a good alternative material for use apart from carbon steel alloys, recording a low corrosion rate of 0.05 mm/year. The EDS analysis supported the findings showing higher weight percent of iron and sulphur on surface of the alloys after exposure to the SRB media. This implies that the presence of the sulphur ion indeed increased the corrosion rate. ASTM A516-70 carbon steel was chosen as a suitable alternative material to the stainless steel in this environment. The Tafel plot recorded a corrosion rate of 1.08 mm/year for ASTM A516-70 when exposed to SRB media.

Key words: Corrosion, sulphate-reducing bacteria (SRB), cooling tower, heat exchanger, carbon steels

Acknowledgements

I would like to thank my husband, Ashish Prithiraj for his support and motivation. I would also like to thank my supervisors Professor Iyiola Olatunji Otunniyi and Professor Peter Osifo whom have had so much patience with me, supported and guided me, James Daniels with his specialist knowledge whom trained me for a week on practising sterile techniques when handling bacteria and microorganisms, Lekala Barclays Makgale from the University of Witwatersrand for his friendship, support and assistance with electrochemical testing, Professor Josias van der Merwe from University of Witwatersrand, for allowing me to utilise the lab equipment. Deon Slabbert, for his guidance. Mthobeli Ngcemu and Leanne Matthysen, for their support with SEM analysis and EDS analysis, Stephanus Roux and his team in assisting me with the sample taking process and specialist advice.

Table of Contents

List of Figures

List of Tables

List of Acronyms/Definitions/Abbreviations

Anode	Site of oxidation – where electrons are lost
Cathode	Site of reduction – where electrons are gained
ASME	American Society of Mechanical Engineers
ASTM	American Section of the International Association for Testing Materials
ATCC	American Type Culture Collection
CMIC	Chemical microbially influenced corrosion
CS	Carbon steel
EDS	Energy dispersive spectroscopy
EMIC	Electrical microbially influenced corrosion
ESEM	Environmental electron microscopy
EPS	Extracellular polymetric substance
F	Faraday's constant
FCC	Face center cubic
IOB	Aerobic iron-oxidizing bacteria
IRB	Iron reducing bacteria
IRIS	Internal rotary inspection system
MIC	Microbially induced corrosion
OCP	Open Circuit Potential
PCR	Polymerase chain reaction
SAF	Sandvik
SCC	Stress corrosion cracking
SCE	Saturated Calomel Electrode
SEM	Scanning Electron Microscope
SHE	Standard Hydrogen Electrode
SRB	Sulphate-reducing bacteria
SSC	Sulphide stress cracking
SSRT	Slow strain rate test
WE	Working electrode

List of Symbols

CR	Corrosion rate
E	Potential
E°	Revised standard potential
E_{corr}	Corrosion potential
E_{cp}	Passivation is complete
E_h	Redox potential
E_{pp}	Primary passivation potential
E_{trans}	Transpassive potential
E_p	Passivation potential
E_w	Applied potential
I_{corr}	Corrosion rate current density
I_{crit}	Critical current density
I_{pass}	Passive current density
α	Transfer coefficient
n	Number of electrons involved in the reaction
$\eta_{act,c}$	Activation over potential
i_L	Limiting current density
i_c	Cathodic current density
p	Constant used to shape the passivation peak

Draft Manuscript: (Submitted)

Prithiraj, A., Osifo, PO., Otunniyi, IO. (2018). Corrosion behaviour of carbon steels exposed to sulphate-reducing bacteria in industrial heat exchangers. *Engineering Failure Analysis*. (Ready for Decision)

Chapter 1

1. Background to the research study

Sulphate-reducing bacteria, known as *Desulfovibrio Desulfuricans* in the scientific community, are anaerobic and non-pathogenic bacteria, which attach to substrate surfaces and form biofilms, and are capable of causing severe corrosion of iron in water systems due to their ability to produce enzymes which accelerate reduction of sulphate, and a corrosive hydrogen sulphide product is formed. SRB utilise thiosulphates and sulphites as final electron acceptors and various organic nutrients as electron donors. SRB acts as a catalyst in the reduction reaction process. In order for this reduction to occur, the components present should be sulphates, an external energy source in the form of free electrons and the temperature of the water.

Bacteria, algae and fungi are capable of synthesising a vast number of enzymes, many of which are secreted into the surrounding environment. These enzymes can break down a variety of inorganic and organic molecules to provide the organism with the food and energy it needs to grow and multiply (Choudhary 1998:93).

All living organisms require an energy source. Organisms such as green plants and algae are capable of using light (daylight or direct sunlight) as their energy source which has the unique ability to use reduced inorganics such as elemental sulphur and hydrogen sulphide (Choudhary 1998:93).

The energy needed for growth of sulphate-reducing bacteria is obtained through the oxidation of organic compounds:

$$SO_4^{2-} + organic\ matter = HS^- + H_2S + HCO^{3-} \quad (1)$$

Microbiologically induced corrosion (MIC), caused by SRB, has been known and studied for many years, and the damage it causes is still of considerable concern to many industries that suffer great economic losses due to this form of corrosion. MIC is always coupled with the electrochemical process, and SRB are recognised as detrimental bacteria to most common metals used in the industry. SRB are well known for attacking carbon steel (CS) in the form of pitting corrosion (Hamilton 1985:195; Hardy & Brown 1984:650). The damaging effects caused by pitting are typically much more severe than those by uniform corrosion. Pitting can lead to perforation or crack initiation and, accordingly, has been the root cause to many corrosion failures (McCafferty 2010:20; Javaherdashti 1999:173). Pitting corrosion is much

more difficult to detect in the field than the uniform corrosion because pits are often micron-sized and are concealed under the corrosion products and/or biofilm. Pitting has also been considered to be of a stochastic nature (Shibata & Takeyama 1976:260; Shibata & Takeyama 1977:243). Corrosion pits induced by SRB were reported to cause catastrophic problems, especially in the oil and gas industry (Cord-Ruwishch 1987:97; Javaherdashti 1999:173).

Researchers have developed several methods of detection, and water treatment companies have used these methods of detection in many industries (Tan & Halim, 2015). Methods include, periodic visual inspection of equipment for pitting caused by MIC together with SRB attack, bacteria or SRB counting or qualitative measurement via culture growth and bacteria or SRB evaluation of attack on corrosion coupons.

Given the service conditions (Lutey & Saito 1996:127) MIC by SRB is a probable cause for corrosion in shell and tube heat exchangers in petrochemical processing plants. In the basic design of a heat exchanger, cooling water flows in the tubes, and used as a cooling medium. Pitting in the form of localised corrosion has been noted in the tubes during IRIS (Internal Rotary Inspection System) inspections (according to plant records). These incidences lead to leaking tubes, make-up plugging and consequential downtimes. This has prompted the need for further study on basic research to increase our understanding of the microbial corrosion and their interactions with metal surfaces in the heat exchanger environment.

1.1. Focus of this study

Shell and tube heat exchangers that use cooling water on the tube side are experiencing tube failures, in a petrochemical plant in South Africa, requiring tubes to be plugged (specially machined metal plugs inserted at the entrance of a tube to seal the leaking tube) occasionally resulting in unintended downtimes. Due to the leaks and excessive plugging, tube bundles are being replaced every two years, whereas the shell and tube heat exchangers are designed to last 15 to 20 years. To ensure integrity and reliability of the heat exchanger, maintenance strategies in the form of Risk Based Inspections (RBI) are conducted, using a condition based approach. During inspections pitting in the form of localised corrosion (Javed *et al*. 2015:56) using IRIS could be seen. With pitting and localised corrosion, the activity of sulphate-reducing bacteria (SRB) is probable (Chen *et al*. 2014:767; Abdullah *et al*. 2014:2; Xu *et al*. 2006:829; Hamilton 1985:195; Hardy & Brown 1984:650). Stainless steel tube is now being considered (Lemoine *et al*. 1985:1260; Viera *et al*. 2000:205, Scott & Davies 1989:57) for replacing the carbon steel tubes currently in use. This requires careful consideration because of remarkably higher costs, and should the problem be due to SRB, stainless steels may as well not be a solution.

Many engineering materials considered to be corrosion resistant such as steel, copper, nickel, zinc, aluminum, titanium and their alloys-have been reported to experience MIC (Microbially Induced corrosion) by SRB (Javaherdashti 2011:1513). Duplex stainless steels SAF 2205, for instance, have been reported for its vulnerability to MIC (Scott & Goldie 1991:55; Wagner & Little 1993:65). Studies have shown that SAF 2205 can corrode and, have pitting initiated due to the presence of SRB after immersion into seawater for 18 months (Neville & Hodgkies 1998:111). Corrosion rates of 10 mm/year (Romero *et al*. 2004:2) in oil treatment plants and 0.7-0.74 mm/year due to the action of SRB and/or acid-producing bacteria in soil environments have been reported (Li *et al*. 2001:826). Duplex stainless steel ASTM-A789-S31803 is also reported vulnerable in the heat exchanger environment with pitting noted on the tube side where cooling water flows. Other stainless steels respond to various extents under MIC have been reported (Enos 1996:831; Neville & Hodgkies 2000:62; Antony *et al*. 2008:2689; Brennenstuhl *et al*. 1996:186).

Since MIC is still possible with stainless steels, this work seeks to explore behavior of different grades of carbon steel, which are inexpensive structural metals, in the presence of SRB. Copper alloys will be included for a wider scope of performance options, due to use in heat exchangers for its good resistance to corrosion, combined with mechanical workability,

excellent electrical and thermal conductivity, and ease in soldering and brazing (Javed *et al*. 2016:1).

Many authors have reported on MIC by SRB in different environments on different materials: soils, concrete, reinforcement, sea water, etc. (El Mendili *et al*. 2015:76; El Mendili *et al*. 2014:1350; Li *et al*. 2001:815; Usher *et al*. 2015:354; Abdullah *et al*. 2014:2; Melchers 2004:824), but reports isolating and growing SRB from the heat exchanger environment in these plants' cooling towers is still scarce.

It is worthwhile to explore how grades of carbon steel respond to MIC by SRB for this peculiar environment. This will assist shell and tube heat exchanger designers to prevent degradation by SRB in industries without resorting to the more expensive stainless steel materials.

In an attempt to establish presence of SRB in this system bacteria from three selected cooling towers were isolated. Corrosion behavior of carbon steels typically found in the petrochemical industry, for construction of shell and tube heat exchangers, when exposed to SRB media were studied. The corrosion rates along with corrosion behavior of alloys were compared to identify a carbon steel of relatively promising performance in this environment.

Specification of carbon steels already in use and others probable for better performance were investigated, specifically ASTM A179, ASTM A106-B, ASTM A516-70 and 2205 duplex stainless steel, ASTM B111 grade C 70600 and ASTM B111 grade C71500.

1.2. Objectives and scope of this work

The main objective of this study is to investigate SRB presence in the heat exchanger environment, isolate it and asses how it affects corrosion of different alloys.

The specific objectives are to:

- Grow SRB under conditions applicable and that which is obtained in heat exchangers
- Determine the corrosion susceptibility and rate of selected grades of carbon steels under exposure to SRB at such conditions that are obtained in heat exchangers.
- Characterise and compare surface structural degradation of the carbon steels exposed to SRB media.

1.3. Research scope

The research scope consists of a comprehensive literature and theory review. It includes objectives, results, conclusions and recommendations.

Chapter 1: introduces the concept of SRB and how detrimental it can be to the industry, the chapter also includes the main objective and specific objectives. Limitations and assumptions are listed, following an outline of the research problem.

Chapter 2: this chapter focuses on the mechanisms of MIC by SRB and the typical environments in which SRB can be found. SRB can be found in the heat exchanger environment, where basic concepts are presented on the heat exchanger, this flows into the techniques for detecting SRB and basic concepts of electrochemistry, as this will be the chosen methodology, other methodologies from literature are further presented. Lastly, the chapter gives some insight into anodic and cathodic behaviour when biofilm is formed on the surface of a metal, and corrosion rate calculations, this forms part of data interpretation.

Chapter 3: presents a brief introduction into what is anticipated by the study. A research design is included, highlighting possible research designs, following the chosen detailed methodologies of the study.

Chapter 4: In this chapter the metal elemental composition before exposure to SRB media and cooling water composition are compared with EDS results, after exposure of metals exposed to SRB media, results for growing and incubating the SRB media at 35°C are presented, and potentiodynamic curves, corrosion rates, SEM and EDS analysis, are showcased. Each section is concluded.

Chapter 5: Concludes the results and proposes carbon steel best suited for operation in industrial heat exchangers when SRB is present in the cooling system, the chapter also includes recommendations for future work.

1.4. Limitations and assumptions of the study

Limitations:

- SRB identification will be characterised only by visual inspection, smell, EDS sulphur weight percent with the corrosion products and biofilm presence. Therefore no gene

sequencing was conducted on the bacterial culture to determine the bacterial species present.

- It was impossible to produce a fully anaerobic environment when collecting bacteria at the cooling towers, but anaerobic conditions were met during incubation and growth of SRB.
- Chemical dosing is done at different times on plant A, B and C, this is an uncontrollable factor, possibly leading to negative indication of SRB.
- Industry SEM, EDS and microscopes were used.

- SEM and EDS analysis of the biofilm was conducted a day after the specimens were exposed to SRB. The machine did not produce spectra graphs due to not saving as a project file, but gave a spectrum of elemental compositions in weight.

It is assumed that:

- the positive identification of the culture of bacteria is regarded as SRB**.**
- all specimens sourced were packaged as new as provided by the industry.
- the presented water quality results obtained by the industry is acceptable.
- the training that was received for a week from the industry in handling bacteria is acceptable.
- the elemental analysis conducted using ASTM standard E415 is acceptable.
- industry EDS and SEM equipment used to produce results is acceptable.

1.5. Research problem

Figure 1.1 is the diagram that illustrates the research problem which includes a brief explanation of the problem statement.

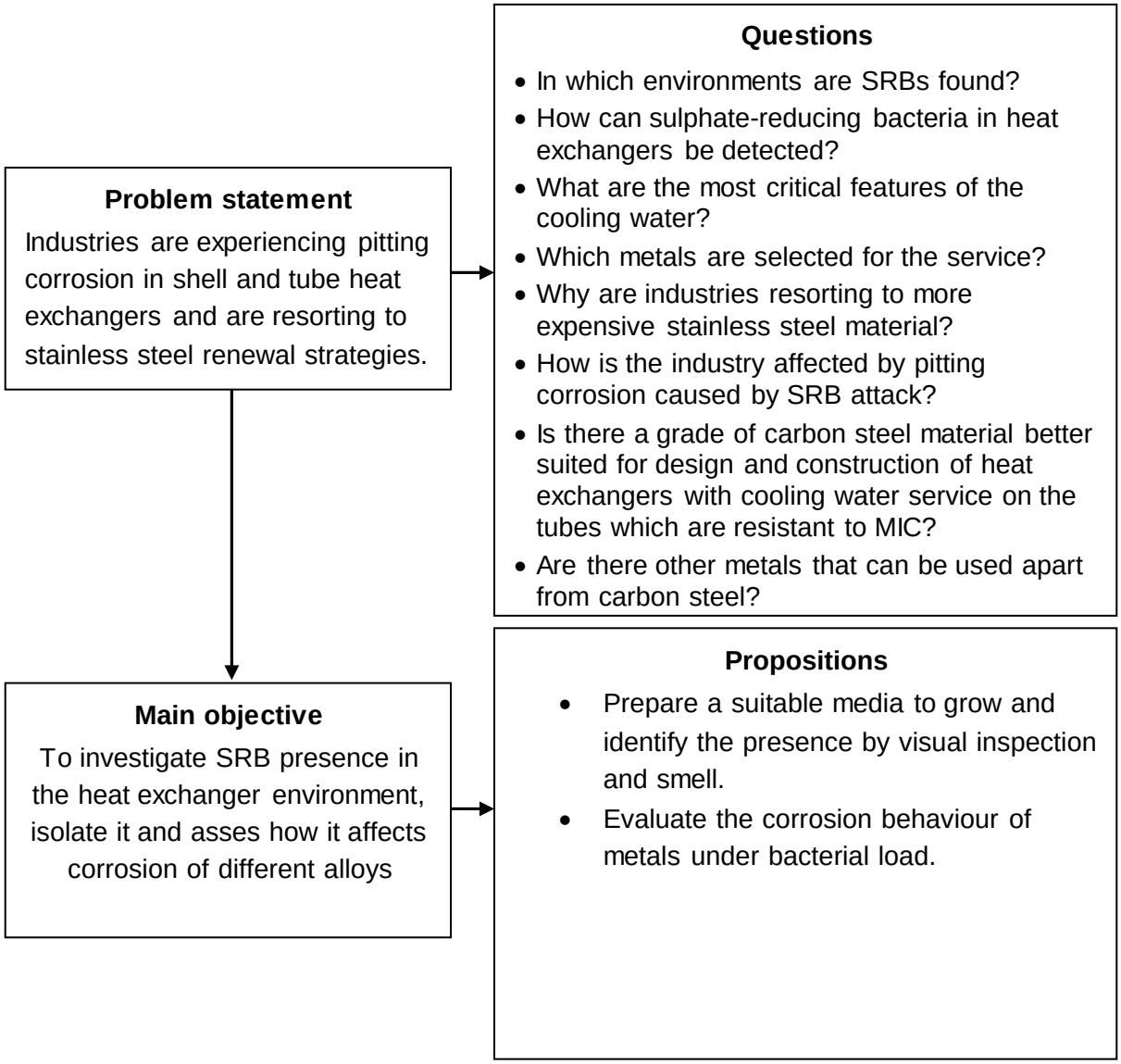

Figure 1.1: Outline of the research problem

Chapter 2

2. Literature Survey

2.1. Introduction

The literature survey focuses on mechanisms of MIC by SRB. The order presented, describes the environments in which SRB can be found from literature, zooming in to the heat exchanger environment, following techniques on detection of SRB and electrochemistry basic concepts. Methodologies from literature are further presented, with an insight into anodic and cathodic behaviour when biofilm is formed on the surface of a metal, followed by corrosion rate calculations.

2.2. Cathodic depolarisation theory

The first evidence for an involvement of SRB in anaerobic corrosion was provided more than a hundred years ago. Gaines (1910:128) reported the analysis of high percentage of sulphur in rust from anaerobically corroded iron constructions and hypothesised about a connection to the bacterial sulphur cycle. Von Wolzogen and Vlugt (1934:147) identified SRB as the prime cause of widespread iron pipe failures in the sulphate-rich soils of North Holland. Those authors proposed a purely lithotrophic microbial process, with iron as the only source of reducing equivalents. They attributed microbial corrosion to a prominent physiological trait, the utilization of cathodic hydrogen (Equation 3, in Table 2.1) as the sole electron donor by SRB (Von Wolzogen & Vlugt 1934:147). The mechanistic explanation became famous as the (classical) “cathodic depolarisation theory.” Much controversy followed in the subsequent decades. Most authors initially favored the theory (Booth 1964:174; Butlin *et al*. 1949:26; Starkey 1947:193), while only a few questioned the idea that microbial H_2 scavenging would accelerate corrosion (Spruit & Wanklyn 1951:951; Wanklyn & Spruit 1952:928). With the beginning of the 1960s, the hypothesis was subjected to a series of electrochemical investigations (Booth & Tiller 1960:1689; Booth & Tiller 1962a:110; Booth & Tiller 1962b:2510).

The mechanism postulated by Von Wolzogen and Vlugt (1934:147) attempts to explain the corrosion problem in terms of the involvement of SRB. According to this explanation (Stott 1993:667; Javaherdashti 1999:173), the bacteria used the cathodic hydrogen through consumption by an enzyme called hydrogenase. It has been postulated that the main probable effect of SRB on corroding metal is the removal of hydrogen from the metal surface by means of hydrogenase and catalyzing the reversible activation of hydrogen. Sequences of

reactions of the classical theory can be divided into three categories: metal, solution and microorganism as given in Table 2.1:

Table 2.1: Sequences of reactions of the classical theory (Javaherdashti 2011:1512)

Metal	Anodic reaction	$4Fe \rightarrow 4Fe^{2+} + 8e^{-}$	Electrochemical cell
Solution	Cathodic reaction	$8H^{+} + 8e^{-} \rightarrow 8H_{ad}$	Electrolyte
Solution	Cathodic reaction	$8H_2O \rightarrow 8H^{+} + 8OH^{-}$	Electrolyte
Micro-organism	$SO_4^{2-} + 8H_{ad} \rightarrow S^{2-} + 4H_2O$		Microbial depolarisation
	$Fe^{2+} + S^{2-} \rightarrow FeS$		Corrosion products
	$3Fe^{2+} + 6OH^{-} \rightarrow 3Fe(OH)_2$		Corrosion products
	$4Fe + 4H_2O + SO_4^{2-} \rightarrow 3Fe(OH)_2 + FeS + 2OH^{-}$		Overall reaction

In the absence of oxygen, the cathodic areas of a metal surface quickly become polarized by atomic hydrogen. In anaerobic conditions, the alternative cathodic reaction to hydrogen evolution, such as oxidation by gaseous or dissolved oxygen, is not available either. These conditions will result in the dissociation of water as to become the main cathodic reaction with the hydrogen ions thus produced both adsorbed on the metallic surface (polarisation) and consumed by the hydrogenase enzyme. Figure 2.1 schematically summarises the classical theory. Although the classical theory could explain MIC by SRB for the first time based on electrochemistry, it suffered from serious flaws, some of which are as follows: Research has confirmed that it is impossible for hydrogenase to contribute to the depolarisation of a cathode by removal of atomic hydrogen as “hydrogenase cannot work on atomic hydrogen at all” (Stott 1993:667). According to this theory, the ratio of corroded iron to iron sulphide must be 4:1; however, in practice, this ratio varies from 0.9 to 1 (Tiller 1983).

In a study by Cord-Ruwisch (1996:8), a culture of nitrate-reducing SRB that could grow and consume hydrogen faster and more efficiently was used. When sulphate was replaced by nitrate, these nitrate-reducing bacteria proved to efficiently oxidize the cathodic hydrogen from the metal, but unlike sulphate-reducing bacteria, cultures failed to stimulate corrosion. This study then showed that MIC by SRB could not just be attributed to the uptake of cathodic hydrogen.

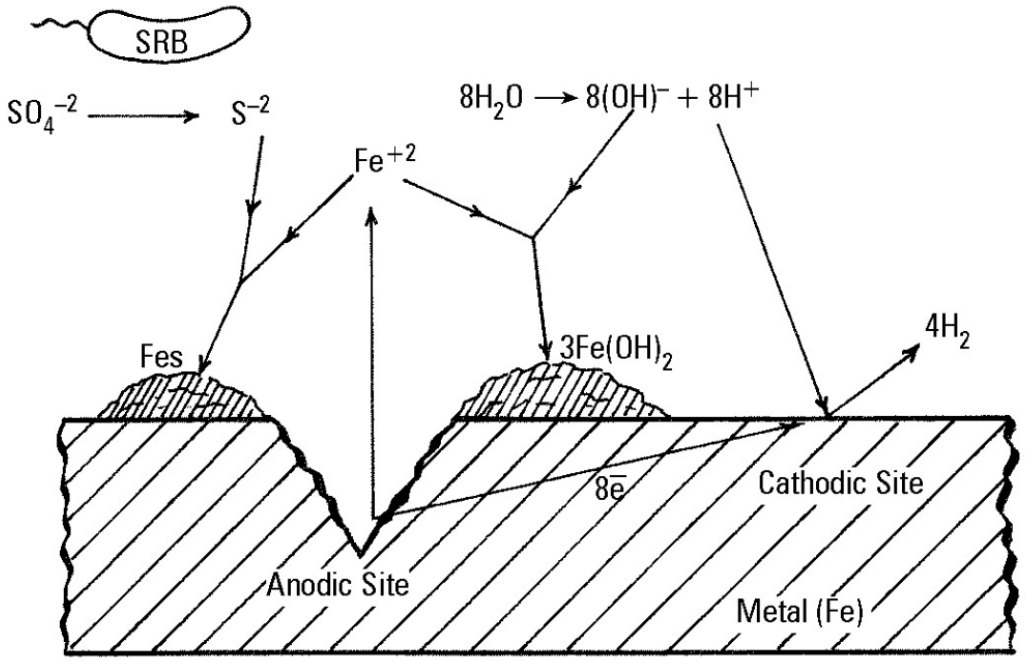

Figure 2.1: Schematic of the cathodic depolarisation "classical" theory of SRB activity (Javaherdashti 1999:174)

2.3. EMIC and CMIC

The classical theory does not take into consideration the corrosive effects of H_2S and its corrosion products, iron sulphide (Li *et al*. 2001:816).

In 2004, experimental evidence for a novel corrosion mechanism was furnished through isolation of SRB from enrichment cultures, with metallic iron as the only electron donor (Dinh *et al*. 2004:829). Sulphate reduction by these peculiar strains was directly fueled by bacterial consumption of iron-derived electrons, without the involvement of cathodic hydrogen gas as an intermediate. While the most efficient hydrogen-utilizing SRB did not accelerate iron corrosion compared to sterile tests, when grown in organic matter-free (lithotrophic) cultures, these novel isolates accelerated iron oxidation up to 71-fold under the same conditions (Enning *et al*. 2012:1778). The existence of such a direct mechanism of electron uptake had previously been considered by some investigators (Ferris *et al*. 1992:1320; Widdel *et al*. 1992:277) but without the availability of defined model organisms for experimental validation. The process was able to be studied in greater detail (Enning *et al*. 2012:1781; Venzlaff *et al*. 2012:88) and the term "electrical microbially influenced corrosion" (EMIC) was proposed (Enning *et al*. 2012:1781). EMIC, which is fundamentally different from the corrosive effects of biogenic H_2S, can destroy metallic structures at rates of high technological relevance (Enning *et al*. 2012:1781; Beese *et al*. 2013:239). While EMIC has so far been observed in

only a limited number of highly corrosive SRB isolates, all SRB, by definition can influence corrosion through excretion of the chemical H_2S ("chemical microbially influenced corrosion"; CMIC) if sulphate and suitable electron donors are present.

SRB act as either direct or indirect catalysts of anaerobic iron corrosion (EMIC and CMIC, respectively) and there are species-specific differences in this respect.

2.3.1. MIC or anaerobic biocorrosion

Javaherdashti (2011:1507) explains that except for some cases caused by erosion or mechanical stress, the corrosion of iron is mostly an electrochemical process, coupling metal oxidation to the reduction of a suitable oxidant (Revie 2011:356, Whitney 1903:394). In contrast to redox reactions of nonmetals, it is not necessarily the case that iron oxidation and reduction of the oxidizing agent must occur at the same locality. Spatial separation of oxidative (anodic) and reductive (cathodic) reactions is possible as the metallic matrix allows the free flow of electrons from anodic to cathodic sites. Central to iron corrosion is the high tendency of the metal to give off electrons according to the following anodic reaction:

$$Fe^{\circ} \leftrightarrow Fe^{2+} + 2e^{-1} \quad (2)$$

$$E^{\circ} = -0.47\ V$$

where, E° is the revised standard potential (Enning *et al*. 2012:1772, Rickard & Luther 2007:514). Hydrated ferrous ions move into the solution only if electrons, which cannot enter the aqueous phase, are removed from the surface by a suitable chemical reactant. The most common reactant in iron corrosion is molecular oxygen ($E^{\circ\prime}$= +0.81 V), and corrosion of iron in oxygen environments ultimately leads to the formation of various iron hydroxides ("rust"). In the absence of oxygen, on the other hand, the most common electron acceptors for iron oxidation are protons from dissociated water. Here, the cathodic reaction consisting of proton reduction to molecular hydrogen occurs as follows:

$$2e^{-} + 2H^{+} \leftrightarrow H_2 \quad (3)$$

$$E^{\circ\prime} = -0.41\ V$$

Owing to the condition of electroneutrality, the anodic and cathodic half-reactions are stoichiometrically coupled, which in the case of Equations 2 and 3 yields the following net reaction:

$$Fe^{\circ} + 2H^{+} \rightarrow Fe^{2+} + H_2 \quad (4)$$

$\Delta G^{\circ\prime} = -10.6kJ\ mol(Fe^{\circ})^{-1}$

Ferrous iron from Equation 2, readily precipitates in most anoxic environments (e.g., as $FeCO_3$) such that the activity of Fe^{2+}(aq), usually remains low, thus making reaction of Equation 3 even more favourable e.g., $\Delta G_{environ} = -27.7kJ\ (mol\ Fe^{\circ})^{-1}$ at $a_{(Fe^{2+})} = 10^{-3}$ and pH 7 (otherwise standard conditions). However, reaction Equation 2 in Table 2.2 is particularly slow at pH>6, where proton availability is limiting (Piron 1994). Hence, iron corrosion is technically insignificant in the absence of oxygen or acid and iron constructions in many anoxic environments (e.g., marine sediment, water-logged soil) could, in principle, last for centuries. However, the scenario described above changes in the presence of microorganisms, some of which dramatically accelerate corrosion kinetics. This is particularly true in environments with little or no oxygen and pH>6, i.e., where, from a purely chemical point of view, corrosion rates should be low. In technology, the phenomenon is referred to as (anaerobic) microbially influenced corrosion (MIC) or anaerobic biocorrosion.

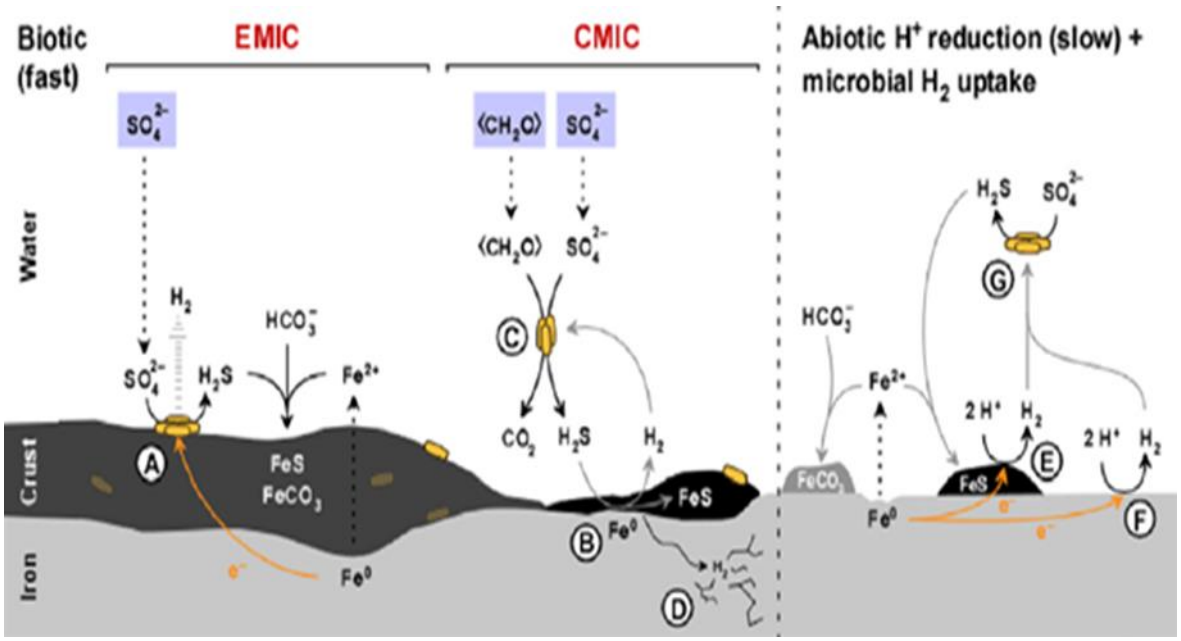

Figure 2.2: Schematic illustration of different types of ion corrosion by SRB at circumneutral pH. Biotic and abiotic reactions are shown (Enning & Garrelfs 2013:1232)

Depicted biotic reactions tend to be much faster than abiotic corrosion reactions. SRB attack iron via electrical microbially influenced corrosion (EMIC) or chemical microbially influenced corrosion (CMIC). The depicted processes, as illustrated in Figure 2.2 and Table 2.2, may occur simultaneously on corroding metal surfaces but differ in rates and relative contributions to corrosion. (A) Specially adapted lithotrophic SRB withdraw electrons from iron via

electroconductive iron sulphides (EMIC). Excess of accepted electrons may be released as H_2 (via hydrogenase enzyme). Participation of possibly buried (encrusted) SRB in sulphate reduction and hydrogen release is currently unknown. (B) Biogenic, dissolved hydrogen sulphide reacts with metallic iron. (C) Overall representation of CMIC. Organotrophic SRB produces hydrogen sulphide which reacts with metallic iron. (D) Sulphide stress cracking (SSC) of iron due to biogenic hydrogen sulphide. (E) Catalytic iron sulphides may accelerate reduction of H^+ ions to H_2. (F) Slow, kinetically impeded reduction of H^+ ions to H_2 at iron surfaces. (G) Consumption of H_2 from reaction E or F by SRB does not accelerate the rate of H_2 formation (no "cathodic depolarisation"). Note that CMIC quantitatively depends on the availability of biodegradable organic matter (here schematically shown as carbon with the oxidation state of zero, CH_2O) (Enning & Garrelfs 2013:1232).

Table 2.2: Stoichiometry of corrosive reactions (Enning & Garrelfs 2013:1232)

Electrical microbially influenced corrosion (EMIC):	A $4Fe^{\circ} + SO_4^{2-} + 3HCO_3^- + 5H^+ \rightarrow FeS + 3FeCO_3 + 4H_2O$
Chemical microbially influenced corrosion (CMIC):	B $H_2S + Fe^{\circ} \rightarrow H_2 + FeS$ C $3 < CH_2O > + 2Fe^{\circ} + 2SO_4^{2-} + H^+ \rightarrow 3HCO_3^- + 2FeS + 2H_2O$
Sulphide stress cracking	D $2H_{abs} \rightarrow H_2$
Abiotic	E $Fe^{\circ} + 2H^+ \xrightarrow{FeS} Fe^{2+} + H_2$ F $Fe^{\circ} + 2H^+ \rightarrow Fe^{2+} + H_2$ G Same as A but slower

2.4. Sulphate-reducing bacteria found in different environments

Cultures of bacteria can be obtained from different environments. Bacterial cultures from a number of environments have showed positive identification of bacteria.

Suo *et al*. (2017) examines and characterises the attachment and colonization of *Bacillus sp*. on their surfaces in artificial seawater, and their effects on anticorrosion performances of coatings. Results from this study show that *Bacillus sp*. opt to settle on low-lying spots of the coating surfaces in early stage, followed by recruitment and attachment of extracellular polymeric substances (EPS) secreted through metabolism of *Bacillus sp*. The bacteria survive with the protection of EPS.

Javed *et al*. (2016:7) studied copper nickel alloys under pure strain bacterial load, and the results were quite remarkable. Black corrosion products formed on the surface of the alloys containing high content of elemental iron, copper and sulphur, indicating the presence of FeS and/Cu_2S. After removal of the biofilm, CuNi (90-10) showed grain boundary attack, and CuNi (70-30) showed localised pitting attack.

Javed *et al*. (2015:48) studied the effect of ferrous ions on the initial attachment of sulphate reducing bacteria (SRB) and subsequent corrosion of carbon steel. The sulphate-reducing bacterium (SRB) used in this study, *Desulfovibrio desulfuricans* (*D. desulfuricans*) ATCC 27774, was obtained from the American Type Culture Collection (ATCC), USA. Short and long term exposure of carbon steel to SRB was investigated, in static batch mode at 21 °C under anaerobic conditions.

Liu *et al*. (2015:485) studied both SRB and IOB (Aerobic iron-oxidizing bacteria), isolated from the sludge in Sinopec oilfield. 16S rDNA sequencing was done to identify bacterial species. A sample of the oilfield water was also collected and, the water composition presented showed sulphate content of 854 mg/l.

Guan *et al*. (2012:1648) obtains a slime culture from cooling tower bottom of circulating water. A pure strain of iron bacteria was obtained through the separation, purification and enrichment culture. The strain is identified by the morphological observation, physiological and biochemical identification. The isolated bacteria are carried on gram staining. A tubular heat exchanger dynamic simulation was used (to simulate the industrial environment) to study the biofouling formation with iron bacteria in circulating cooling water system. The experimental conditions are 30 °C± 0.2 °C for water and flow rate at 0.4 m/s. Results show that the fouling resistance increased.

Kuang *et al*. (2007:6084) investigates the influence of the growing process of sulphate-reducing bacteria (SRB) in seawater system on the medium state and corrosion behaviour of carbon steel (D36) was studied by detecting solution state parameters and using corrosion electrochemical methods. Mixed seeds of SRB used in this study were separated from effluent samples collected from the mud and 50 ml SRB culture was diluted into 500 ml purified seawater. Experiments were carried out at 28 °C and in airtight system. Hydrogen sulphide generated by the metabolism of SRB during its growing process caused the change of environment parameters.

Little *et al*. (2006:1008) diagnoses MIC from other works explaining use of equipment such as ESEM (Environmental electron microscopy) which is ideal in capturing bacteria in wet biofilm, further explaining that three types of evidence must be used when diagnosing bacteria in different environments these are, metallurgical, chemical and biological which are independent measurements, and must be consistent with the mechanism for MIC.

Li *et al*. (2001:815) investigates microbiologically influenced corrosion (MIC) of plain carbon steel in anaerobic soil, using field survey, and provides evidence from conventional electrochemical experiments, that activity of sulphate-reducing bacteria alter the corrosion mechanism of steel by the production of hydrogen sulphide and iron sulphide film on the steel surface, which reduces the polarisation resistance and therefore increases the corrosion rate. Detection of bacteria was done using dilution tubes containing Postgate's medium B, and blackening was seen after 21 days at an incubation period of 35 °C.

Neville and Hodgkiess (2000:61) grow SRB culture, obtained from a source of estuarine mud extracted from the Clyde Estuary on the west coast of Scotland. Media was prepared using Postage's B medium, in synthetic sea water. Austenitic and duplex stainless steels were exposed to the SRB media for 9 months using potentiodynamic studies, and results show increased susceptibility to localised and general corrosion. Growth of SRB culture was accompanied with a characteristic blackening of the solution and increase in the measured partial pressure of hydrogen sulphide, indicating that sulphate reduction was proceeding.

Henry *et al*. (1987:1406) investigates microbial sulphate reduction rates in acidic peat from a New Jersey Pine Barrens cedar swamp in 1986, and freshwater lake sediments, and present a range of sulphur content. Peat was incubated over 24 h and removed from the incubator at selected intervals for determination of the time course of sulphate reduction.

Suo *et al*. (2017) concludes that biofilm secreted by a pure strain of bacteria, acts as a protective shield ensuring survival, biofilm formation is greatly anticipated in this study however, the study does not obtain a bacterial culture from the heat exchanger environment. Javed *et al*. (2016:7) uses pure strain bacteria on copper nickel alloys (same as in this study) to evaluate corrosion behaviour, however it would be fascinating to compare the corrosion behaviour of these alloys when exposed to a mixed culture of bacteria. There is not enough data available when exposure tests are conducted. Javed *et al*. (2015:49) focuses on the effects of pure strain bacteria and does not obtain cultures, however sulphur weight percent was presented in the results and, similar results can be anticipated in this work, to give an indication of strains of bacteria present. Lui *et al*. (2015:484) presents water composition where SRB and IOB were found, in the study that follows water composition will be analysed

for sulphate content. Techniques in identifying species of bacteria presented by Guan *et al*. (2012:1650) are also useful for future work. Kuang *et al*. (2007:6085) investigates corrosion behaviour of carbon steels used in marine equipment, the study does not address carbon steels used as tube material in a heat exchanger. Little *et al*. (2006:1008) discusses 16S rDNA genetic techniques in identifying microbial populations and the use of ESEM, these techniques are useful for future work. The investigation done by Neville and Hodgkiess (2000:61) characterises positive indication of bacteria. These are the results that can be expected in the study that follows, although not in the heat exchanger environment, a mixed culture of bacteria was investigated.

The heat exchanger environment was selected to investigate the presence of SRB. Figure 2.3 represents the classification of heat exchangers according to process function, classification of condensers and liquid to vapour phase change exchangers, these types of condensers are widely used throughout petrochemical industries.

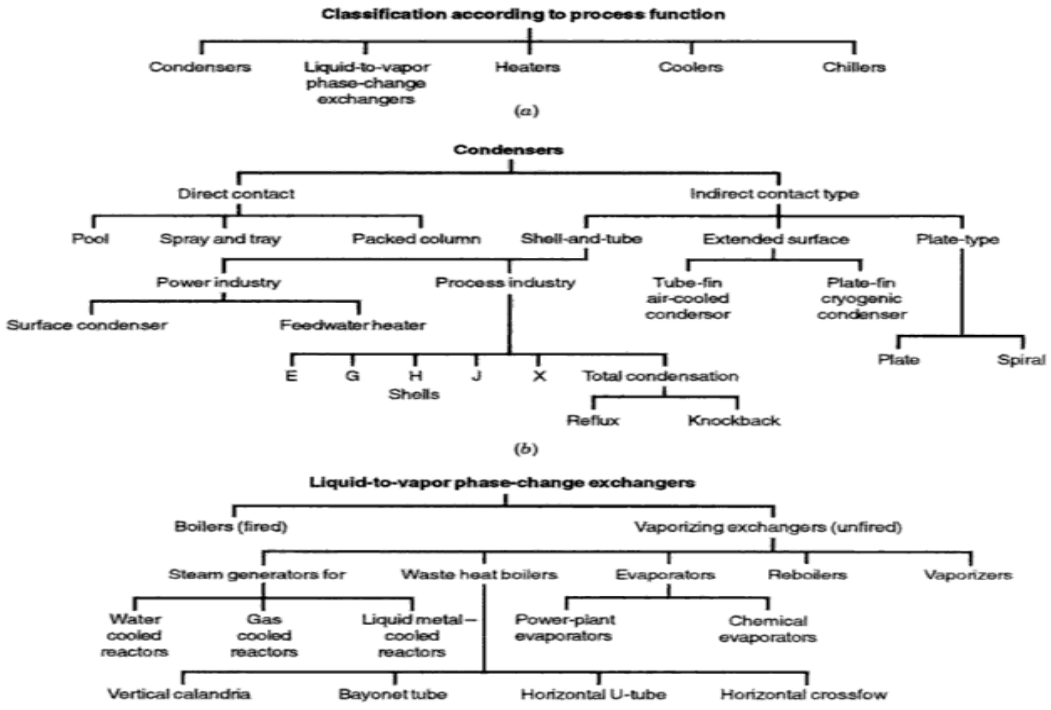

Figure 2.3: (a) Classification according to function; (b) classification of condensers; (c) classification of liquid to vapour phase change exchangers (Ramesh & Dusan 2003:13)

The shell and tube exchanger as shown in Figure 2.4 as described by Ramesh & Dusan (2003:13), are used widely in the petrochemical industry, to cool and condense gas. When there are tube leaks, this leads to unintended downtimes. The heat exchangers are generally built of a bundle of round tubes mounted in a cylindrical shell, with the tube axis parallel to that of the shell. One fluid flows inside the tubes, the other flows across and along the tubes.

The major components of this exchanger are the tubes (or tube bundle), shell, front-end head, rear-end head, baffles, and tubesheets. Three most common types of shell and tube heat exchangers are; fixed tubesheet design, U-tube design, and floating head type.

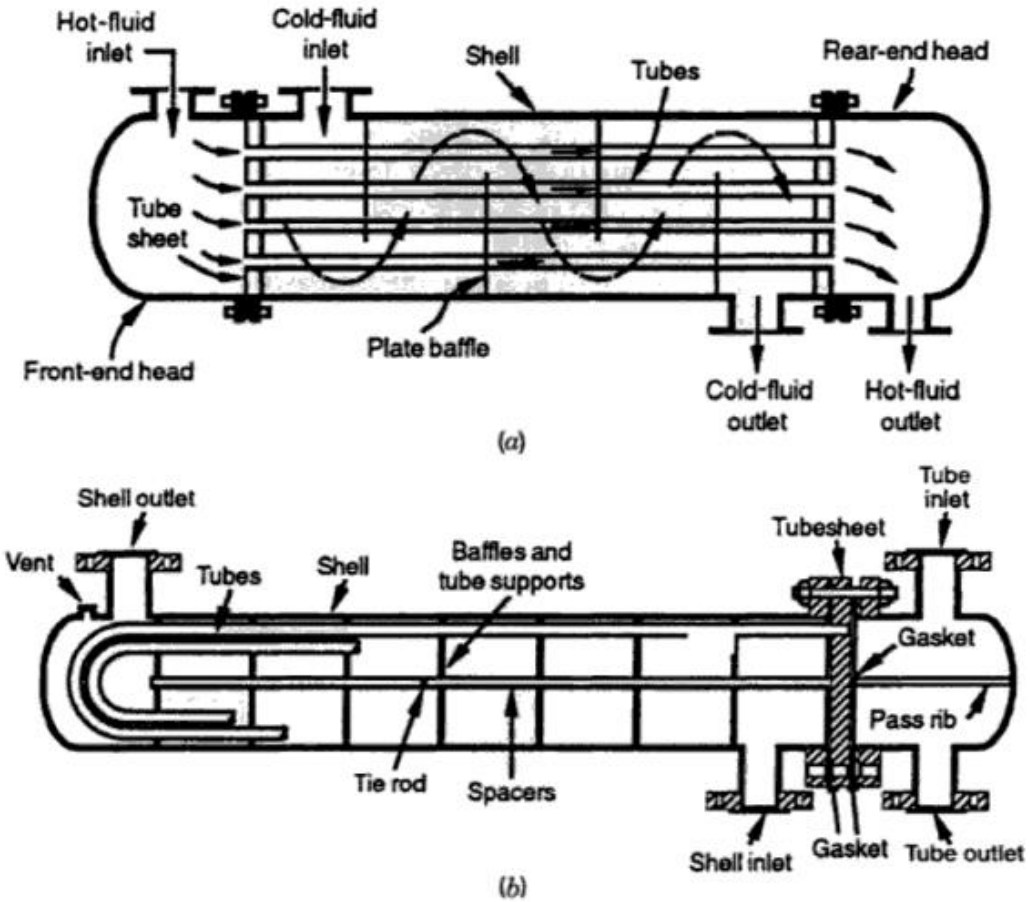

Figure 2.4: (a) Shell and tube exchanger (BEM) with one shell pass and one tube pass; (b) Shell and tube exchanger (BEU) with one shell pass and two tube passes (Ramesh & Dusan 2003:13)

2.5. Methods to detect SRB

In order to detect SRB in the heat exchanger environment, some approaches according to Tan & Halim (2015:121) can be used. The approaches employed to detect the presence of SRB are divided into two main categories: culture-based and molecular-based methods. The mechanisms of these two methods are briefly discussed.

Culture based

Typically, the investigation of SRB using culture-based approach involves the isolation and characterisation of the microorganisms by using different growth media, such as nutrient agar. According to the previous reports, the isolation of the SRB requires selective growth

medium and several findings claimed that there is no growth of the bacteria takes place in the media rendered “biologically free” of iron (Ghazy *et al*. 2011:604). Currently, there are a wide range of different growth media which have been formulated to cultivate the growth of SRB, such as Postgate, Starky and Baar's (Postgate 1984). There are slight differences in the chemical composition of each media which results in different efficiency on the detection of SRB growth. Typically, the detection of SRB can be done by using the culture based approach by the human observer. There will be some blackening in the sample as illustrated in Figure 2.5, when the colonies of SRB are sufficiently high enough to be observed. A current finding by Ghazy *et al*. (2011:607), reported that the growth of SRB isolated from the failure shipping pipeline, could only be observed and detected after 2 to 7 days of incubation.

Molecular-based approach

Investigation and analyses of microbial populations using culture independent molecular technique catches an expertise's interest. One of the common techniques used to detect and quantify SRB populations is based on the analyses of polymerase chain reaction (PCR). The common procedure using PCR approach for SRB detection involves the extraction of RNA from an environmental sample. The result generated by the PCR reflects a mixture of microbial gene signatures from all organisms presented in a sample (Rastogi & Sani 2011:29). PCR amplification of conserved genes such as 16S rRNA has been used extensively in the analyses of SRB distribution, using the molecular-based approach. However, this approach required experts to conduct the testing, and it is not convenient for field test. In addition, there are several problems encountered during the process, for example, the difficulties of using rRNA fluorescent probes in sediments or industrial wastewater (Eitan *et al*. 2007:439).

The best practice of detecting SRB was given by Benham (2010:50) and, has utilised and examined the following methods for detecting the presence of SRB in water systems:

Periodic inspection of equipment for pitting caused by MIC/SRB attack

Periodic equipment inspection is considered to be the best method for MIC/SRB induced corrosion identification, but it may be possible to do this only after a failure. Pitting caused by SRB sometimes is difficult to differentiate from other types of corrosion (e.g. Chloride induced pitting). Hence, more failure analysis is needed to appropriately distinguish the root causes of the corrosion.

Bacteria/SRB counting qualitative measurement via cultured growth

A widespread method for SRB detection is to cultivate SRB by means of test kits and detect SRB either qualitatively or quantitatively. These test kits are frequently utilized by water treatment and the results may be marred by many inaccuracies. If the water sample is taken from the bulk water, it is only indicative of SRB in the bulk water. It is often considered that if the test is positive, SRB are active throughout the system. It is possible to have negative results on SRB test kits, but there could be severe attacks happening somewhere else in the system.

Bacteria/SRB evaluation attack on corrosion coupons

The use of corrosion coupons to detect MIC and SRB is simple, reliable and indicative. The mild steel corrosion coupons are inserted into the system at appropriate locations such as supply and return lines or heat exchanger outlets to determine the general corrosion rate over a specific time. It is suggested that the inserted coupons be periodically inspected visually and if a black local deposit is observed on a coupons surface, the following may be performed to identify MIC/SRB-induced corrosion. The coupon, which is covered by some localised black deposits, should be removed and immediately put in 200 ml of hydrochloric acid (HCl). Close the cap and leave it for a couple minutes, then open the cap and smell the solution (with precaution). If a rotten-egg odour is detected, it is attributed to hydrogen sulphide (H_2S) released by the reaction of HCl with iron sulphide (FeS). (FeS is a corrosion product of SRB-induced corrosion.) This test should be performed on fresh mild steel corrosion coupon in situ. This test has been used on carbon steel (CS) corrosion coupons inserted in water systems. Lead acetate paper may be used to identify the presence of a sulphur compound (e.g. H_2S) after the fresh CS corrosion coupon has been dipped in HCl. This method is a qualitative test and is based on the discolouration of the lead acetate paper. The unexpected paper colour is white and turns to a yellow/light brown colour thereafter progressing to a dark brown/black colour. The colour is proportional to the concentration of sulphur/sulphur based compounds. The shape of the pits after acid cleaning of the corrosion coupon should also be examined. The pits are typically characterised as follows: Pits are filled with black corrosion product/deposits, metal surfaces beneath the corrosion products are often bright and active, the pits are round at the outer surface and conical in cross section, with concentric rings inside the pits, the pits are typically hemispherical and they are overlapped and clustered.

Figure 2.5: Indication of the presence of SRB in a sample (Tan & Halim 2015:121)

The culture based approach is promising for the heat exchanger environment, and this approach will be discussed in Chapter 3.

2.6. Basic terminology in electrochemistry

Once SRB cultures are detected, electrochemical experiments can be conducted to evaluate corrosion rates. Presented are some basic concepts in electrochemistry, followed by experimental works of others from Section 2.7 to 2.9.

Three-electrode cells and e-log i plots:

The three electrode cell is the standard laboratory apparatus for the quantitative investigation of the corrosion properties of materials. It is a refined version of the basic wet corrosion cell and a typical example is illustrated in Figure 2.6. It can be used in many types of corrosion experiments (Trethewey & Chamberlain 1995:111).

Components:

The working electrode is the name given to the electrode being investigated. The counter electrode (auxiliary) electrode is the name given to the second electrode. The counter electrode is present specifically to carry the current created in the circuit by the investigation; it is not required for measurements of potential. Usually, a carbon rod is used, but can be any material that will not introduce contaminating ions into the electrolyte. Platinum and gold can

also be used with success, especially if space is at a premium, when smaller electrodes can be used; titanium is also suitable (Trethewey & Chamberlain 1995:111).

The reference electrode is present to provide a very stable datum against which the potential of the working electrode can be measured. It cannot itself carry more than the most negligible current. If it did, it would participate in the cell reactions and its potential would no longer be constant, hence the requirement for the counter electrode would not be met. By far the most convenient reference electrode to use in such an experiment is saturated calomel electrode (SCE). The external circuit can be varied considerably. The essential components are current measuring device, a potential-measuring device and a source of potential. The current-measuring device should be capable of reading microamps potential. The potential-measuring device should draw no current during the act of measurement; traditionally potentiometers have been used for this purpose. The modern digital meter, however, can have impedance of the order of gigohms, and may be used with as good accuracy as a potentiometer. The source of potential must 'drive' the working electrode to produce the desired cell reactions (Trethewey & Chamberlain 1995:111).

The e-log i plot, or potentiodynamic polarisation curve, is one of the most common methods of examining the corrosion behaviour of materials. It has become common practice in e-log i plots for all current densities to be treated as positive. This is just a convenience for it reduces the size of the graphs and gives a much clearer indication of the value of potential when the current density changes from negative to positive (Trethewey & Chamberlain 1995:111).

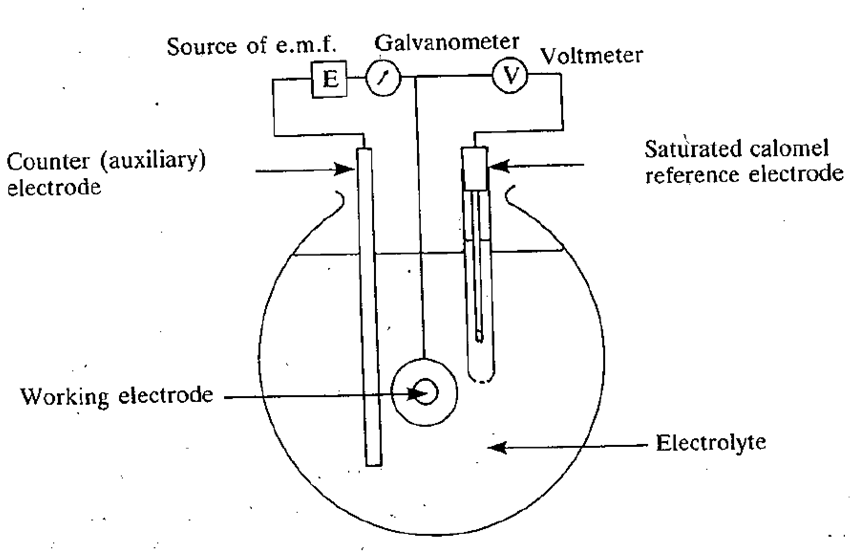

Figure 2.6: Three electrode cell (Trethewey & Chamberlain 1995:111)

2.7. Experimental setups according to literature

Different methods of experiments were used by works of others. More detail and results can be obtained in the articles stated.

Javed *et al*. (2015:49) investigates triplicate steel coupons which were tested for each exposure time, after which the tests were repeated to give n = 6 for each set of conditions. During tests, the coupons were fully immersed in the medium with the polished side facing upward. All experiments were carried out in static batch mode at 21 °C under anaerobic conditions.

Chen *et al*. (2014:767) uses six containers, each holding 4 CS coupon specimens that were set up in the study. Three of the containers were inoculated with SRB cells, each as a sacrificial system for the coupons to be collected and evaluated on Day 3, 21 or 43. The other three were corresponding cell-free controls. The containers used were 600 ml glass beakers closed with rubber stoppers. The coupons were hung vertically, using plastic tie wraps, on stainless steel hooks that were anchored to the rubber stopper. The coupons were completely submerged in the medium.

Abdullah *et al*. (2014:2) performed an experiment using a 125 ml sealed anaerobic vial and in a 1 liter electrochemical glass cell. An open circuit potential (OCP) measurement was conducted by using a saturated calomel electrode (SCE) as the reference electrode and carbon steel as the working electrode in a standard electrochemical glass cell with the SRB medium as electrolyte. A multimeter (Kyoritsu KEW1051) was utilized to read the OCP value. Potential dynamic polarisation curves were conducted in an ASTM standard cell (Ahammed 1997:988) with a three electrode system, a carbon steel coupon as a working electrode, a platinum electrode as a counter electrode, and a saturated calomel electrode as a reference electrode. An Autolab PGSTAT 30 with General Purpose Electrochemical System (GPES) software was used to monitor the corrosion rate of the experiments.

Beimeng *et al*. (2012:1) describes the method of three electrode system which was applied to obtain the E_{corr} of specimens immersed in culture of IRB and SRB to understand the effect of mixture of bacteria on the corrosion process.

Venzlaff *et al*. (2012:89) describes the method of electrochemical cells. Duran glass bottles (250 ml) filled with 200 ml of anoxic sterile electrolyte was used as electrochemical cells. Each bottle was equipped with a magnetic stir bar and the two sterilised ion coupons (WE and CE) in such a way that only the lower 5 cm of the coupons were immersed. Silver wires

providing electrical contact to the coupons were pierced through the butyl-rubber septum. For connection with the reference electrode, a sterilised steel cannula (13.201 stainless steel; Unimed S.A., Lausanne, Switzerland) of 0.8 mm in diameter was introduced into the cell through the top septum and connected to a glass holder via gas-tight butyl rubber tubing. The glass holder contained two compartments separated by a glass diaphragm. The electrode compartment of the glass holder was filled with a 3M KCl electrolyte and equipped with a standard Ag/AgCl reference electrode (type 6.0750.100 by Metrohm AG, Herisau, Switzerland).

Kuang *et al*. (2007:6085) used the three electrode cell setup. The corrosion potential (E_{corr}), potentiodynamic polarisation curves and the electrochemical impedance spectroscopy were performed with Solartron SI1287 electrochemical interface and SI1260 impedance/gain-phase analyser control systems.

Javaherdashti *et al.* (2006:29) explains SCC failure in terms of the possibility of hydrogen embrittlement, a few SSRT tests (Figure 2.7) had been carried out under imposed electrochemical potential on specimens that had been charged with hydrogen prior to the SSRT tests. The open circuit potential (OCP) was determined from previous experiments by carrying out the OCP tests on the carbon steel in biotic and abiotic environments (Javaherdashti 2005).

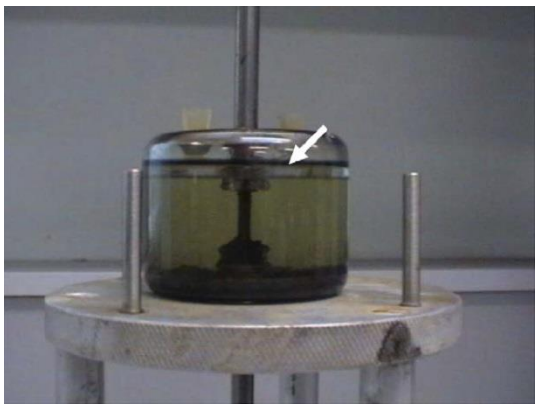

Figure 2.7: SSRT carbon steel sample in the anaerobic chamber inoculated with SRB. Note the oil layer (arrow) to avoid oxygen entrance (Javaherdashti *et al.* 2006:29)

Neville & Hodgkiess (2000:62) explains that the corrosion monitoring techniques used were electrochemically based measurements of free corrosion potential E_{corr} and, more importantly, dc potentiodynamic (anodic and cathodic), potentiostatic, and galvanic type tests performed in the presence of an active culture of SRB.

Natishan *et al.* (1999:1063) explains that anodic polarisation curves for tungsten were obtained in deaerated 0.6 M NaCl solution or 0.6 M NaCl to which 3.5 g/L of sodium sulphate (Na_2SO_4) was added. Specimens were immersed for 24 h to establish a steady state open-circuit potential. Anodic polarisation curves were determined using a potential step technique. Potentials were reported relative to the saturated calomel electrode (SCE).

Open circuit potential and potentiodynamic studies, will be used in this study as presented in the works of Kuang *et al*. (2007:6085), Natishan *et al.* (1999:1063), Abdullah *et al*. (2014:2), Neville & Hodgkiess (2000:62) and Beimeng *et al*. (2012:1). These methods will provide understanding of polarisation curves, indicating behaviour of the carbon steels, and other alloys when exposed to the SRB. It will give indication of the activity and corrosion effects of the bacteria.

In light of the above, this study will explore behaviour of different grades of carbon steel when exposed to SRB, using electrochemical methods (three electrode cell system). Corrosion rates will then be evaluated. Exposure tests by Javed *et al*. (2015:49), will not produce data for e-log i plots.

2.8. Media preparation according to literature

Different SRB growth media are used, and the table below presents the types of nutrients bacteria need in order to grow or survive, the media presented was used as a basis, and adjusted slightly for this work.

Table 2.3: SRB growth media used from literature

Article	Media per L
Abdullah *et al.* (2014:2)	$C_3H_5NaO_3$ (Sodium Lactate) 6 g, $NaSO_4$ 4.5 g, NH_4Cl 1.0 g, Yeast extract 1.0 g, KH_2PO_4 0.5 g, $Na_3C_6H_5O_7$ (Sodium citrate) 0.3 g, $CaCl_2.6H_2O$ 0.06 g, $MgSO_4.7H_2O$ 0.06 g, $FeSO_4.7H_2O$ 0.004 g in water.
Javed *et al.* (2015:49)	KH_2PO_4 0.5 g, NH_4Cl 1.0 g, $NaSO_4$ 4.5 g, $CaSO_4.2H_2O$ 0.05 g, $MgSO_4.7H_2O$ 4.1 g, $C_3H_5NaO_3$ (Sodium Lactate) 5.67 g, Yeast extract 1.0 g, $Na_3C_6H_5O_7$ (Sodium citrate) 5.0 g added for each MilliQ of water. The media contains Fe^+ ions.

Chen *et al.* (2014:767)	$C_3H_3NaO_3$ (Sodium Lactate) 6 g, $NaSO_4$ 4.5 g, NH_4Cl 1.0 g, Yeast extract 1.0 g, KH_2PO_4 0.5 g, $Na_3C_6H_5O_7$ (Sodium citrate) 0.3 g, $CaCl_2.6H_2O$ 0.06 g, $MgSO_4.7H_2O$ 0.06 g, $FeSO_4.7H_2O$ 0.004 g in deionised water.
Kuang *et al.* (2007:6084)	$C_3H_3NaO_3$ (Sodium Lactate) 4ml, Na_2SO_4 0.5 g, NH_4Cl 1.0 g, Yeast extract 1.0 g, KH_2PO_4 0.5 g, $CaCl_2$ 1.0 g, $MgSO_4$ 2 g, in sea water.
Media adjusted and used in this study	KH_2PO_4 0.5 g, NH_4Cl 1.0 g, $NaSO_4$ 4.5 g, $CaCl_2.2H_2O$ 0.05 g, $MgSO_4.7H_2O$ 0.06 g, $C_3H_5NaO_3$ (Sodium Lactate) 6 g, Yeast extract 1.0 g, $FeSO_4.7H_2O$ 0.004 g, $Na_3C_6H_5O_7$ (Sodium citrate) 5.0 g in distilled water.

2.9. Metal preparation according to literature

Table 2.4 gives carbon steel preparation methods, before exposure to SRB media. Standards can be obtained in the articles.

Table 2.4: Preparation of metals for exposure to SRB media

Article	Preparation method
Abdullah *et al.* (2014:2)	The corrosion specimens were machined from an actual segment of API 5L X-70 pipe obtained from a local gas operator. The composition of the carbon steel is as follows: 97.093% Fe, 0.078% C, 1.67% Mn, 0.15% Ni, 0.012% P, 0.3% Si, 0.023% Cu, 0.275% Cr, 0.11% Ti, and 0.002% S (Noor *et al*. 2012:312). Prior to use, the metal specimen were polished with a SiC grit paper graded 200, 400, and 600, followed by cleaning with acetone and coated with Teflon, leaving only the flat surface exposed to the medium in an anaerobic bottle experiment.
Javed *et al.* (2015:49)	Carbon steel (1010) specimen with the chemical composition of 99.38% Fe, 0.10% C, 0.44% Mn, 0.02% Si, 0.01% S, 0.02% P and 0.03% Al, were cut with dimensions of 25 mm × 25 mm × 3 mm from a plate sample using an automatic abrasive wheel cutting machine (Struers Tegramin-25, Australia). First the specimen was ground sequentially up to 1200 grit silicon carbide paper to obtain a smooth surface finish. Finally, the specimens were polished through a sequence of fine polishing with 9 and 3µm diamond suspensions to a final 0.04 µm finish using silica suspension (Struers OPU, Australia). The polished specimens were ultrasonically cleaned with acetone

	for 10-15 min, rinsed with distilled water followed by ethanol, and then dried under warm air. Prior to testing, specimens were ultrasonically cleaned with acetone followed by sterilisation via immersion in absolute ethanol (100%) and then aseptically dried within a level 2 physical containment (PC2) cabinet. The surface roughness of a material has been reported to affect the attachment of bacterial cells (Chen *et al*. 2015:89) The surface roughness of the polished specimens were therefore characterised using a 3D optical profilometer (Contour GTK1, Bruker, Germany).
Chen *et al.* (2014:767)	The carbon steel specimens (UNS G10100) used were rectangular (25 by 11 by 0.3 mm). One side of the specimen was polished following the polishing procedure described below. The unpolished side was marked with a number by scratching the specimen surface using stainless steel tweezers. For sterilisation, specimens where soaked in pure ethanol for 2 days at room temperature and sonicated during the periods of 0 h to 2 h and 46 h to 48 h to remove gas bubbles, if not removed, could prevent complete wetting of the specimen surfaces by ethanol and compromise the effectiveness of sterilisation. CS specimens were polished with abrasive papers (240/P280, 600/P1200, 800/P1500, 1200/P2500, 8 inch diameter) using a grinding and polishing machine (Struers. Inc., model DAP-7) at 200 rpm. An abrasive paper (240/P280) was secured on the machine, and then the acrylic holder was pressed down to polish the specimens with abrasive paper for 5 min. During the polishing process, water was added to rinse and cool the specimens and the abrasive paper. The process was repeated 3 times, each with a higher grit (finer) abrasive paper, i.e., 600/P1200, 800/P1500), and then 1200/P2500, respectively. The polished specimens were immediately rinsed with DI water to remove particles and then sonicated, first in ethanol and then in DI water, each for 5 min. The cleaned specimen were dried under a stream of nitrogen.
Kuang *et al.* (2007:6085)	D36 carbon steel composed of the following elements with a mass ratio of 0.4% C, 0.5% Mn, 0.17% Si, 0.035% P, 0.25% Cr, 0.00104% Mo, 0.25% Ni, 0.015% Al, 0.0053% Co, 0.25% Cu, 0.015% Nb, 0.02% V, 0.010% W, 0.02% Ti, 0.014% Sn, 0.035% S and 98.0% Fe was used as the working electrode. No specific method of preparation was mentioned.

2.10. Biofilm: cathodic and anodic behaviour on e-log i plots

During electrochemical experiments it is anticipated that biofilm will start to form on the surface of the metals, below gives insight into the nature of the biofilms formed by SRB.

Passive films form on the surface of the metal in the presence of SRB, and the anodic and cathodic behaviour originates from sulphide precipitation with Fe^{2+} ion to form iron sulphide films. These film are good electric conductors, and have low over voltage for hydrogen evolution (Da Silva *et al.* 2002; Cabrera *et al.* 2000:487), and consequently tend to change the E_{corr} of the metal where it deposits (Da Silva *et al.* 2002; Benetton 2017:41). Additionally, it is thought that iron sulphide films may be both protective and detrimental (Vedage & Ramanarayanan 1993:114) due to (1) Iron sulphide films formed in the absence of oxygen are usually unstable (Benetton 2017:81), and have a porous structure (Da Silva *et al.* 2002); (2) iron sulphide films has many forms, and it is greatly influenced by the changes of hydrogen sulphide concentration and pH; (3) additionally, ferrous ion diffusion can also be a rate limiting step (Vedage & Ramanarayana 1993:114). In this case the films may relate to unstable protection of the steel, protecting the material initially, but with changes in environmental conditions, breaking down and resulting in structural transformation, leading to an increase in corrosion rate (Da Silva *et al.* 2002; Benetton 2017:52). The latter relates to inhomogeneous film formation on the surface as some parts of the metal surface may remain uncovered (become anodic) and some parts may be covered by the iron sulphides (become cathodic), thus resulting in localised corrosion (Da Silva *et al.* 2002; Benetton 2017:81), if the anode to cathode ratio is small.

Typically, the anodic half reaction is step 1 (mentioned above), in this reaction, $Fe(OH)_2$ is considered to be the primary corrosion product in the absence of sulphide:

$$Fe + 2H_2O \rightarrow Fe(OH)_2 + 2e^- + 2H^+ \quad (5)$$

SRB are facultative anaerobes that utilise sulphate as a terminal electron acceptor during energy generation, producing sulphide as a by-product by the following cathodic reaction:

$$SO_4^{2-} + 9H^+ + 8e^- \rightarrow HS^- + 4H_2O \quad (6)$$

2.11. Corrosion rates can be calculated using ASTM standard G102-89(2015)e1

In order to calculate corrosion rates ASTM standard G102-89(2015)e1 can be used. Some machines used to conduct electrochemical experiments, readily provide corrosion rates and

are built with corrosion rate formulas. However, equivalent weight and density were manually calculated, and the surface area remained constant, refer to Appendix A.

The current density of coupons can be determined using the following formula as per ASTM standard G102-89(2015)e1:

$$i_{corr} = \frac{Icorr}{A} \quad (7)$$

where:

i_{corr} = corrosion current density, $(\frac{\mu A}{cm^2})$,

I_{corr} = total anodic current, μA, and

A = exposed specimen area, cm^2.

The equivalent weight of the coupon can be determined using the following formula as per ASTM standard G102-89(2015)e1:

Equivalent weight may be thought of as the mass of metal in grams that will be oxidized by the passage of one Faraday (96 489 ± 2 C (amp-sec)) of electric charge.

Note 1: The value of EW is not dependant on the unit system chosen and so may be considered dimensionless.

For pure elements, the equivalent weight is given by:

$$EW = \frac{W}{n} \quad (8)$$

where,

W = the atomic weight of the element, and

n = the number of electrons required to oxidise an atom of the element in the corrosion process, that is, the valence of the element.

For alloys, the equivalent weigh is more complex. It is usually assumed that the process of oxidisation is uniform and does not occur selectively to any component of the alloy. If this is not true then the calculation will need to be adjusted to reflect the observed mechanism. In addition, some rationale must be adopted for assigning values of n to the elements in the alloy because many elements exhibit more than one valence value.

To calculate the alloy equivalent weight, the following approach may be used. Consider a unit mass of alloy oxidised.

The electron equivalent for 1 g of an alloy, Q is then:

$$Q = \sum \frac{nifi}{Wi} \quad (9)$$

were,

fi = the mass fraction of the ith element in the alloy,

Wi = the atomic weight of the ith element in the alloy, and

ni = the valence of the ith element in the alloy.

Therefore, the alloy equivalent weigh, EW, is the reciprocal of this quantity:

$$EW = \frac{1}{\sum \frac{nifi}{Wi}} \quad (10)$$

The corrosion rate of coupons can be determined using the following formula as per ASTM standard G102-89(2015)e1:

Faraday's law can be used to calculate the corrosion rate, either in terms of penetration rate (CR) or mass loss rate (MR):

$$CR = K_1 \frac{i_{corr}}{\rho} \text{EW} \quad (11)$$

$$MR = K_2 \, i_{corr} \, EW \quad (12)$$

where,

CR is given in mm/yr, i_{corr} in $\frac{\mu A}{cm^2}$,

$K_1 = 3.27 \times 10^{-3}$, mm g/ μA cm yr,

ρ = density in $\frac{g}{cm^3}$

EW is considered dimensionless in these calculations. For more detail refer to G102-89(2015)e1.

The polarisation resistance can be determined using the following formula as per ASTM standard G102-89(2015)e1:

$$B = \frac{babc}{2.303\ (ba+bc)} \quad (13)$$

where,

B = Stern-Geary constant, V.

ba = slope of the anodic Tafel reaction, when plotted on base 10 logarithmic paper in V/decade,

bc = slope of the cathodic Tafel reaction when plotted on base 10 logarithmic paper in V/decade, and

Stern-Geary constant may be calculated:

$$B = \frac{b}{2.303} \quad (14)$$

where,

b = the activation controlled Tafel slope in V/decade

In cases where the reaction mechanism is known in detail, the Tafel slopes may be estimated from the rate controlling step in the mechanism of the reaction. In general Tafel slopes are given by (Glasstone 1941:552):

$$b = \frac{KRT}{nF} \quad (15)$$

where,

K = a constant

R = the perfect gas constant

T = the absolute temperature

n = the number of electrons involved in the reaction step,

F = Faraday's constant

At 25°C, $(\frac{RT}{2.303F})$ is 59.2 mV/decade. For simple one electron reactions, K is usually found to be 2.0.

The corrosion current density may be calculated from the polarisation resistance and the Stern-Geary constant using the following formula as per ASTM standard G102-89(2015)e1:

$$i_{corr} = \frac{B}{R_p} \quad (16)$$

The effect of solution resistance is a function of the cell geometry, but the following expression may be used to approximate its magnitude.

$$R_p = R_a + \rho l \quad (17)$$

where:

R_a = the apparent polarisation resistance, ohm cm^2,

ρ = the medium resistivity in ohm cm,

l = the distance between the specimen electrode and the Luggin probe tip, or the reference electrode in cm, and

R_p = the true polarisation resistance in ohm cm^2.

Potentiodynamic techniques introduce an additional error from capacitive charge effects. In this case, the magnitude of the error is proportional to scan rate. The error is illustrated by the following formula as per ASTM standard G102-89(2015)e1:

$$I_{total} = I_f + c(\frac{dV}{dt}) \quad (18)$$

where,

I_{total} = the cell current,

I_f = The Faradaic current associated with anodic and cathodic processes,

c = the electrode capacitance, and

$\frac{dV}{dt}$ = the scan rate

Chapter 3

It is suspected that the root cause of pitting corrosion in the heat exchanger tube is due to MIC by SRB. This chapter presents detailed methodologies to collect and grow bacteria, anticipating positive identification of SRB. Positive identification will lead to further corrosion investigations.

3. Research design

The approach used in this study, was based on the works of Kuang *et al.* (2007:6085) and Neville and Hodgkiess (2000:61) and modified accordingly to suit specific requirements. Kuang *et al.* (2007:6085) and Neville and Hodgkiess (2000:61) used a culture of SRB from the soil environment. Modifications to the methodology was made, to imitate the heat exchanger environment. Kuang *et al.* (2007:6085) identifies bacterial presence by concentration of hydrogen sulphide generated by the metabolism of the SRB, and increase in corrosion rate of carbon steel when exposed to SRB media. Neville and Hodgkiess (2000:61) reported characteristic blackening of the solution containing SRB culture, Tan & Halim (2015:121) also presented a similar approach in detecting a culture of SRB. Electrochemical methods were used to produce e-log i plots.

Knowing that bacteria will survive under anaerobic conditions, a limitation exists. Coupons were inserted in the cooling towers, to collect a mixed culture of bacteria, then exposed to atmospheric conditions for a short period of time when removed, this could have possibly contaminated the prepared media, and produce negative indication of SRB presence (media will not turn black). The prepared media that was taken to the cooling tower site was exposed to atmospheric conditions and other impurities for a short time, adding to oxygen content, possibly contaminating the media.

In light of the above, once bacterial presence was positive (media will turn black), potentiometry studies commenced using the PGSTAT 302 machine, selected to give accurate measurements of corrosion rates, this is used widely in academic institutions.

3.1. Experimental Procedure

A detailed methodology is presented in this Chapter, it includes the materials used, a process overview of cooling tower plants where coupons were inserted and collected, preparation of media, growing of SRB, microstructural analysis and preparation of metals for electrochemical testing.

3.2. Experimental setup

3.2.1. Materials

Table 3.1 summarises the materials used during the experimental runs and includes the use of each piece of equipment. Figure 3.1 describes the experimental process used to recommend the best carbon steel suited for use in industrial heat exchangers.

Table 3.1: Materials used in experimental runs

Equipment	Use
Mettler Toledo AB204-S scale	To measure the weight of each component
Erlenmeyer beaker with magnetic stirrer	Contain media
Stnart halogen hotplate HT4	Mixing media
Autoclave machine HICALVE HV-50	To sterilize media and bottles
Gas generating kit (OXOID Code BR38):	Produces 1800 ml hydrogen and 350 ml carbon dioxide to produce anaerobic environment
Saphire 520 automatic grinder	To grind coupons
Olympus BX61	To evaluate microstructure of the metal before exposing to SRB media
INCA X-act with energy dispersive X-ray spectroscopy (EDS) by Oxford instruments	To determine elemental composition
Autolab potentiostat, PGSTAT 302	Potentiometry tests

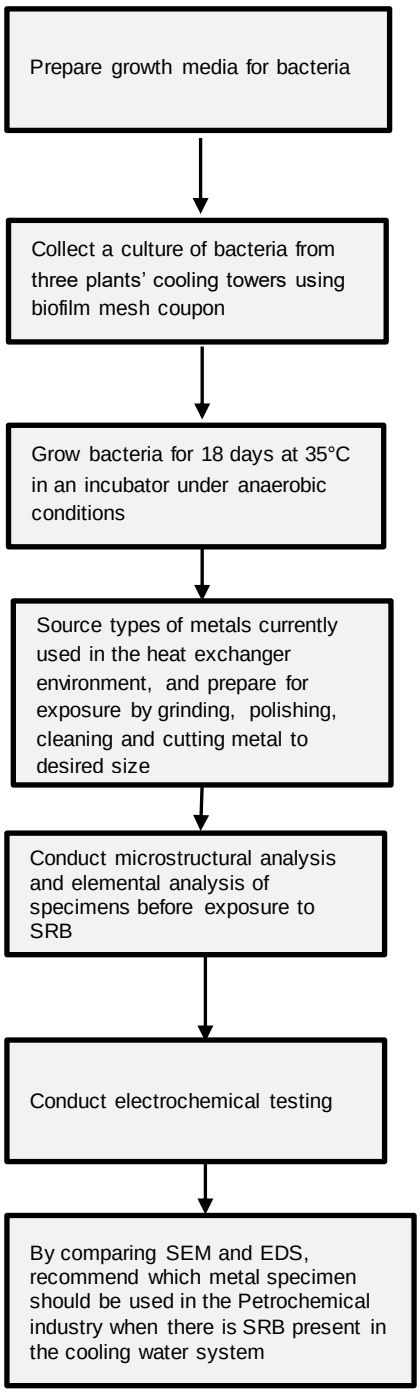

Figure 3.1: Experimental Process

3.3. Process overview of plants: A, B and C

Figure 3.2 represents a process flow diagram of the plants where SRB cultures were obtained. All plants have separate cooling towers and heat exchanger equipment. SRB cultures were obtained at plant B cooling tower, which dam X supplies. The cooling water from plant B, was sent to plant C, where cultures were obtained at this cooling tower. Cultures were lastly collected at plant A cooling tower, where plant X supplies make up water from time to time. In conclusion, Plant B supplies cooling water to a number of plants, which use water as a cooling medium in heat exchangers. Cooling water was chemically dosed differently at each plant, giving rise to further uncertainties in achieving positive indications of SRB presence.

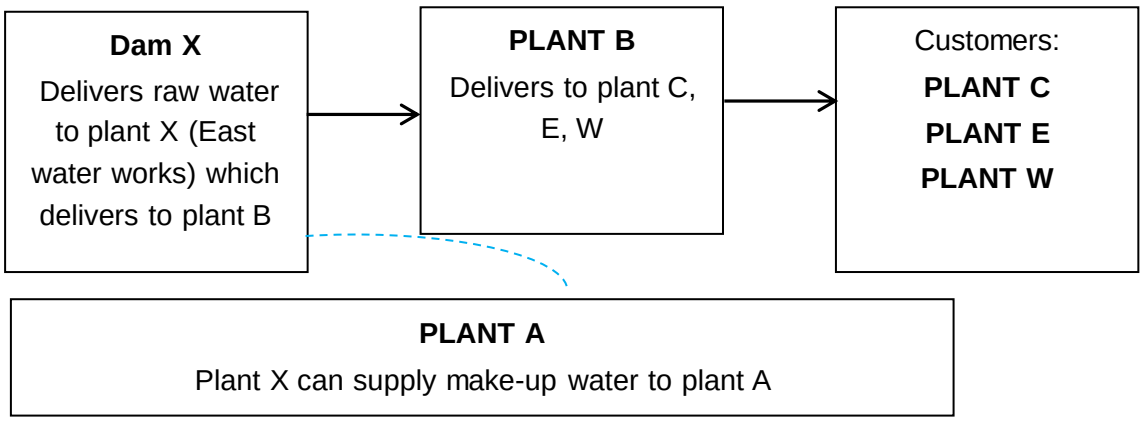

Figure 3.2: Process overview of where samples were obtained

3.4. Media preparation

A 0.178 mm × 12.7 mm × 76.2 mm biofilm mesh coupon was inserted for approximately three months in the selected cooling towers in three plants designated A, B and C. Mixed culture of SRB was collected as biofilms on the mesh coupons. After calibration, a Mettler Toledo AB204-S scale was used to weigh each constituent for culture media preparation.

Using recipes in literature as a basis (Table 2.3) with adjustment, per liter: 0.5 g KH_2PO_4; 1.0 g NH_4Cl; 4.5 g $NaSO_4$; 0.05 g $CaCl_2.2H_2O$; 0.06 g $MgSO_4.7H_2O$; 6 g $C_3H_5NaO_3$ (sodium lactate); 1.0 g yeast extract; 0.004 g $FeSO_4.7H_2O$; 5.0 g $Na_3C_6H_5O_7$ (sodium citrate) in distilled water mixed in a 2000 ml Erlenmeyer beaker with a magnetic stirrer on top of a Stnart halogen hotplate HT4 with no heat. To measure pH, a Multi 3401 pH meter was used with two controls, WTW pH 4.01 Technical buffer 50 ml and WTW pH 7.00 technical buffer 50 ml, pH of the media was found to be 6.47 and then adjusted to 7 by addition of NaOH at

12 ^{0}C. Bottles used had plastic seal rings. A total of 5 bottles were prepared then autoclaved in an HICALVE HV-50 at 121 ^{0}C for 15 min to sterilise the media and the bottles. Five bottles were used, three for holding the mesh coupons, one for a control and one for topping-up.

3.5. Collection of plant SRB coupons

Four bottles were taken to the cooling tower site (with contents specified in Section 3.4), three for holding the mesh coupons and one bottle for topping-up the bottles after inserting coupons. A tweezer was used to remove mesh coupons. The tweezer was immersed in ethanol and ignited with a flame to sterilize the tool. The coupon slot had to be opened manually. The coupons were removed with a tweezer from the slot in the line. The coupons were then immediately inserted into the prepared media. After the coupons were inserted into the media, another bottle with the same sterilized media was used to top-up the three bottles, preventing as little oxygen in the bottles as possible. The three 250 ml bottles with a seal were closed air tight and placed into a cooler box and taken to the incubator.

3.6. SRB incubation and growth

The mesh coupons taken from plants A, B and C cooling water towers were incubated in the prepared media to allow any bacteria that may be present on the coupon to grow. The coupon was considered to have collected a mixed culture of SRB. A separate bottle containing media without a coupon designated plant D, as a control, was also incubated. The methods as described by Kuang *et al*. (2007:6085), which conforms with ASTM standard D 4412-84) was used in timing the growth of SRB, where one to four days was taken to be the 1st stage called the exponential phase. During this stage the number of active SRB increases quickly and the SRB population achieves the maximum value at the 4th day. After the 4th day the growing process of SRB reaches the 2nd stage namely the death phase. The number of active SRB decreases quickly during this stage. After the 14th day, the growing process of SRB reaches the 3rd stage: residual phase. During this stage, the number of SRB returns to the original number and the active SRB almost disappeared. Detection of the number of active SRB was not covered in the study that follows.

Traditional SRB media contain sodium lactate as the carbon source (RP-38 1965; Postgate 1979). When SRB are present in the sample, sulphate is reduced to sulphide, which reacts with iron (either in the solution or solid) to produce black ferrous sulphide (Little *et al.* 2006:1006). These bottles with the control bottle were kept in a pressure container with a gas release kit to prevent any explosions while under incubation. The gas release kit is an

OXOID type with Code BR38 for anaerobic systems. The Oxoid gas generating kit is a reliable and convenient method for producing anaerobic conditions in standard jars containing active catalysts. Each sachet contains tablets of sodium borohydride, tartaric acid and sodium bicarbonate. When used as directed, they will produce approximately 1800 ml hydrogen and 350 ml carbon dioxide. The volume of hydrogen produced is adequate to ensure virtually complete anaerobiosis in the presence of an active catalyst in jars of up to 3.5 liters capacity, whilst the carbon dioxide evolved will give a final concentration of 7-10% depending on the jar used. The sachet was cut, 10 ml water was added to the sachet, and placed in an upright position in the pressure container with the lid closed. The gas release kits were inserted in a WTW TS 606/2-I incubator. The incubator was set at 35 ^{0}C, which was the cooling water temperature measured in the heat exchanger environment.

3.7. Alloys investigated

These alloys were obtained as tubes and sheets. The tubes were cut to 40 mm from 1 m pipes, and then sectioned into 4 quarters, giving approximately 40 mm × 15 mm rectangular specimens. Six specimens of the same size and surface finish were prepared from each material. The specimens were labelled A1-A6 for specimens machined from the alloy ASTM A516-70, as in Table 4.3, B1-B6 for specimens machined from alloy ASTM A179 the second in the table, and in that order. The cut specimens were surface finished to 800-grit. The 40 mm x 15 mm specimens were then cut to 10 mm × 10 mm using a hacksaw to suite electrochemical setup (Figure 3.3), Appendix B.1 shows the size of the metal used in the experiment. The specimens were then cleaned with acetone and ethanol (sterilisation). The surface roughness has been reported to affect the attachment of bacterial cells (Javed *et al*. 2015:48) but according to industrial conditions, it was chosen to grind specimens to 400 grit finish. Elemental analysis conducted for all metallic specimens were carried out at Vaal Metallurgiese Laboratoriums (PTY) Ltd, conforming to ASTM standard E415.

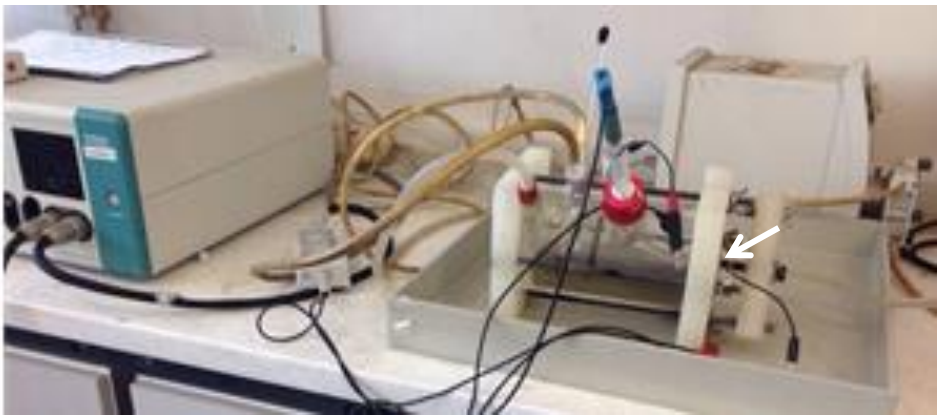

Figure 3.3: The Figure shows the three electrode cell setup and the white arrow indicates where the working electrode was inserted

3.8. Microstructural analysis

All microstructures and elemental composition of all the specimens used in this study were obtained, conforming to ASTM 407, ASTM E3 and ASTM E415 standards. For microstructural analysis, the 40 mm × 15 mm pipe specimens were sectioned longitudinally and cut with a band saw to 5 mm, plates were also cut with a saw to 5 mm × 2 mm. The specimens were mounted with a MultiFast Phenolic hot mount resin using a Struers CitoPress-15, set at 180 °C. The mounted specimens were polished with a polish disk from 220-grit to 1200-grit and cleaned with acetone. In order to reveal the microstructures of the specimens, different etchants were used for the different types of alloys. Etching is a form of controlled chemical attack, thus different metals and alloys are attacked differently by different chemicals. The three carbon steels ASTM A516-70, ASTM A179 and ASTM A106-B, were etched by immersing specimens in nital (2 ml HNO_3 and 98 ml ethyl alcohol) for 15 s, then cleaned with water and acetone. Electrolytic etching, was done for duplex stainless steel (2205) and copper alloys using, 56 g potassium hydroxide, 100 ml H_2O (added slowly) for 60 s and 1 to 3 V (this is a highly caustic solution). Specimens were electro-contacted for 40 seconds using a Buehler Polinat 2 electro-chemical etching machine. The microstructures were obtained using Olympus BX61 optical microscope. Elemental composition of the biofilm was determined using INCA X-act with energy dispersive X-ray spectroscopy (EDS) by Oxford instruments. Etched specimens were not used for electrochemical tests, but separate specimens were used.

3.9. Electrochemical Tests

Some of the 10 mm x 10 mm specimens cut from the tube and plate, were prepared for the electrochemical tests by polishing an area to be exposed using 400 grit silicon carbide emery paper, the chosen grit finish is used in industrial heat exchangers. The specimens were cleaned in acetone for 3 min to degrease, and sterilised in ethanol for 5 min before air-drying. The aqueous media from plant B, which showed highest indication of SRB growth (discussed in Section 4.2), was used for all the corrosion investigations. The specimens were then exposed to the media in the three electrode cell setup for the potentiometry studies. The tests were done in duplicates and control tests for each alloy were also done in distilled water. The pH value of the media before exposure to the alloys was recorded as 8.2 and the media temperature was kept at 35 °C during the tests using a thermostat-controlled bath. The corrosion performance of the different specimens was evaluated by electrochemical polarisation measurements using Autolab potentiostat, PGSTAT 302. The setup utilises graphite as the counter electrode and saturated silver-silver chloride electrode as the reference electrode in a three electrode cell setup. The working electrode (10 × 10 mm metal specimens) was held in place using a circular rubber piece with an internal exposure surface area of 0.50265472 cm^2. This was the exposed working electrode surface area; the rubber piece acts to create a constant surface area and is not reactive with the SRB media. A long screw secures the rubber piece and the working electrode in place. All appliances used in this experiment were sterilised in a MERK GEMMY HL-341 autoclave for 15 min at 121 °C. Nitrogen was purged continuously throughout the experiment to create an anaerobic environment. All inputs of the cell were sealed using thread tape and foil tape. The electrochemical setup consists of a computer connected to the potentiostat, water pump, water bath, nitrogen supply and the three cell electrode. Potentiodynamic polarisation was carried out for each alloy at a scanning rate of 0.01 V/s, from -2 V to 2 V and at a step voltage of 0.001.

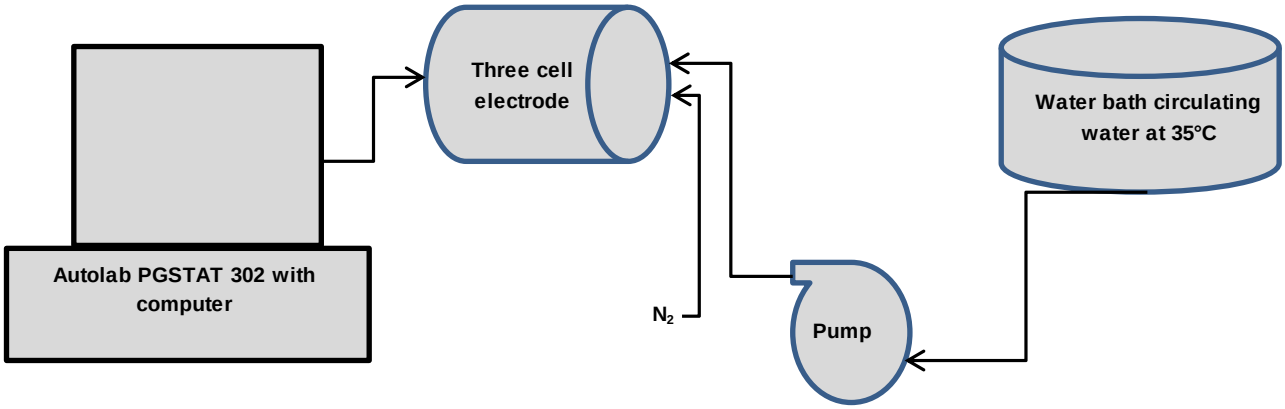

Figure 3.4: Electrochemical setup

Chapter 4

4. Results and discussion

4.1. Introduction

In this chapter the metal elemental composition before exposure to SRB media and cooling water composition are compared with EDS results after exposure of metals exposed to SRB media, results for growing and incubating the SRB media at 35 °C are presented, and potentiodynamic curves, corrosion rates, SEM and EDS analysis, are showcased. Each section is concluded.

4.2. SRB incubation and growth

The presence of SRB was detected based on visual observation after an incubation period of 18 days. Culture media are typically incubated over several days, and 30 days may be required for SRB growth (Little *et al*. 2006:1006) but in this instance, the results after 18 days were glaring. In this study, no genetic sequencing was conducted to identify the type of SRB. This will be undertaken as future work for this research. After 3 to 4 days of incubation upon visual inspection, the aqueous media became murky mostly and a slight black colour could be seen at the bottom of the bottles containing coupons taken from plants A and B. After 18 days of incubation, media B was completely black, as can be seen in Figure 4.1. Media A (in bottle A) showed slight blackening as compared to media B, while media C (having the coupon from plant C) and media D (in control bottle D) both showed no positive identification for SRB. According to Abdullah *et al*. (2014:2), when the media turned to black after an incubation period of 3 to 4 days at 37 °C, the black precipitate is indicative of iron sulphide (FeS) produced from the reduction of sulphate ions (SO_4^{2-}) to sulphide (S_2). This is also accompanied by a strong smell of rotten- eggs, indicating the production of H_2S as a result of sulphide-reducing activity of SRB (Abdullah *et al*. 2014:2).

When Media B bottle was opened, a strong smell of rotten-eggs was detected and gave an indication that there was production of H_2S gas, further confirming that SRB was grown in the media. Media B, with clear indication of presence of SRB, was therefore chosen as the media for potentiodynamic tests.

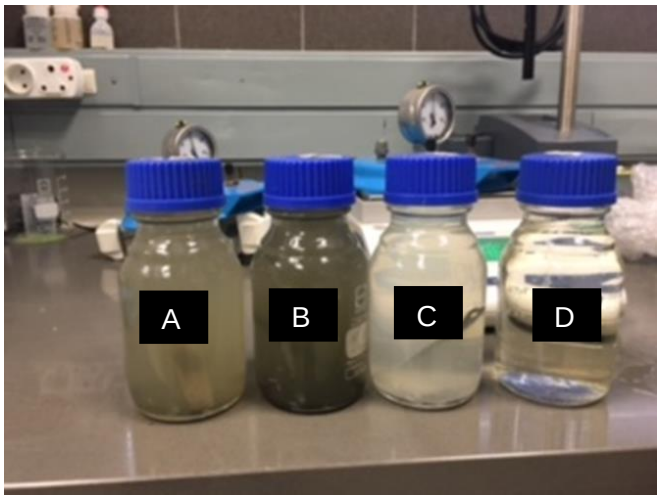

Figure 4.1: 250 ml bottles after 18 days of incubation

After fully anaerobic incubation for 18 days, positive indications of presence of SRB were obtained from mixed cultures, collected from industrial cooling water plants, which supply heat exchanger tubes. Positive indications are seen in bottle A and B as black precipitates. The media composition used in this study proves to be the recommended media for this type of environment.

4.3. Comparative corrosion rates for the different alloys

The e-log i plots in Figures 4.2 to 4.7, show the responses of carbon steel ASTM A516-70, ASTM A179, ASTM A106-B, duplex stainless steel (2205), and copper alloys B111 grade C70600 (90-10) and B111 grade C71500 (70-30) during the potentiodynamic investigation under the media with and without bacterial load. More general data from tests are also shown in Table 4.1 and Table 4.2. A general observation is that an increase in corrosion rate is seen when specimens were exposed to SRB media. Comparing the carbon steel alloys, a corrosion rate of 1.23 mm/year was computed for ASTM A179, and 1.08 mm/year for ASTM A516-70 carbon steels when exposed to SRB loaded media. Generally the plots show the potentials shifted to the right when steels were exposed to SRB media compared to when it was in the control media. This graphically indicated that the presence of SRB indeed increased the corrosion rate. It can be seen that the corrosion current densities (I_{corr}) in the presence of the SRB media are greater than that in control media, indicating the occurrence of MIC (Liu *et al.* 2015:485). Refer to Appendix B.2 for reference to data obtained by Liu *et al*. (2015:485).

Table 4.1: Potentiodynamic tests data for different alloys in medium without SRB (control medium)

Alloys	βa (V/dec)	βc (V/dec)	I_{corr} (A/cm^2)	E_{corr} (V)	Corrosion Rate (mm/year)
ASTM A516-70 Carbon Steel	0.441	0.436	8.08E-05	0.041	0.953
ASTM A179 Carbon Steel	0.215	0.273	8.58E-05	-0.014	1.005
2205 Duplex stainless steel	0.266	2.588	7.91E-06	0.423	0.080
ASTM A106-B Carbon Steel	0.541	0.282	3.11E-05	0.168	0.364
ASTM B111 grade C70600 (90 - 10) Copper nickel	0.325	0.344	3.98E-6	0.244	0.046
ASTM B111 grade C71500 (70 - 30) Copper nickel	0.200	0.797	6.74E-5	0.165	0.777

Table 4.2: Potentiodynamic tests data for different alloys in medium with SRB

Alloys	βa (V/dec)	βc (V/dec)	I_{corr} (A/cm^2)	E_{corr} (V)	Corrosion Rate (mm/year)	% Increase in corrosion rate
ASTM A516-70 Carbon Steel	0.201	0.274	9.16E-05	-0.293	1.081	13.43%
ASTM A179 Carbon Steel	0.254	0.250	1.05E-04	-0.230	1.230	22.39%
2205 Duplex stainless steel	0.812	0.923	8.88E-05	0.102	0.908	1035%
ASTM A106-B Carbon Steel	0.300	0.486	4.51E-05	-0.192	0.529	45.33%
ASTM B111 grade C70600 (90 - 10) Copper nickel	0.703	0.403	8.60E-5	0.332	0.979	2028%
ASTM B111 grade C71500 (70 - 30) Copper nickel	0.529	0.357	2.15E-4	0.082	2.511	223%

In Figure 4.2 for ASTM A516-70, passive film formation was seen in the cathodic polarisation region. This peak was not seen on the control curve. By visual observation the control curve had an I_{corr} 8 × 10 $^{-5}$ A/cm^2 of and E_{corr} of 0.1 V. Under SRB media, I_{corr} (corrosion current density) was visually observed in the cathodic region at approximately 2 × 10 $^{-4}$ A/cm^2 with E_{corr} of -0.3 V, the reaction taking place in the absence of oxygen yields the equation $2H^+ + 2e^- \leftrightarrow H_2$. The data in the table computed 9.16 × 10 $^{-5}$ A/cm^2 with E_{corr} of -0.293 V and is an acceptable range. The corrosion was under cathodic control within this short potential range. With slight further polarisation, the situation was altered and cathodic activity continued. Indication of I_{crit} (critical current density) in the active passive phase indicates the onset of passivation, this is when there is a loss of electrochemical activity, or drastic decrease in corrosion rate is observed, and where a protective film began to form (indicated by the arrows). The anode branch transitioned from the active phase to the active passive phase, and the “nose” can be seen as the critical current density. In this case I_{crit} under SRB media was visually observed from the graph as 5 × 10 $^{-4}$ A/cm^2 with E_{pp} (primary passivation potential) of -0.8 V. At this point a film began to form as the corrosion current density

suddenly decreased, leading to localised corrosion. As the anodic branch moves out of the active passive phase, it reached the passive phase at a positive potential of approximately E_{trans} (transpassive potential) 0.5 V, at this point I_{pass} (passive current density) is visually observed from the plot as 9 × 10 $^{-3}$ A/cm^2, maintaining a steady current density, then breaking down the protective film, this is when iron (Fe) is dissociated to form Fe^{2+} ions and can be represented by the half reaction equation $Fe^{2+} + 2e^{-} \rightarrow Fe$. The anodic branch then reached a transpassive phase, where a steady state was reached at a potential of approximately 2 V, where current density increased, and the localised corrosion attack increased. The passive film originated due to bacterial activity producing sulphide ions (S^{2-}). Sulphide precipitation with Fe^{2+} ion will form iron sulphide films. This can be confirmed by the high sulphur concentration found in the EDS results in Table 4.5. This film protected the metal at first, decreasing the $E_{corr,}$ then broke down leading to localised corrosion. Visually, the control plot displays no critical points, and the anode branch reaches steady state at a potential of approximately 1.58 V. Localised corrosion could be seen in SEM images (Figure 4.8c).

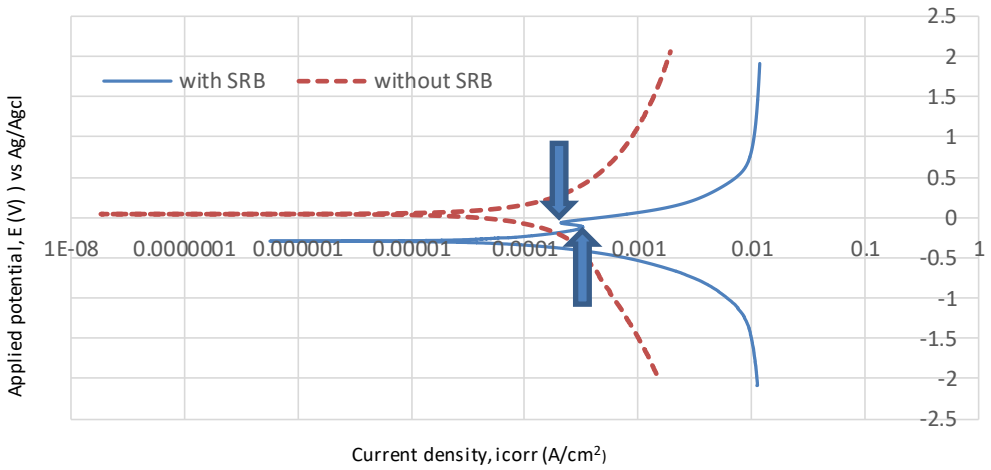

Figure 4.2: E-log I plot from ASTM A516-70 under potentiodynamic scan at 0.01 V/sec in aqueous media with and without SRB load, anaerobic conditions and temperature kept at 35 °C

In Figure 4.3, ASTM A179 visually showed no passivation peaks under SRB and control media. The control plot showed I_{corr} in the anodic region as seen in Table 4.2, at approximately 8.60 × 10 $^{-4}$ A/cm^2 and E_{corr} of 0.1 V. The curve under SRB media, shifted to the right of the control plot, where i_{corr} was visually observed at approximately 1 × 10 $^{-4}$ A/cm^2 with E_{corr} of -0.2 V in the cathodic region, Table 4.2 computed similar potential. Current density was maintained from approximately 0.48 V. The anodic branch of the control and

SRB media curve both continued to steady state of 2 V. Intergranular corrosion could be seen from SEM images (Figure 4.9c).

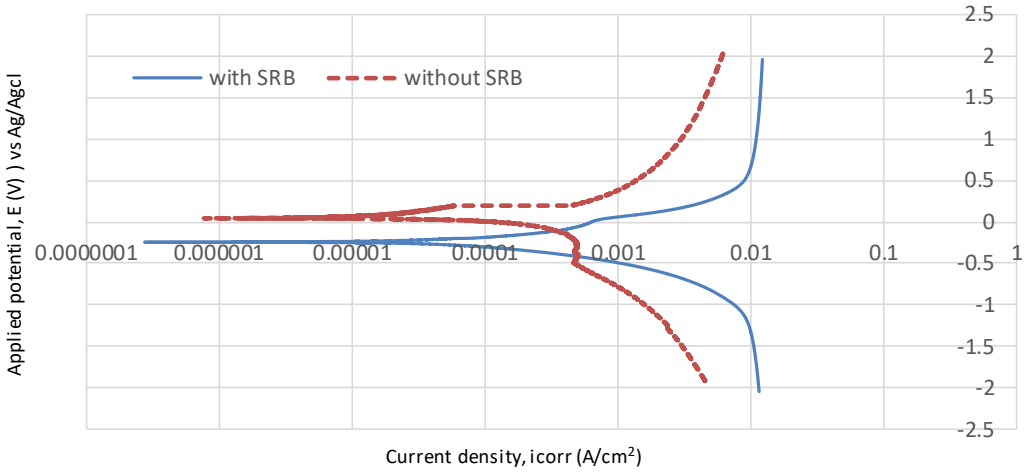

Figure 4.3: E-log I plot from ASTM A179 under potentiodynamic scan at 0.01 V/sec in aqueous media with and without SRB load, anaerobic conditions and temperature kept at 35 °C

In Figure 4.4, duplex stainless steel showed dynamic passivation and breakdown over a wide range of anodic polarisation under the control media. In the control plot I_{corr} was visually observed at approximately 8 × 10 $^{-6}$ A/cm^2 with E_{corr} of 0.3 V, similar data was obtained in Table 4.2. The anodic branch reached the active passive region with I_{crit} approximately 3.5 × 10 $^{-5}$ A/cm^2 and E_{pp} at 0.55 V where film formation began (indicated by the arrow), the branch transitioned to the passive region with I_{pass} at approximately 4.5 × 10 $^{-4}$ A/cm^2 and E_{trans} at 1.8 V. At approximately 1.8 V the current density was stable for a short time, then suddenly reaching a breakdown point at 2.3 V. Then showed some stable behavior at 2 V where current density increased. The nature of the curve shows corrosion resistance, this could be due to more than 12%-Cr element alloyed into the metal (Table 4.3). A Cr-rich passive film was formed (EDS results in Table 4.5 shows high concentrations of the Cr element). The oxidation half reaction taking place is represented by the equation $Cr^{3+} + e^{-} \rightarrow Cr^{2+}$.

Under bacteria media, passivation is absent and anodic currents were much higher, about two orders of microamperes. It showed that the bacteria had a remarkable impact on the corrosion resistance of the stainless steel, accelerating it by a factor of about 100. Although, this is still below the current density values obtained with the carbon steels. From the plot anodic polarisation could be visually observed with an I_{corr} of 9 × 10 $^{-5}$ A/cm^2 and E_{corr} of 0.2 V.

At 0.5 V the current density was steadily maintained, then at about 1.8 V current density started to increase. The SEM images in Figure 4.10c show no indication of pitting or localised corrosion, however general corrosion could be noted, this type of uniform corrosion increased the corrosion rate from 0.08 mm/year to 0.908 mm/year.

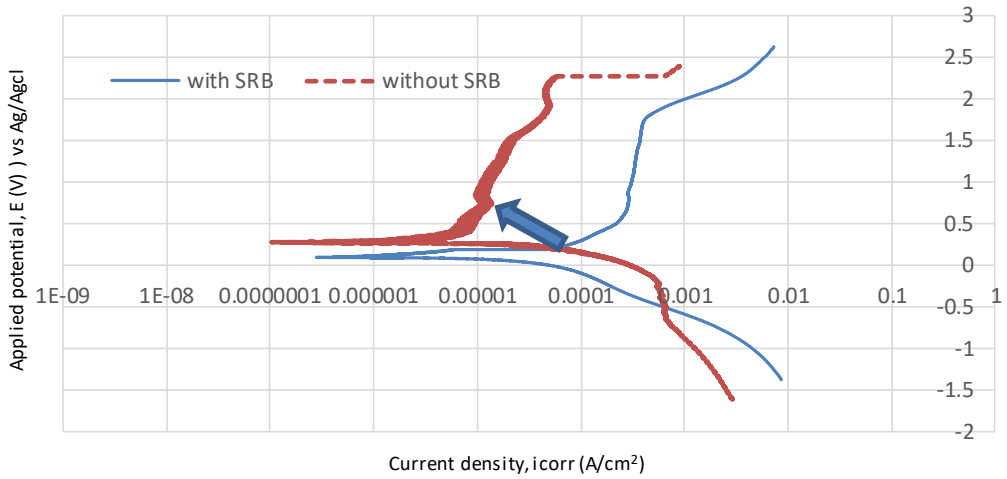

Figure 4.4: E-log I plot from 2205 duplex stainless steel under potentiodynamic scan at 0.01 V/sec in aqueous media with and without SRB load, anaerobic conditions and temperature kept at 35 °C

In Figure 4.5, alloy ASTM A106-B showed passivation under anodic polarisation, indicating local accelerated corrosion, but the I_{pass} through the film at the most developed state at approximately 9×10^{-3} A/cm^2 and E_{trans} of 1 V, was still well above the I_{corr} at 4.5×10^{-5} A/cm^2 at E_{corr} of 0.2 V under the control media. This showed the film was not very protective under the prevailing condition, and with little further anodic polarisation, the pitting potential/critical breakdown point was reached. Under SRB media, the anodic branch showed I_{corr} as 5×10^{-5} A/cm^2 at approximately E_{corr} -0.15 V. Then reaching the active passive region and critical breakdown point with I_{crit} of 5×10^{-4} A/cm^2 and E_{pp} of 0.3 V (indicated by the arrow). From 1 V current density was steady until a breakdown of the film could be seen after this point. The easy breakdown of the film is possibly an indication of sufficient anions such as S^{2-} from the bacteria metabolites in the media, which destabilise the passivation film. This caused localised breakdown of the film, exposing the underlying metal for corrosion current to continue flowing. This response led to pitting, as confirmed in Figure 4.11c.

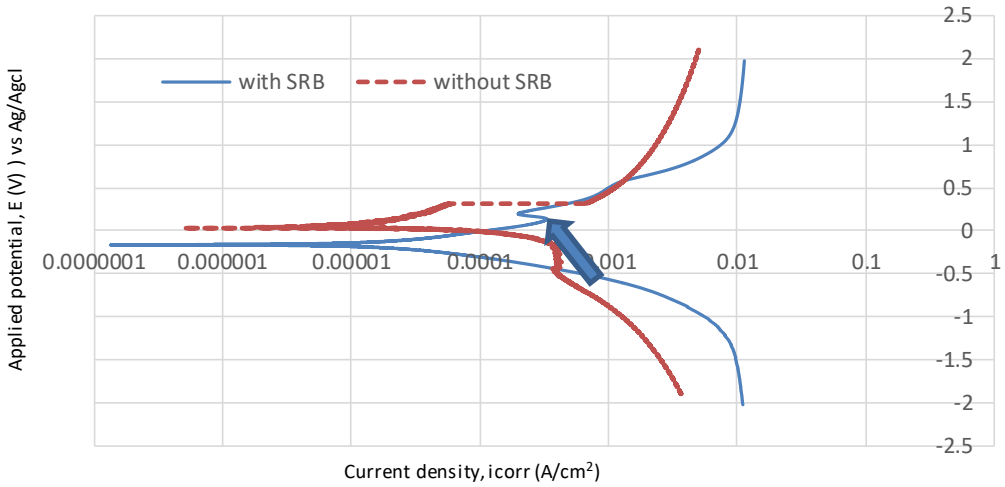

Figure 4.5: E-log I plot from ASTM A106-B under potentiodynamic scan at 0.01 V/sec in aqueous media with and without SRB load, anaerobic conditions and temperature kept at 35 °C

In Figure 4.6, alloy B111 grade C70600 (90-10) showed no passivation under control and SRB media. The anodic branch becomes steady at approximately 1 V. Under control media I_{corr} was observed as 9 × 10 $^{-6}$ A/cm^2 and E_{corr} 0.6 V. Under SRB media, I_{corr} was observed at approximately 3 × 10 $^{-4}$ A/cm^2 at an E_{corr} of 0.2 V. The anodic branch under SRB media curve stabilised in current density from 1.3 V. The alloy doesn't show film breakdown or passivity under SRB media, but a thin film was seen in SEM images (Figure 4.12b). Revie (2011:153) explains that the passive film substantially lowers the rate of corrosion. The film protects the metal at first, then breaking it is broken down by anions in the media. The corrosion behaviour of this alloy showed low corrosion rates under SRB load, computed as 0.979 mm/year, similar to that of duplex stainless steel. The corrosion observed was denickelification, which is uniform, thinning the metal layer by layer, and depositing nickel on the surface (Figure 4.12c). Using the table of standard electrode potentials, the cathodic half reaction for nickel is represented by the equation $Ni^{2+} + 2e^- \rightarrow Ni$ and the anodic half reaction gives $Cu^{2+} + e^- \rightarrow Cu^+$.

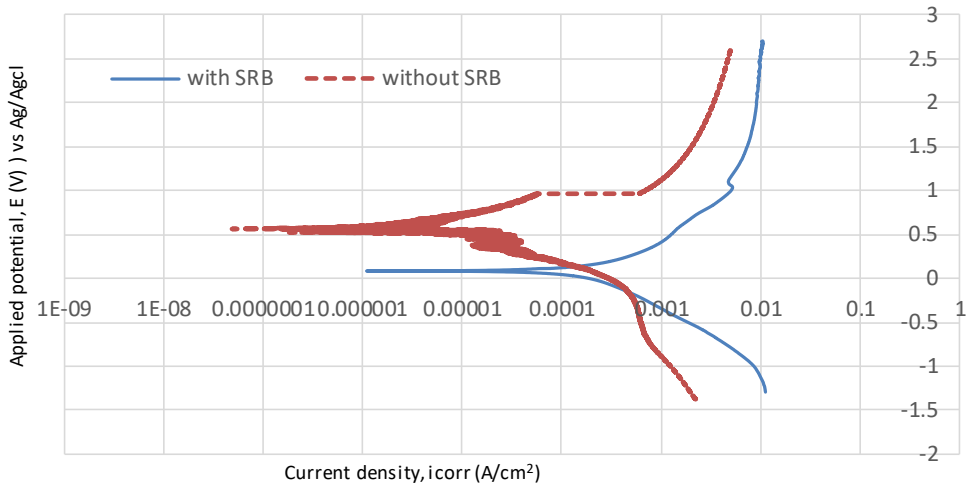

Figure 4.6: E-log I plot from B111 grade C70600 (90-10) under potentiodynamic scan at 0.01 V/sec in aqueous media with and without SRB load, anaerobic conditions and temperature kept at 35 °C

In Figure 4.7, no pitting potential/critical breakdown point could be seen on both curves under control and SRB media. In the control plot, I_{corr} was visually observed as 7 × 10 $^{-6}$ A/cm^2 at an E_{corr} of 0.3 V. From about 1 V the current density stabilised. From the plot under SRB media I_{corr} could be observed at approximately 2.5 × 10 $^{-4}$ A/cm^2 at an E_{corr} of 0.1 V. Current density stabilised from approximately 1 V, reaching potentials higher than 2.4 V, the half reaction taking place for copper is represented by the equation $Cu^{2+} + e^{-} \rightarrow Cu^{+}$. A drastic increase in corrosion rate from 0.78 mm/year to 2.5 mm/year was computed as seen in Table 4.1 and 4.2. Pitting was observed on the surface of the alloy as seen in Figure 4.13c.

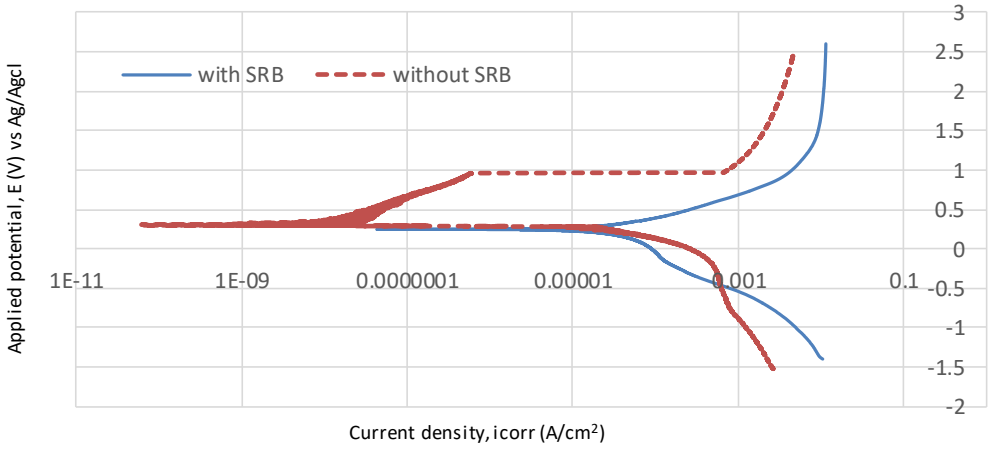

Figure 4.7: E-log I plot from B111 grade C71500 (70-30) under potentiodynamic scan at 0.01 V/sec in aqueous media with and without SRB load, anaerobic conditions and temperature kept at 35 °C

All three carbon steels ASTM 516-70, ASTM A179, ASTM A106-B, duplex stainless steel and copper alloys subjected to potentiodynamic tests in the presence of SRB loaded media showed increased corrosion rate; the potentials on the e-log i plots all shifted to the right, compared to the control media. The specific corrosion responses of the alloys differ. ASTM 516-70 shows a short potential range of cathodic passivation, but the film was very unstable, ASTM A106-B also shows anodic passivation, also with an unstable film easy broken by sulphide species in the medium. ASTM A179 did not passivate. The stainless steel also showed high corrosion rates relative to the control condition in media without SRB. Copper alloy B111 grade C70600 (90-10) showed film breakdown under control media, but B111 grade C71500 (70-30) showed film breakdown under control media and SRB load. In comparison to Table 4.1 and 4.2. I_{corr} values may differ slightly, because the Tafel plot extrapolation method was done using the PGSTAT software. The values obtained in the above discussions, are all observed visually from the plots.

4.4. Surface microstructures of alloys before and after exposure to SRB

Section 4.4 to 4.6 discusses SEM and EDS results obtained from analysing biofilm on the surfaces, and comparing them to the elemental composition of the metals. It should first be mentioned that the proximity of the SEM and metallurgical laboratories prevented the observation of wet biofilm. The biofilm was observed when dry. Also, degradation could not be effectively captured against microstructural grains, as specimens exposed to SRB load were not etched before exposure, separate specimens were used for etching and exposure tests. Acetone was used to faintly clean the biofilm from the metal surface, before polishing with 3 micron suspension. During removal of the mesh coupon from plant B, slight biofilm could be seen by visual inspection. Biofilm is the term used to describe micro-organisms encased in a matrix of extracellular polymeric substances (EPS). These biofilms have been shown to influence the corrosion of metallic materials, especially ferrous alloys. When SRB is present in the biofilm formed on these surfaces, they are usually associated with pitting corrosion attack (Hamilton 1985:195; Hardy & Brown 1984:650; Javed *et al*. 2015:51; Postgate 1984; Wade *et al*. 2011:75; Xu *et al*. 2006:829).

In Figures 4.8 to 4.13, give microstructures labelled (a) before exposure to SRB media, those labelled (b) show the microstructure of corresponding alloys after exposure to SRB media with biofilm on the surface, those labelled (c) show images after cleaning the surface with acetone followed by 3 micron polish, and (d) showing higher magnification images of the metals microstructure.

The micrograph labelled Figure 4.8a, showing pearlite in a ferrite matrix, Nital etched. After cleaning the biofilm (Figure 4.8b) from the surface of ASTM A516-70 with acetone, localised corrosion could be seen (Figure 4.8c), the type of localised corrosion was seen on a specific area of the metal, the grain boundaries were attacked in the specific area, and grains were dislodged as seen in a high magnification image in Figure 4.8d.

The microstructure in Figure 4.9a showed narrow grain boundaries and spheroidisation, according to Shin *et al* (2003:1360), this process is the transformation of cementites (iron carbide) from lamellar morphology to spherical shapes. Spheroidisation treatment of cementites in steels is used to increase their formability, etched with Nital. The image in Figure 4.9b showed biofilm thinly layered across the surface of the alloy, enhancing the shape of the grains. In Figure 4.9c steel alloy ASTM A179 was cleaned with acetone, and intergranular corrosion was revealed along the grain boundaries, leaving the bulk of the grains unaffected the attack was observed in Figure 4.9c. Intergranular attack along the grain boundaries was seen throughout the exposed area of the metal.

The microstructure in Figure 4.10a showed directional grains and electrolytic etched with KOH. A clear interface was seen in Figure 4.10b, where the corroded area was the darker zone, and the unexposed area was the lighter zone. On visual observation the thickness in the darker zone was shown to be significantly reduced. Leaving a wall-like interface slightly elevated from the exposed area. In Figure 4.10c, duplex stainless steel showed no signs of severe corrosion on the exposed surface, however the corrosion rate increased under SRB load, the type of corrosion that can be noted on the surface of the metal is general corrosion, identified by light brown stains on the surface of the metal (Figure 4.10c). Figure 4.10d gives a higher magnification image of the exposed area after cleaning with acetone, where no significant corrosion attack could be seen on the grains.

In Figure 4.11a, the microstructure of ASTM A106-B showed spheroidisation over the pearlite area, etched with Nital. Figure 4.11b showed that the biofilm covered the exposed area and filled the pit. After cleaning the biofilm with acetone, pitting was revealed on the surface. Pitting in Figure 4.11c and Figure 4.11d, is characterised as rounded at the edge, deepened in the center, with circular rings around the pit. Pit dimensions are about 100µm.

The Figure 14.12a shows the microstructure of B111 grade C70600 (90-10) electrolytic etched with $FeCl_2$. In Figure 14.12b the biolfilm was seen as a thick uneven layer on the surface of the metal, this could be a combination of sulphide and nickel. The elemental analysis is discussed in Section 4.6. After cleaning the surface of B111 grade C70600 (90-10) with acetone, there was indication of denickelification (Mansfeld & Little 1992:2291),

results differ compared to Javed *et al*. (2016:7), this further proves the uniqueness of the culture of bacteria used in this study. Denickelification is observed as uniform corrosion, where the attack is layer type, decreasing the metal thickness and leaving denickelified metal behind (Figure 14.12c and Figure 14.12d).

In Figure 4.13a depicts the microstructure of B111 grade C71500 (70-30), electrolytic etched with $FeCl_2$. In Figure 4.13b biofilm formed on the surface of the metal and resembled a bulge or thick layer, possibly indicating high sulphur content in that specific area. After cleaning the biofilm with acetone (Figure 4.13b), pitting was observed on the surface of the metal, the center pit had smaller pits clustered around (Figure 4.13c), however took rounded shapes at the edges. In a higher magnification image (Figure 4.13d), the pit took a rounded shape at the edge and cracks could be observed within the pit, at the center. The pits differ in size and range from 25 µm to 50 µm.

For carbons steels investigated, ASTM A516-70 can be considered better in this service environment, because of pitting on ASTM A106-B and pitting susceptibility observed on SA 179 only by visual inspection of the microstructure. B111 grade C70600 (90-10) showed corrosion rate of 0.979 mm/year, which can be recommended as an additional alloy for better performance, apart from the carbon steels investigated. Duplex stainless steel is most corrosion resistant under SRB load.

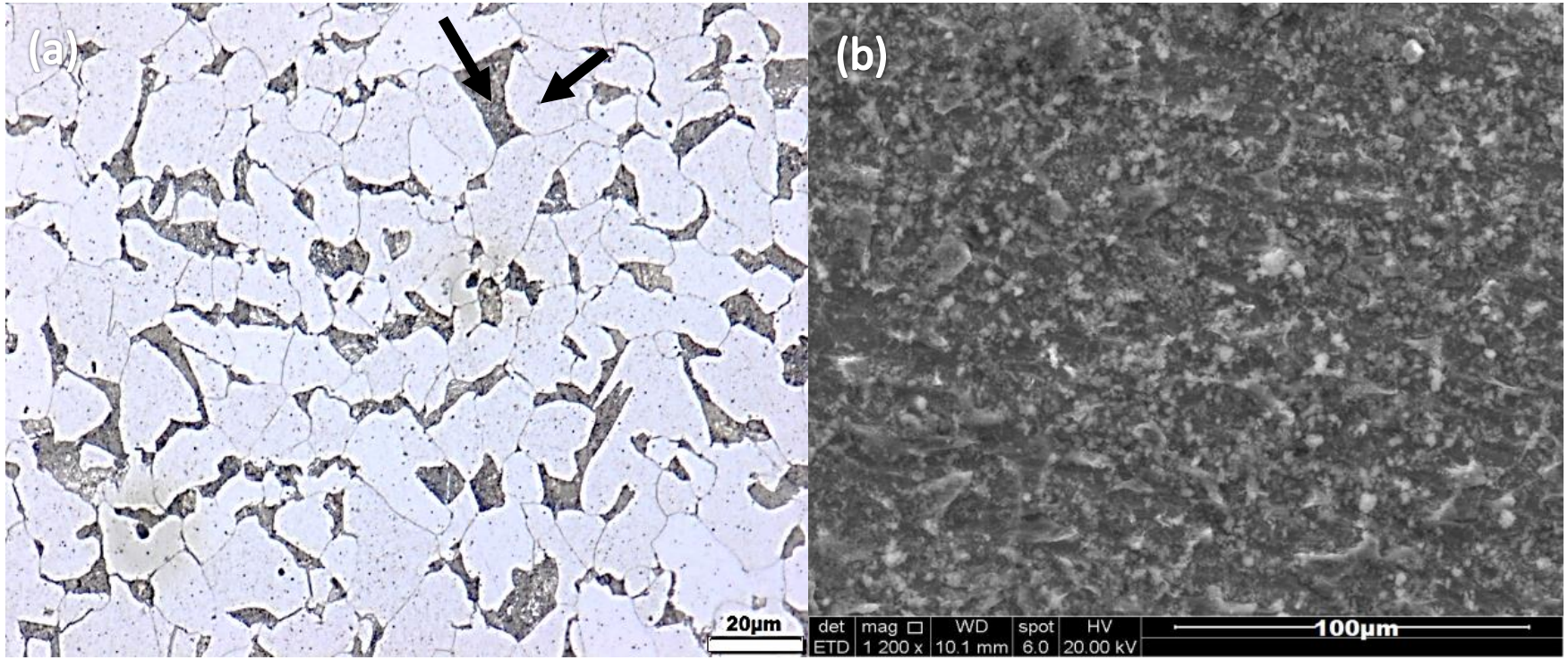
(a)
20µm
(b)
det mag WD spot HV
ETD 1 200 x 10.1 mm 6.0 20.00 kV
100µm

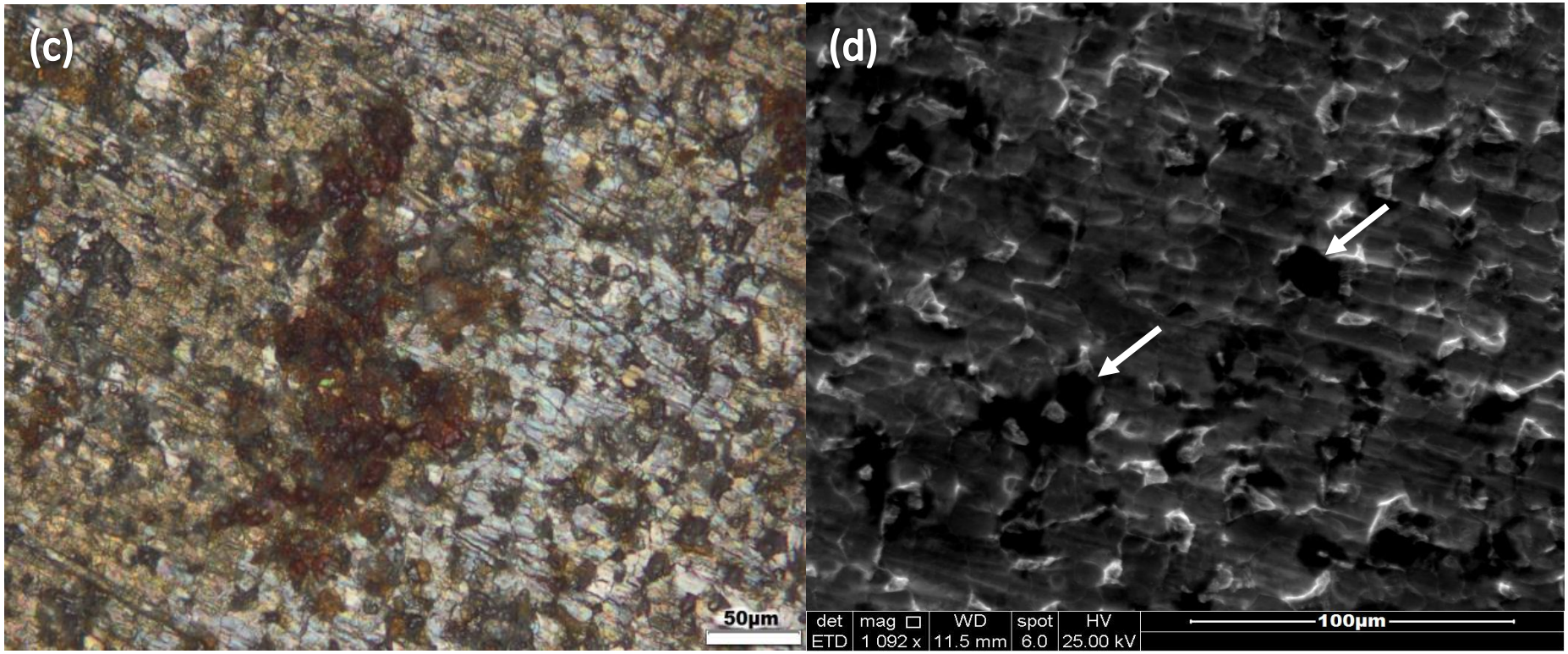

Figure 4.8: Microstructure of steel alloy ASTM A516-70 (a) before exposure to SRB media, with dark phase being pearlite and light phase being the ferrite (indicated by black arrows), Nital etched, (b) after exposure to SRB media with biofilm on the surface, (c) after cleaning the surface with acetone, showing localised corrosion (d) image showing localised attack along the grain boundaries, only seen on a selective area, and grains dislodged, arrows point to areas where grains were dislodged, leaving bulk of the other areas unaffected.

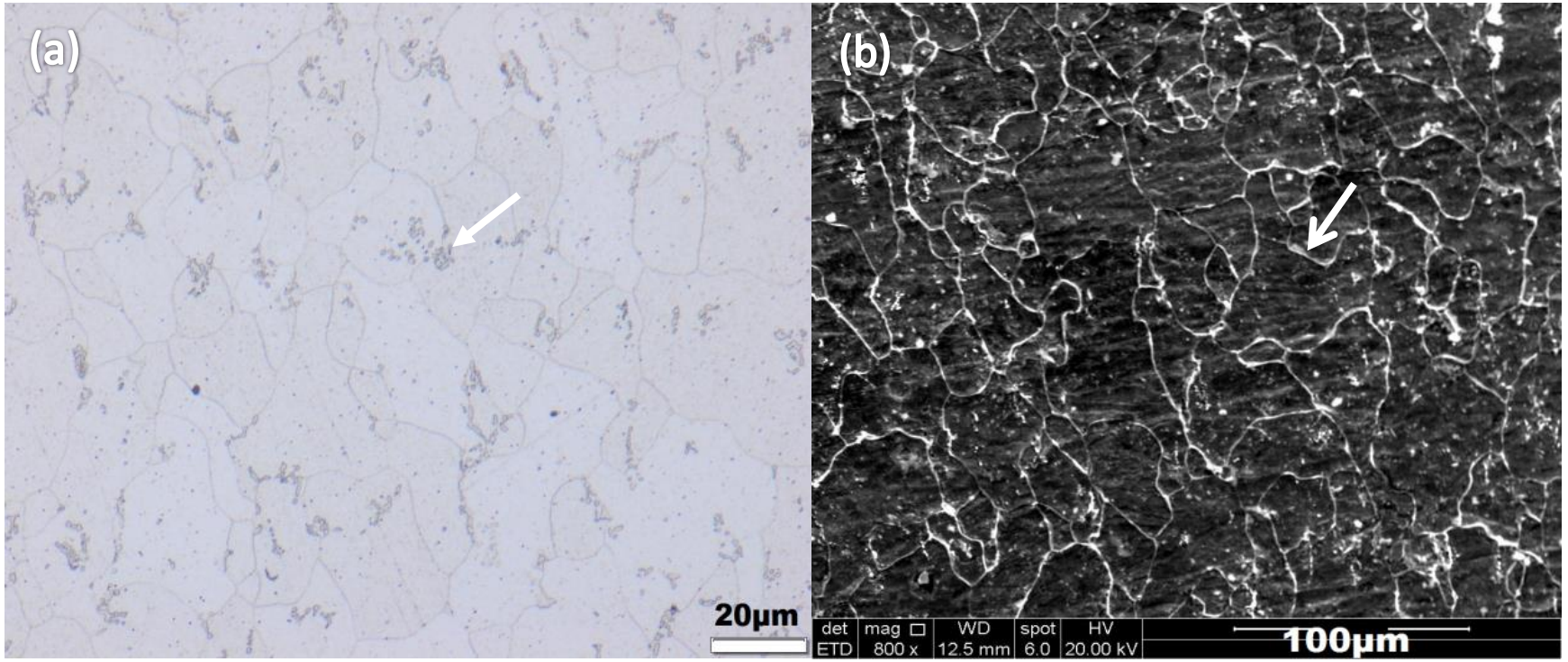
(a)
20µm
(b)
det mag WD spot HV
ETD 800 x 12.5 mm 6.0 20.00 kV
100µm

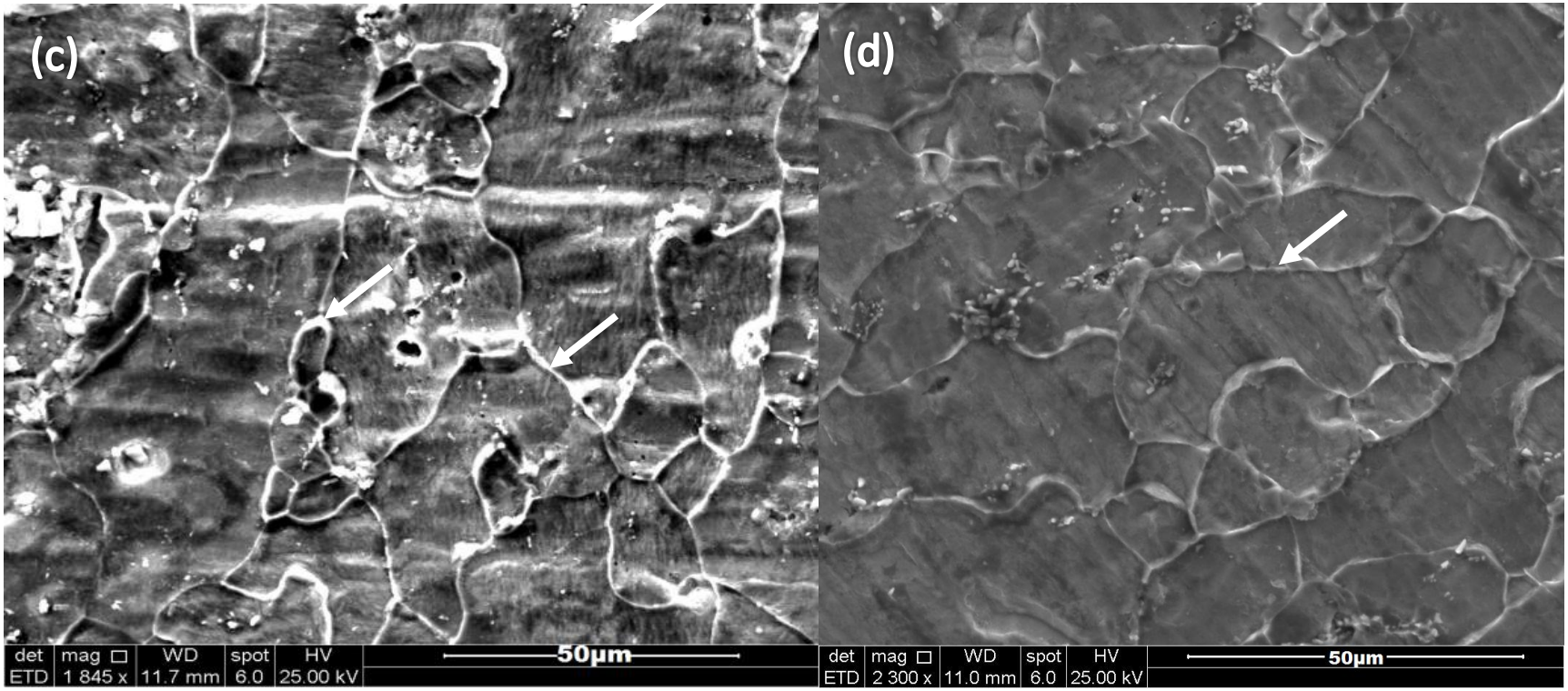

Figure 4.9: Microstructure of steel alloy ASTM A179, (a) before exposure to SRB media, showing spheroidisation (white arrow) Nital etched, (b) image after exposure to SRB media with biofilm on the surface, (c) after cleaning the surface with acetone showing intergranular corrosion, indicated by white arrows, and (d) high magnification image of intergranular corrosion.

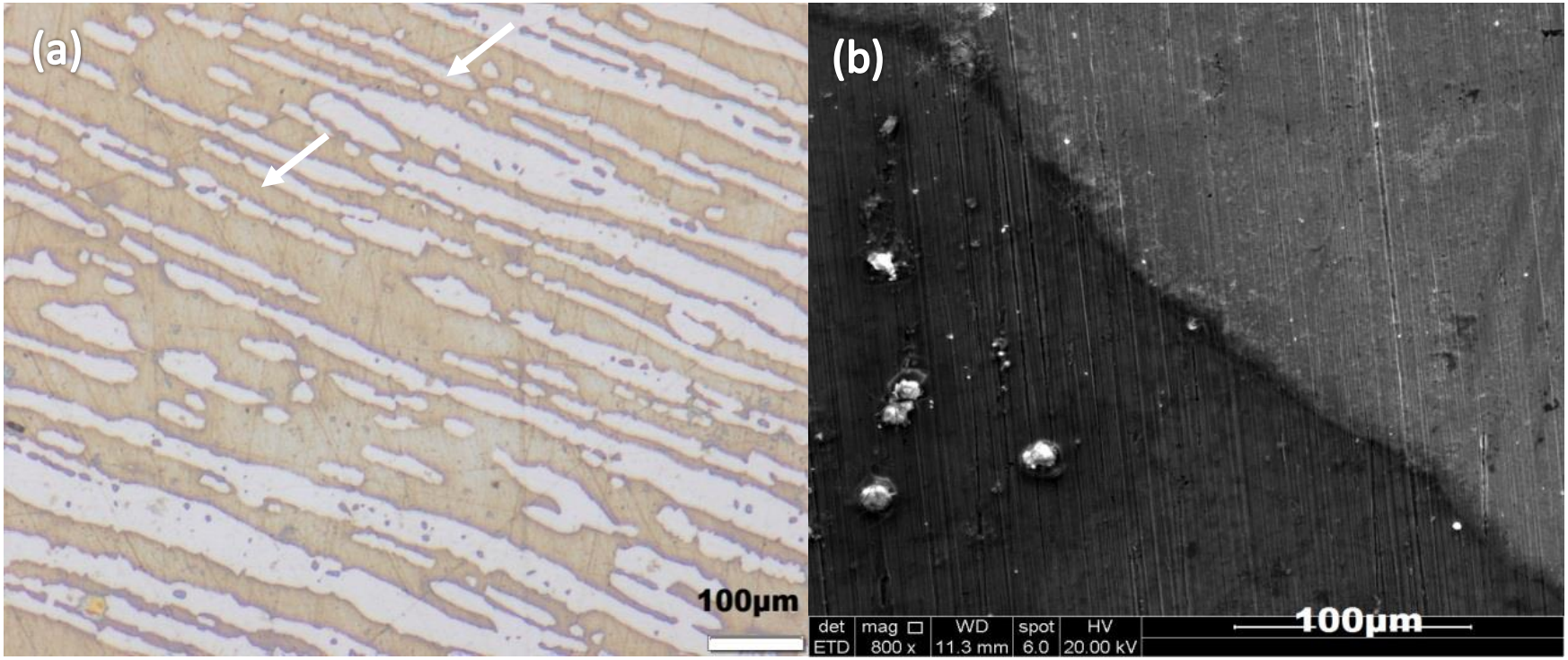
(a)
100µm
(b)
det ETD
mag 800 x
WD 11.3 mm
spot 6.0
HV 20.00 kV
100µm

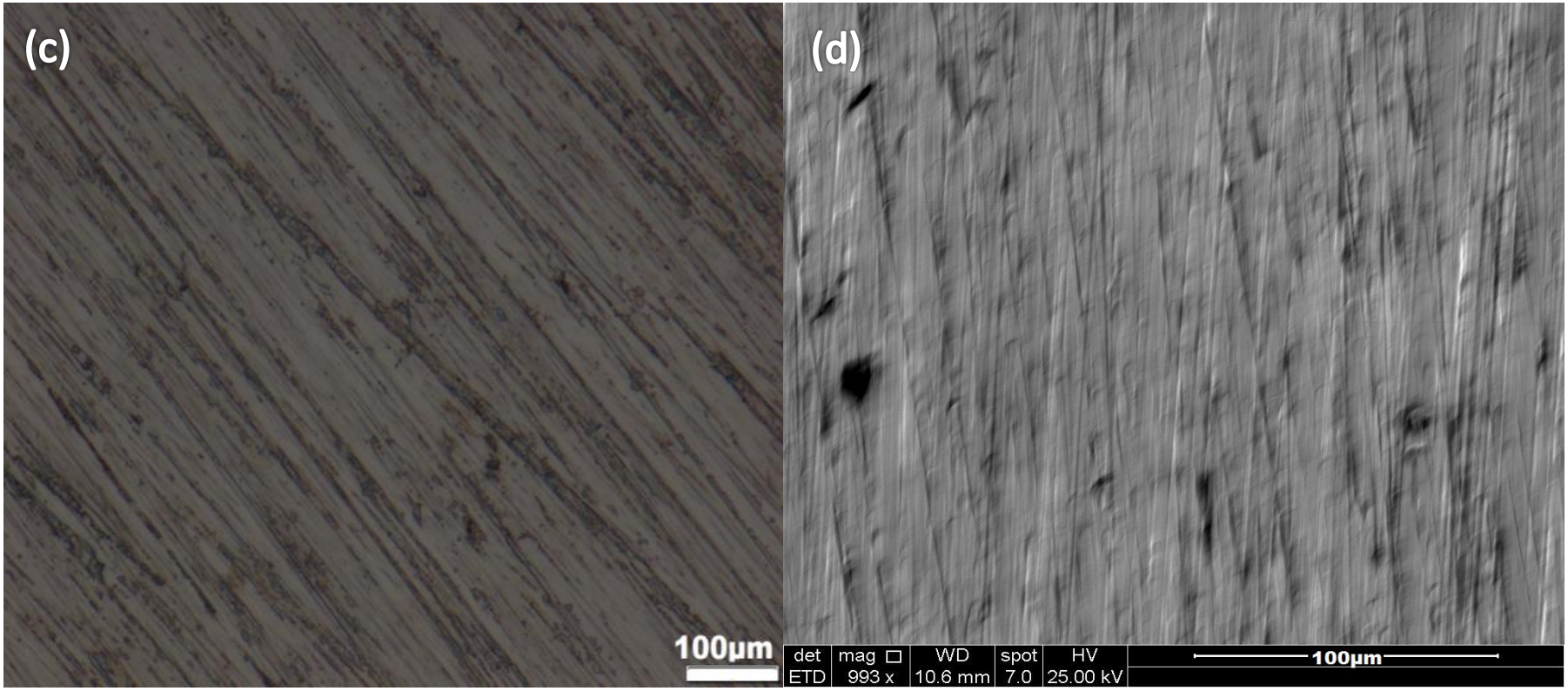

Figure 4.10: Microstructure of 2205 duplex stainless steel (a) before exposure to SRB media, with light phase being the ferrite and dark phase being austenite (indicated by white arrows), directional grains can be seen indicative of forming or rolling bodies, KOH electrolytic etched. (b) after exposure to SRB media with biofilm on the surface (darker zone), (c) after cleaning the surface with acetone, showing general corrosion identified by brown stains on the surface of the metal, and (d) high magnification image showing surface is not severely corroded.

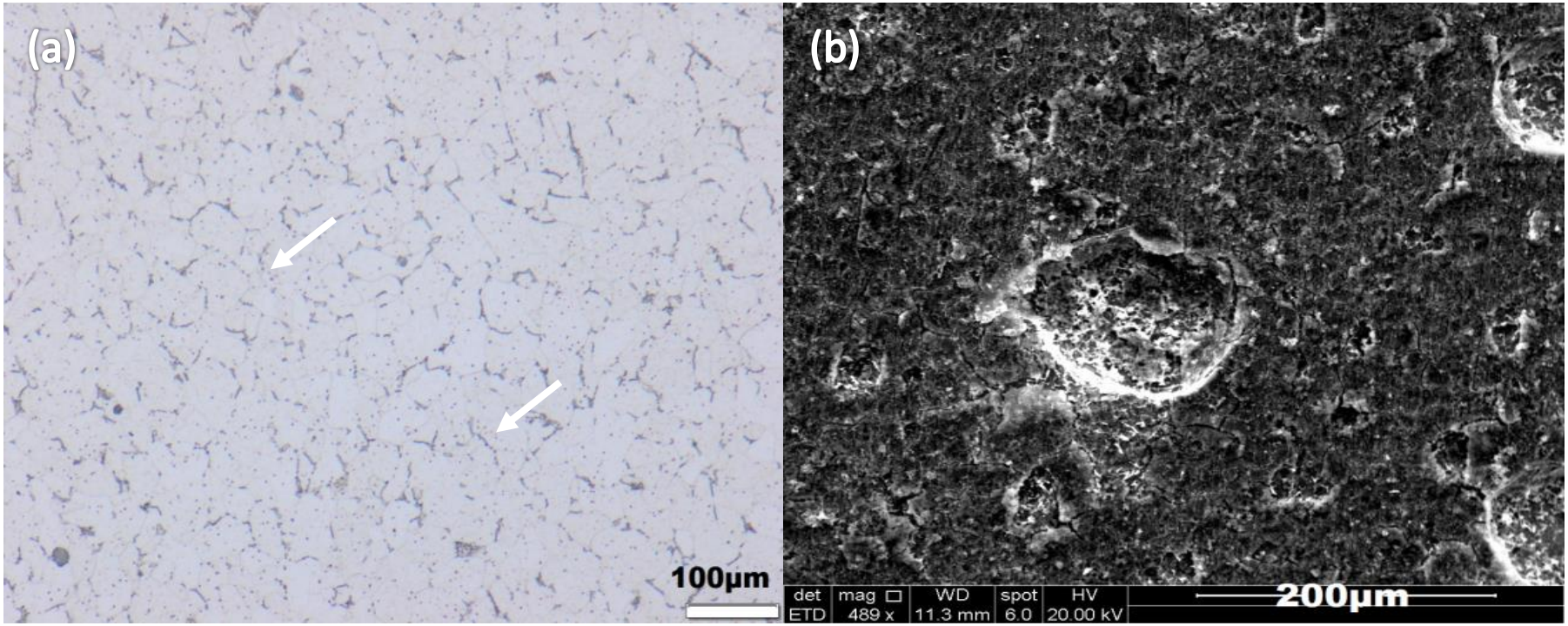
(a)
100µm
(b)
det mag WD spot HV
ETD 489 x 11.3 mm 6.0 20.00 kV
200µm

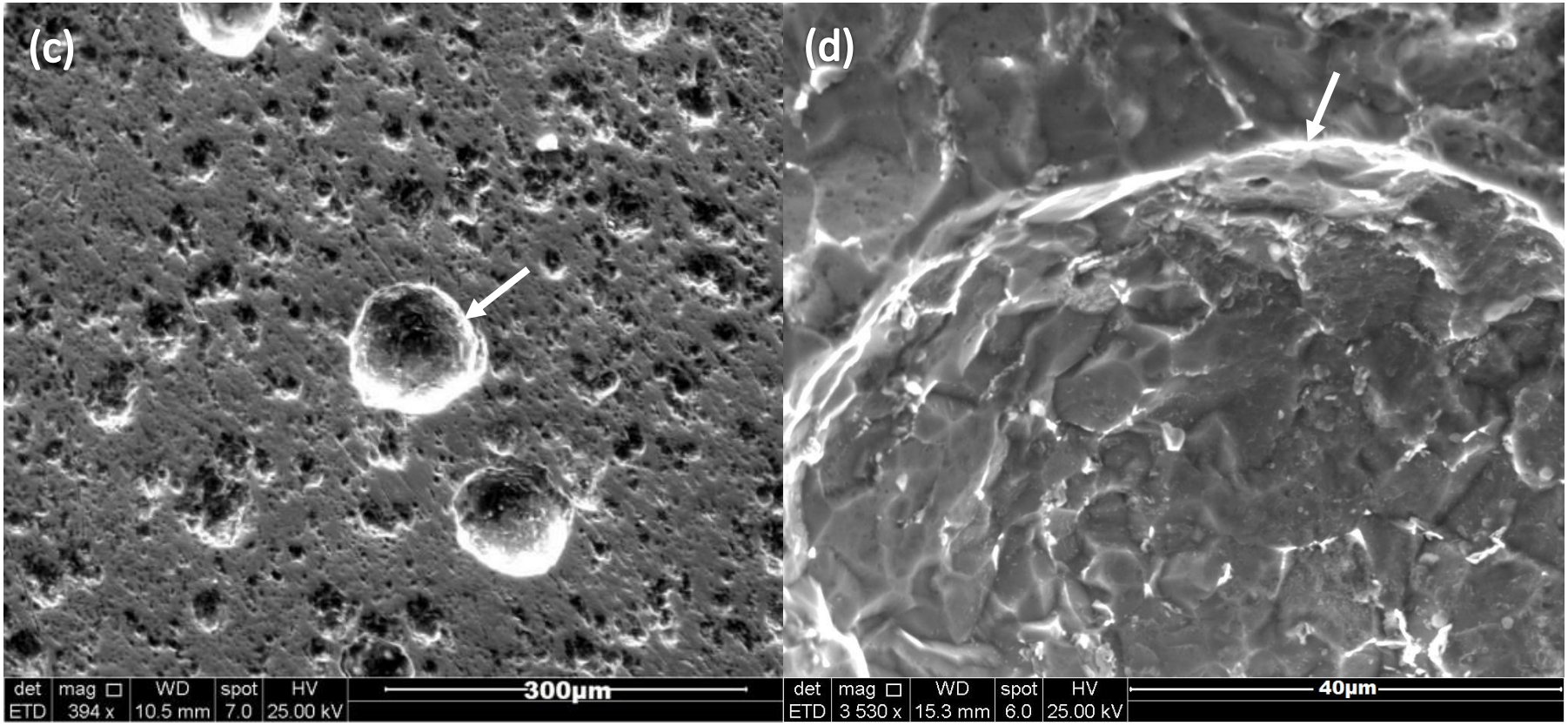

Figure 4.11: Microstructure of ASTM A106-B (a) before exposure to SRB media, showing spheroidisation marked by carbides scattered (indicated by white arrows) leaving little traces of the original pearlite area, Nital etched (b) after exposure to SRB media with biofilm on the surface, (c) image of pits on ASTM A106-B after cleaning with acetone and 3 µm polish, the white arrow indicates the pit, and (d) high magnification image of a pit showing rounded outer surface.

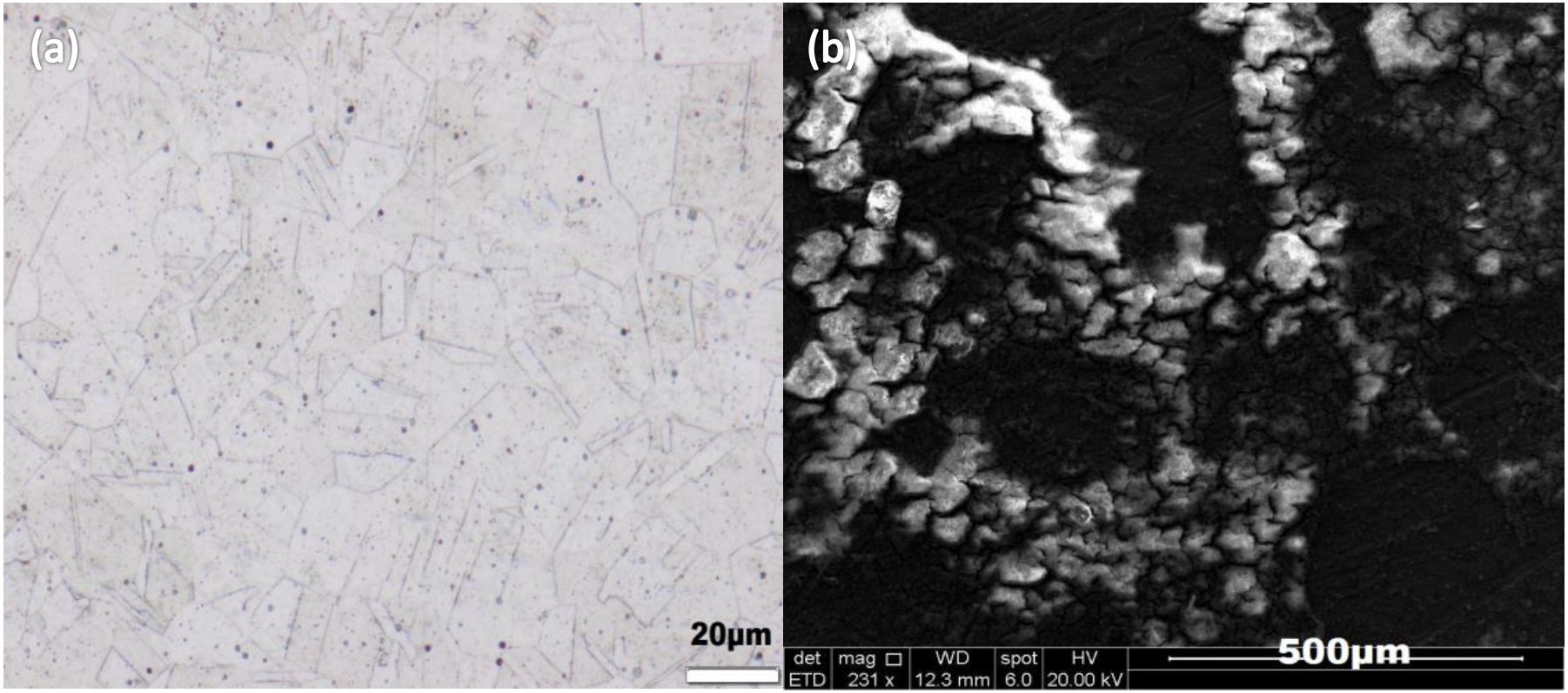
(a)
20µm
(b)
det mag WD spot HV
ETD 231 x 12.3 mm 6.0 20.00 kV
500µm

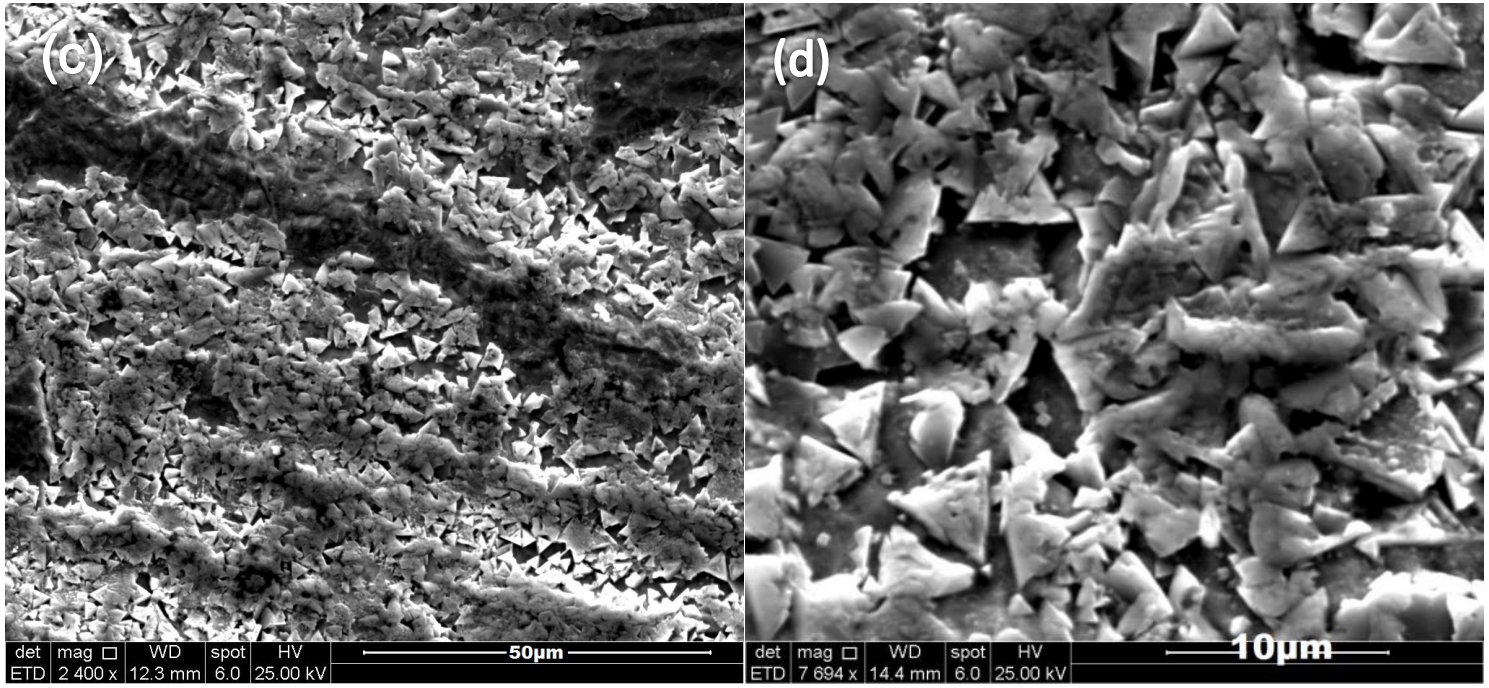

Figure 4.12: Microstructure of B111 grade C70600 (90-10) (a) before exposure to SRB media, showing a fully recrystallized structure which consists of FCC (face centre cubic) alpha grains and annealing twins, $FeCl_2$, electrolytic etched (b) after exposure to SRB media with biofilm on the surface, and (c) overview of the metal showing uniform denickelification, (d) high magnification image of exposed surface after cleaning with acetone, showing nickel residue on the surface of the metal.

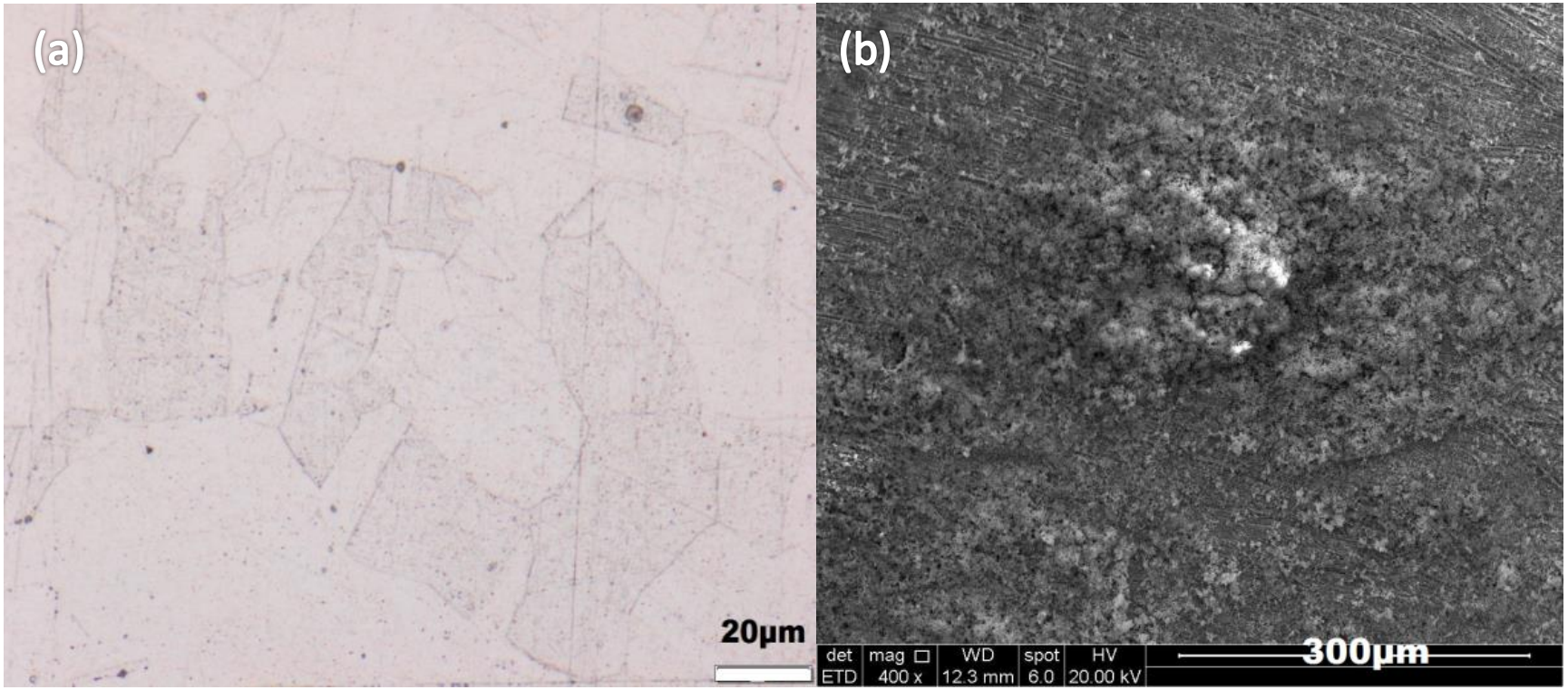
(a)
20µm
(b)
det mag WD spot HV
ETD 400 x 12.3 mm 6.0 20.00 kV
300µm

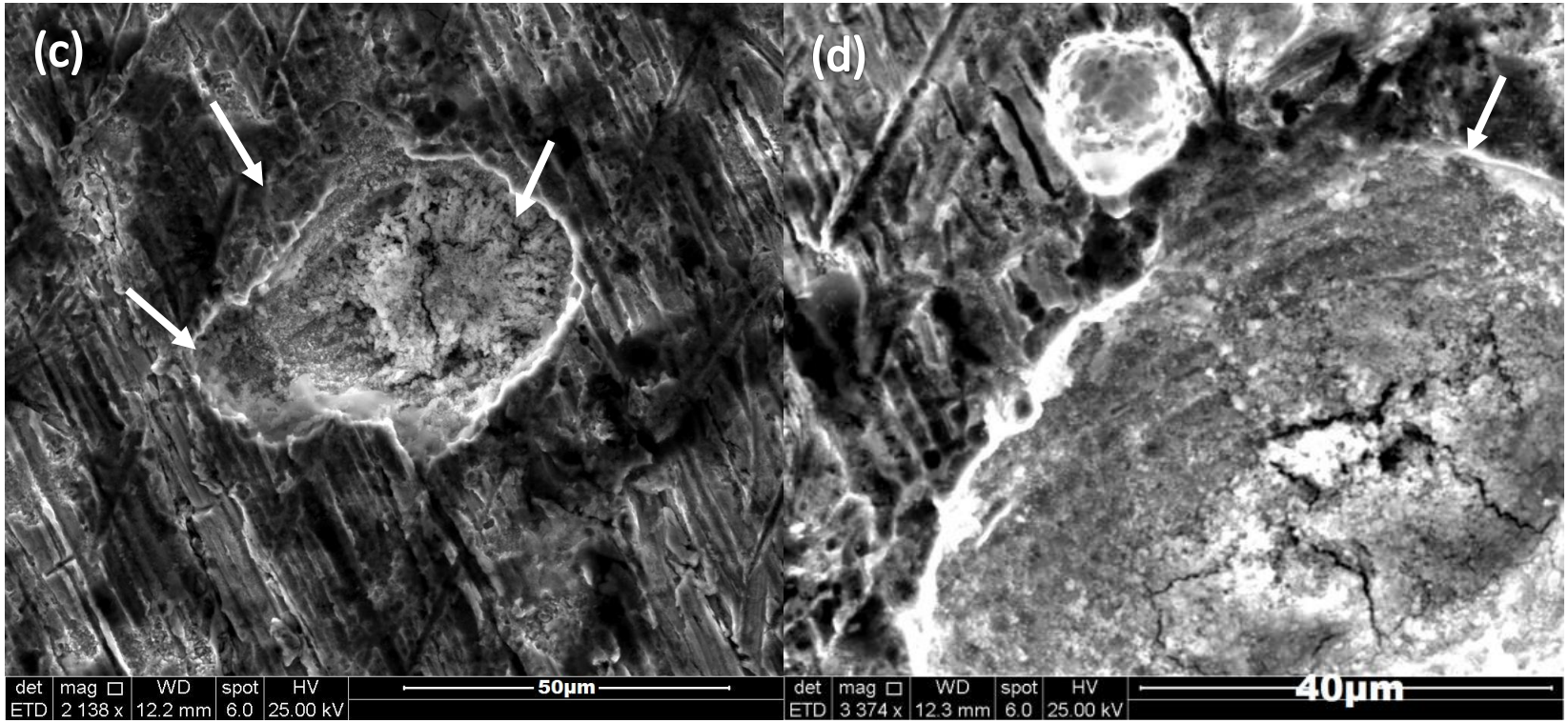

Figure 4.13: Microstructure of B111 grade C71500 (70-30) (a) before exposure to SRB media, showing a fully recrystallized structure which consists of FCC alpha grains and annealing twins, $FeCl_2$, electrolytic etched (b) after exposure to SRB media with biofilm, (c) image of surface after cleaning with acetone, showing smaller pits clustered around the larger pit (indicated by the white arrow), and (d) high magnification image of a pit after cleaning with acetone, showing rounded outer surface (indicated by the white arrow).

4.5. Elemental composition of metals before exposure to SRB media

Table 4.3 shows the actual composition of the metals that were sourced before exposure to control media and SRB media.

Table 4.3: Elemental composition of metals before exposure to SRB media using E415 standard

Elements	ASTM A516 - 70 Carbon Steel Tube (Specimens A1 – A6)	ASTM A179 Carbon Steel Tube (Specimens B1 – B6)	2205 Duplex stainless steel Plate (Specimens C1 – C6)	ASTM A106-B Carbon Steel Plate (Specimens D1 – D6)	ASTM B111 grade C70600 (90 - 10) Copper Nickel Tube (Specimens E1 – E6)	ASTM B111 grade C71500 (70 - 30) Copper Nickel Tube (Specimens F1 – F6)
C	0.122	0.078	0.007	0.064	0	0
Si	0.290	0.208	0.421	0.020	<0.0020	<0.0020
Mn	0.849	0.444	0.877	0.754	1.000	0.743
P	0.0087	0.0096	0.0230	0.0210	0.00050	0.0014
S	0.0047	0.0012	<0.00050	0.0078	<0.0010	<0.0010
Cr	0.010	<0.0020	22.500	<0.0020	0	0
Mo	0.029	0.0024	3.087	0.0015	0	0
Ni	0.147	0.0039	4.040	<0.0015	9.049	31.35
Al	0.036	0.013	0.0043	0.021	<0.0010	<0.0010
Cu	0.050	0.014	0.059	0.012	Balance	Balance
Nb	0.0037	0.0039	0.0040	0.0034	0	0
Ti	0.0011	0.0014	0.0045	0.00066	0	0
V	0.0030	0.00092	0.116	0.0011	0	0
Sn	0.0033	0.0024	0.0049	0.0034	0.0017	0.0023
Sb	<0.0050	0.0100	0	0.0130	0	0
Fe	Balance	Balance	Balance	Balance	1.101	0.575
Zn	0	0	0	0	<0.00050	0.026
Mg	0	0	0	0	<0.00050	<0.00050
Pb	0	0	0	0	<0.0030	<0.0030

Table 4.4 shows the composition of the water samples taken in 2016, and indicates sulphate presence in the water, at the period coupons were inserted at the cooling towers.

Table 4.4: Sample analysis of cooling water from plant B over 50 days (Cu, Cr, Pb, Mo, Mn and Ni always < 0.10 mg/l and P < 0.02 mg/l)

Date+ 2016	pH	Conductivity µS/cm	Cl	F	Ca	Fe	K	Mg	Na	SiO_2	Zn	SO_4	TS*	SS*
			mg/l											
01/05	8.26	433	23.3	0.355	33.23	<0.10	5.13	20.56	29.05	5.49	0.25	61.22	71	13
01/12	8.03	443	24.1	0.407	33.69	0.11	4.48	22.7	30.54	5.71	0.54	52.9	63	8
01/19	7.68	453	22.9	0.417	35.38	<0.10	4.62	23.73	28.47	4.64	0.389	61.88	89	15
01/26	6.6	458	26.7	0.462	28.52	<0.10	4.83	20.25	30.18	3.15	0.139	67.56	88	18
02/02	8.08	471	25.8	0.329	39.12	<0.10	6.41	24.85	30.89	2.92	0.248	65	88	14

02/09	8.11	478	25.7	0.5	31.16	<0.10	5.16	20.84	27.14	2.14	<0.10	71.17	90	21
02/16	8.29	479	27.6	0.415	32.85	<0.10	5.43	21.3	28.12	2.69	0.376	70.21	74	16
02/23	8.39	491	25.5	0.45	34.36	0.13	5.83	22.96	29.99	4.24	0.371	74.15	86	17

+ Sample taken at 6.00 hours *TS – Total sulphate; SS – Suspended solids

4.6. Energy Dispersive Spectroscopy (EDS) analysis

Table 4.5 gives the EDS results of biofilm that was formed on the specimens after potentiodynamic polarisation at a temperature of 35 °C at pH 8.2. The data shows presence of sulphur at proportions above the actual composition of the alloys as shown in Table 4.3. It can be inferred that increased sulphur has occurred due to the presence of the SRB the specimens were exposed to. It has been shown that S^{2-} is a catalyst for accelerating metal oxidation (Marcus 1998:109). The cooling water composition as shown in Table 4.4 indicated sulphate content in the water, which SRB reduce to H_2S. In the study of Lui *et al*. (2015:484), sulphate concentrations are presented in higher proportions in the biofilm. The corrosion behavior of the carbon steels differed when exposed to the mixed culture (SRB), the culture formed biofilm rapidly within a short period of time, forming precipitates such as sulphur and phosphorus. In line with the EDS data, the highest weight percent of sulphur among the carbon steel specimens was seen on ASTM A516-70 with a weight percent of 2.1. This can be an indication of higher bioactivity on that surface at that spot. A percentage of phosphorus was also observed only on ASTM A516-70, ASTM A106-B and copper alloys.

Table 4.5: EDS results of biofilm that was formed on specimens during SRB exposure at 35 °C and pH 8.2.

Specimen Wt%	C	O	Na	Al	Si	P	S	Cl	K	Mn	Fe	Cu	Ni	Cr	Ca
ASTM A 516-70	3.7	18.7	3.3	0.3	0.5	1.0	2.1	0.9	0.5	0.6	67.8	0.6	0	0	0
ASTM A 179	0	5.5	1.2	0.3	0.3	0	0.5	0	0.2	0.5	91.5	0	0	0	0
2205 Duplex stainless steel	0	6.0	1.6	0.7	0.7	0	1.8	0.8	0.6	0.9	61.3	0	4.4	21.2	0
ASTM A106-B	0	19.3	1.0	0	0.2	2.1	0.3	0.5	0.4	0.8	75.4	0	0	0	0
B111 grade C 70600 (90-10)	4.6	34.5	0	0	0	2.2	2.3	3.3	0.4	0	1.5	49	2.1	0	0
B111 grade C 71500 (70-30)	0	38	0	0	0	3.3	3	2.9	1.6	0.4	0.5	39.2	10.7	0	0.3

The EDS elemental data concurred with the inference made that the blackening of the media was an indication of sulphur presence in the media. The sulphur proportions obtained here was above the actual composition of the alloys shown in Table 4.3.

Chapter 5

5. Conclusions and recommendations

After fully anaerobic incubation for 18 days, of mixed cultures from industrial cooling water plants supplying heat exchanger tubes, positive indications of presence of SRB were obtained, the media turned black with sulphide precipitates. This was further confirmed with EDS analysis of higher sulphur content on the surface of the steel alloys exposed to aqueous solution of this media under potentiometric studies. Traces of phosphorus were also noted in the EDS data. All three carbon steels ASTM A516-70, ASTM A179, ASTM A106-B and a duplex stainless steel subjected to potentiodynamic tests in the presence of SRB loaded media showed increased corrosion rate; the potentials on the e-log i plots all shifted to high log i values, compared to the control media. The specific corrosion responses of the alloys differ. ASTM A516-70 shows a short potential range of cathodic passivation, but the film is very unstable, ASTM A106-B also shows anodic passivation, also with an unstable film easy broken by sulphide species in the medium. ASTM A179 did not passivate, but even showed some pitting susceptibility as indicated by the surface microstructures after the polarisation tests. The stainless steel also shows higher corrosion rates relative to the control condition in media without SRB. Corrosion rates of 1.23 mm/year, 1.08 mm/year and 0.53 mm/year were obtained for carbon steels ASTM A179, ASTM A516-70 and ASTM A106-B respectively, under SRB media, while the stainless steel alloy gave 0.91 mm/year. ASTM A516-70 can be considered better in this service environment out of the carbon steels investigated because of pitting on ASTM A106-B and pitting susceptibility observed on ASTM A179, only through visual inspection of the microstructure. Though the stainless steel shows least corrosion rate, with this work, a conscious choice can be made in considering carbon steels with a projection of the possible service life and capital cost trade off compared to stainless steel. For the copper alloys, B111 grade C70600 (90-10) showed corrosion rate of 0.979 mm/year, which can be recommended as an optional alloy for better performance, apart from the carbon steels investigated. It cannot be said that all carbon steels are prone to pitting attack when exposed to SRB; for every alloy, the factors behind this type of corrosion behavior include the culture of bacteria prevalent in the process system, environmental conditions, and surface finish of the alloy in service. These service condition factors are unique to every industry. This opens further research into the uniqueness of mixed bacterial cultures found in heat exchanger environments of petrochemical industries.

References

ABDULLAH, A., YAHAYA, N., Md NOOR, N., MOHD RASOL, R. 2014. Microbial Corrosion of API 5L X-70 Carbon Steel by ATCC 7757 and Consortium of Sulphate-reducing bacteria. *Journal of Chemistry*, 2014:2-7. Available from: http://dx.doi.org/10.1155/2014/130345 (Accessed: 09 September 2015).

AHAMMED, M., MELCHERS, R.E. 1997. Probabilistic analysis of underground pipelines subject to combined stresses and corrosion. Engineering Structures, 19(12):988-994, December.

ANTONY, P.J., RAMAN, R.K. SINGH., KUMAR, PRADEEP., RAMAN, R. 2008. Corrosion of 2205 Duplex Stainless Steel Weldment in Chloride Medium Containing Sulphate-Reducing Bacteria. *Metallurgical and Materials Transactions,* 39A(11):2689. Available from: DOI:10.1007/s11661-008-9626-y (Accessed: 04 April 2015).

BEESE, P., VENZLAFF, H., SRINIVASAN, J., GARRELFS, J., STRATMANN, M., MAYRHOFER, K.J.J. 2013. Monitoring of anaerobic microbially influenced corrosion via electrochemical frequency modulation. *Electrochimica. Acta*, 105:239-247. Available from: http://dx.doi.org/10.1155/2014/130345. (Accessed: 05 April 2015).

BEIMENG, Q., CHENGUANG, W., XIAOJUL, C., YIXING, Y. 2012. The effect of sulphate-reducing bacteria and iron bacteria on corrosion in water distribution systems. World Automation Congress, 1.

BENETTON, X.D. 2007. *Biocomplexity and Electrochemical Influence of Biofilms in Carbon Steel Deterioration in Gasoline-containing Environments*. Ph.D. Thesis. Instituto Mexicano del Petroleo Mexico.

BENHAM, S. 2010. Use of Mild Steel Corrosion Coupons to Detect MIC and SRB Corrosion. Materials Performance. Corrosion Abstracts, 49(2):50-52, February.

BOOTH, G.H. 1964. Sulphur bacteria in relation to corrosion. Journal of Applied Bacteriology, 27(1):174-181, April.

BOOTH, G.H., TILLER, A.K. 1960. Polarization studies of mild steel in cultures of sulphate-reducing bacteria. Transactions of the Faraday Society, 56:1689-1696, May.

BOOTH, G.H., TILLER, A.K. 1962a. Polarization studies of mild steel in cultures of sulphate-reducing bacteria. Part 2. Thermophilic organisms. Transactions of the Faraday Society, 58:110-115, June.

BOOTH, G.H., TILLER, A.K. 1962b. Polarization studies of mild steel in cultures of sulphate-reducing bacteria. Part 3. Halophilic organisms. Transactions of the Faraday Society, 58:2510-2516, May.

BRENNENSTUHL, A.M., SIM, B., CLAUDI, R. 1996. A progress report on the use of electrochemical noise to investigate the effects of zebra mussel attachment on the corrosion resistance of AISI type 304 stainless steel and carbon steel in lake water. ASTM Special Technical Publication: 186-200.

BROOK, P.A., LEACH, J.S.L., PEARSON, B.R. 1984. Proceedings 166th Meeting of the Electrochemical Society, Louisiana: 243.

BUTLIN, K.R., ADAMS, M.E., THOMAS, M. 1949. Sulphate-reducing bacteria and internal corrosion of ferrous pipes conveying water. Nature, 163:26–27, January.

CABRERA-SIERRA, R., GARCÍA, I., SOSA, E., OROPEZA, T., GONZÀLEZ., I. 2000. Electrochemical behavior of carbon steel in alkaline sour environments measured by electrochemical impedance spectroscopy, Electrochimica Acta, 46(4):487-497, December.

CHEN, Y., HOWDYSELL, R., HOWDYSHELL, S., STANFORD, J., KWANG, LU. 2014. Characterizing pitting corrosion caused by a long-term starving sulphate-reducing bacterium surviving on carbon steel and effects of roughness. *Corrosion Abstracts*, 70(8):767-780. Available from: https://doi.org/10.5006/1190 (Accessed: 04 April 2015).

CHEN, Y., TANG, Q., SENKO, J.M., CHENG, G., ZHANG NEWBY, B.M., CASTANEDA, H., JU, L.K. 2015. Long-term survival of Desulfovibrio vulgaris on carbon steel and associated pitting corrosion, Corrosion science, (90), 89-100.

CHOUDHARY, S.G. 1998. Emerging microbial control issues in water cooling systems. Hydrocarbon Processing, 77(1):91–102, May.

CORD-RUWISCH, R. 1996. MIC in hydrocarbon transportation systems. Corrosion Australasia, 21(1): 8-12.

CORD-RUWISCH, R., KLEINITZ, W., WIDDEL, F., PETROL, J. 1987. Sulphate- reducing bacteria and their activities in oil production. Journal of Petroleum Technology, 39(1):97, January.

DA SILVA, S., BASSEGUY, R., BERGEL, A. 2002. A new definition of cathodic depolarization in anaerobic microbially influenced corrosion. Corrosion. Conference and Expo in Denver, NACE International.

DINH, H.T., KUEVER J., MUßMANN M., HASSEL, A.W., STRATMANN M., WIDDEL, F. 2004. Iron corrosion by novel anaerobic microorganisms. Nature, 427(6977):829-832, February.

EITAN, B. D., BRENNER, A., KUSHMARO, A. 2007. Quantification of Sulphate-reducing Bacteria in Industrial Wastewater, by Real-time Polymerase Chain Reaction (PCR) Using dsrA and apsA Genes. Microbial Ecology, 54(3), 439-451, October.

EL MENDILI, Y., ABDELOUAS, A., BARDEAU, J.F. 2014. The corrosion behaviour of carbon steel in sulphide aqueous media at 30ºC. Journal of Materials Engineering and Performance, 23(4):1350-1375, April.

EL MENDILI, Y., ABDELOUAS, A., KARAKURT, G., AIT CHAOU, A., ESSEHLI, R., BARDEAU, J.F., GRENECHE, J.M. 2015. The effect of temperature on carbon steel corrosion under geological conditions. Applied Geochemistry, 52:76-85, January.

ENNING, D., GARRELFS, J. 2013. Corrosion of iron by sulphate-reducing bacteria: New views of an old problem. *Applied and Environmental Microbiology,* 80(4): 1226-1236. Available from: http://aem.asm.org/content/80/4/1226.short. (Accessed: 01 April 2015).

ENNING, D., VENZLAFF, H., GARRELFS, J., DINH, H.T., MEYER, V.,MAYRHEFER, K., HASSEL, A.W., STRATMANN, M., WIDDEL, F. 2012. Marine sulphate-reducing bacteria cause serious corrosion of iron under electroconductive biogenic mineral crust. *Environmental Microbiology,* (14), 1772-1787. Available from: https://onlinelibrary.wiley.com/doi/epdf/10.1111/j.1462-2920.2012.02778.x (Accessed: 01 April 2015).

ENOS, D.G. 1996. Influence of sulphate-reducing bacteria on alloy 625 and austenitic stainless steel weldments. Corrosion, 52(11):831-842, November.

FERRIS, F.G., JACK, T.R., BRAMHILL, B.J. 1992. Corrosion products associated with attached bacteria at an oil field water injection plant. Canadian Journal of Microbiology, 38(12):1320-1324, December.

FLITT, H.J., SCHEINSBERG, D.P. 2005. A guide to polarisation curve interpretation: deconstruction of experimental curves typical of the $Fe/H_2O/H^+/O_2$ corrosion system. *Corrosion Science,* 47(2005):2125-2156. Available from: https://www.google.com/url?sa=t&rct=j&q=&esrc=s&source=web&cd=2&cad=rja&uact=8&ved=2ahUKEwiyh5TepZnbAhVqlcAKHbzABQQFjABegQIARAz&url=https%3A%2F%2Fwww.researchgate.net%2Fprofile%2FJuan_Genesca%2Fpost%2FHow_can_we_classify_the_coating_system_in_term_of_the_parameters_obtained_from_Tafel_test%2Fattachment%2F59d6275579197b8077985a03%2FAS%3A323290311135232%401454089824450%2Fdownload%2FHJFlittCorrSci47%25282005%25292125.pdf&usg=AOvVaw3Yh5h6Ta4JvhwjC4RCCEek (Accessed: 09 September 2015).

GAINS, R. 1910. Bacterial activity as a corrosive influence in the soil. *Journal of Industrial and Engineering Chemistry*, 2(4):128-130. Available from: https://pubs.acs.org/doi/pdf/10.1021/ie50016a003. (Accessed: 09 September 2015).

GHAZY, E.A., MAHMOUD, M.G., ASKER, M.S., MAHMOUD, M.N., ABO ELSOUD, M.M., ABDEL SAMI, M.E. 2011. Cultivation and Detection of Sulphate-Reducing Bacteria (SRB) in Sea Water. *Journal of American Science*, 7(2):604-608. Available from: http://www.jofamericanscience.org/journals/am-sci/am0702/63_4707am0702_604_608.pdf (Accessed: 13 June 2015).

GLASSTONE, S., LAIDLER, K.J. and EYRING, H. 1941. Theory of rate processes. New York: McGraw Hill.

GUAN, X., LIU Y., ZHANG, Y., CAO, S. 2012. Dynamic simulation experimental study on biofouling formation of iron bacteria in heat transfer equipment. *Energy Procedia,* 17(2017):1648-1654. Available from: https://ac.els- cdn.com/S1876610212006297/1-s2.0-S1876610212006297-main.pdf? tid=a88bf555-e6c4-4b90-b7891aa329d1c85a&acdnat=1526993190_4bcd194baf7e6b2f823cab89a386b066. (Accessed: 09 September 2015).

HAMILTON, W.A. 1985. Sulphate-reducing bacteria and anaerobic corrosion. Annual Reviews in Microbiology, 39:195-217, October.

HARDY, J., BROWN, J. 1984. The corrosion of mild steel by biogenic sulphide films exposed to air. Corrosion, 40(12):650-654, December.

HENRY, G. SPRATT, JR., MARK, D. MORGAN., RALPH, E. GOOD. 1987. Sulphate-reduction in peat from a New Jersey pinelands cedar swamp. *Applied and Environmental Microbiology,* 53(7):1406-1411. Available from: http://aem.asm.org/content/53/7/1406.full.pdf+html. (Accessed: 21 March 2015).

HINES, J.*G*. 1983. Analysis of Complex Polarisation Curves. British Corrosion Journal, 18(1):10:14, July.

JAVAHERDASHTI, R. 1999. A review of some characteristics of MIC caused by sulphate-reducing bacteria: past, present and future. Anti-Corrosion Methods and Materials, 46(3):173–180. Available from: https://www.emeraldinsight.com/doi/full/10.1108/00035599910273142. (Accessed: 01 June 2015).

JAVAHERDASHTI, R. 2005. *Microbiologically induced corrosion and cracking of mild and stainless steels*. Ph.D. Thesis. Monash University Clayton-Victoria, Australia.

JAVAHERDASHTI, R. 2011. Impact of sulphate-reducing bacteria on the performance of engineering materials. *Applied Microbiology Biotechnology,* 91:1507-1517. Available from: http://dx.doi.org/10.1007/s00253-011-3455-4. (Accessed: 04 April 2015).

JAVAHERDASHTI, R., SINGH RAMAN, R.K., PANTER, C., PERELOMA, E.V. 2006. Microbiologically assisted stress corrosion cracking of carbon steel in mixed and pure cultures of sulphate-reducing bacteria. *International Biodeterioration and Biodegradation,* 58:27-35. Available from: https://doi.org/10.1016/j.ibiod.2006.04.004. (Accessed: 07 April 2015).

JAVED, M.A., STODDART, P.R., WADE, S.A. (2015). Corrosion of carbon steel by sulphate-reducing bacteria: Initial attachment and the role of ferrous ions. *Corrosion Science,* 93:48-57. Available from: https://doi.org/10.1016/j.corsci.2015.01.006. (Accessed: 24 August 2015).

JAVED, M.A., NEIL, W.C., ADAM, G.M., WADE, S.A. (2016). Microbiologically influenced corrosion of copper and its alloys- A review. *Corrosion & Prevention*, 84:1-14. Available from:

https://www.researchgate.net/profile/Muhammad_Awais_Javed/publication/310607836_MICROBIOLOGICALLY_INFLUENCED_CORROSION_OF_COPPER_AND_ITS_ALLOYS_-_A_REVIEW/links/5833886f08ae102f073687af.pdf (Accessed: 23 May 2018).

KUANG, F., WANG, J., YAN, L., ZHANG, D. 2007. Effects of sulphate-reducing bacteria on the corrosion behaviour of carbon steel. *Electrochimica Acta*, 52(20):6084-6088. Available from: https://doi.org/10.1016/j.electacta.2007.03.041. (Accessed: 24 August 2015).

LI, S.Y., KIM, Y.G., JEON, K.S., KHO, Y.T., KANG, T. 2001. Microbiologically influenced corrosion of carbon steel exposed to anaerobic soil. *Corrosion Abstracts*, 57(9):815-828. Available from: https://doi.org/10.5006/1.3280616. (Accessed: 04 April 2015).

LIENING, E.L., in: MONIZ, B.J., POLLOCK, W.I. 1986. Process Industries Corrosion: The Theory and Practice. United States.

LEMOINE, L., GUEZENNEC, J., FESTY, D., FERA, P. 1985. Corrosion and biofouling of OTEC heat exchangers: Ofremer Researches. OCEANS'85: Oceans Engineering and the Environment, 1260-1266.

LITTLE, B.J., LEE, J.S., RAY, I.I. 2006. Diagnosing microbiologically influenced corrosion: A state of the art review, *Corrosion*, 62(11):1006-1017. Available from: https://doi.org/10.5006/1.3278228. (Accessed: 15 March 2018).

LIU, H., FU, C., GU, T., ZHANG, G., LV, Y., WANG, H., LIU, H. 2015. Corrosion behavior of carbon steel in the presence of sulfate reducing bacteria and iron oxidizing bacteria cultured in oil field produced water, *Corrosion Science* 100, 484-495. Available from: https://doi.org/10.1016/j.corsci.2015.08.023. (Accessed: 24 August 2015).

LUTEY, R.W., SAITO, R. 1996. The Occurrence and Influence of Anaerobic Bacteria in Cooling Water Systems, *International Biodeterioration & Biodegradation,* 37(1-2):127-128. Available from: http://search.proquest.com/docview/903200084?accountid=14717

MANSFELD, F., LITTLE, B. 1992. Microbiologically influenced corrosion of copper-based materials exposed to natural seawater. Electrochimica Acta, 37(12): 2291-2297, September.

MARCUS, P. 1998. Surface science approach of corrosion phenomena. Electrochimica Acta, 43(1):109-114, April.

MCCAFFERTY, E. 2010. Introduction to Corrosion Science. New York: Springer.

MELCHERS, R.E. 2004. Pitting Corrosion of Mild Steel in Marine Immersion Environment-Part 1: Maximum Pit Depth. *Corrosion Abstracts,* 60(9):824-836. Available from: https://doi.org/10.5006/1.3287863. (Accessed: 04 April 2015).

NATISHAN, P.M., JONES-MEEHAN, J., LOEB, G.I., LITTLE, B.J., RAY, R., BEARD, M. 1999. Corrosion behaviour of some transition metals and 4340 steel metals exposed to sulphate-reducing bacteria. *Corrosion Abstracts*, 55(11):1062-1068. Available from: https://doi.org/10.5006/1.3283943. (Accessed: 04 April 201).

NESIC, S., POSTLETHWAITE, J., OLSEN, S. 1996. An electrochemical model for prediction of corrosion of mild steel in aqueous carbon dioxide solutions. Corrosion, 52(11):280-294, December.

NEVILLE, A., HODGKIESS, T. 1998. Comparative study of stainless steel and related alloy corrosion in natural sea water. British Corrosion Journal, 33(2): 111–119, July.

NEVILLE, A., HODGKIESS, T. 2000. Corrosion of stainless steels in marine conditions containing sulphate-reducing bacteria. *British Corrosion Journal*, 35(1):60-69. Available from: https://doi.org/10.1179/000705900101501092. (Accessed: 04 April 2015).

NOOR, N.M., YAHAYA, N., ABDULLAH, A., TAHIR, M.M., SING, L.K. 2012. Microbiologically influenced corrosion of X-70 carbon steel by *Desulfovibrio vulgaris*. Advanced Science Letters, 13(1):312-316, June.

OTIENO-ALEGO, V., HOPE, G.A., FLITT, H.J., SCHWEINSBERG, D.P. 1993. The pitting of low alloy turbine disc steel. Corrosion Science, 35(1):103-109.

PIRON, D.L. 1994. The electrochemistry of corrosion. Houston: NACE Press.

POSTGATE, J.R. 1979. The Sulphate-Reducing Bacteria. London: Cambridge University Press.

POSTGATE, J.R. 1984. The Sulphate-Reducing bacteria. 2nd Edition. London: Cambridge University Press.

POURBAIX, M. 1974. Atlas of Electrochemical Equilibria in Aqueous Solutions. 2nd edition. Houston: National Association of Corrosion Engineers.

RAMESH, K.S., DUSAN, P.S. 2003. Fundamentals of Heat Exchanger Design. New Jersey: John Wiley & Sons.

RASTOGI, G., SANI, R.K. 2011. Molecular Techniques to Assess Microbial Community Structure, Function and Dynamics in the Environment. Microbes and Microbial Technology, 29-57, January.

REVIE, R.W. 2011. Uhlig's corrosion handbook. 3rd Edition. New Jersey: John Wiley & Sons. Available: https://the eye.eu/public/Books/Materials%20science%20and%20engineering/M401%20Corosion%20and%20coatings/R%20%20Winston%20Revie%3B%20Herbert%20Henry%20Uhlig%20Uhligs%20corrosion%20handbook.pdf. (Accessed: 23 May 2018).

RICKARD, D., LUTHER, G.W. 2007. Chemistry of iron sulphides. *Chemical Rev*iews, 107(2):514-562. Available from: https://pubs.acs.org/doi/pdf/10.1021/cr0503658. (Accessed: 23 May 2018).

ROMERO, M.F., URDANETA, S., BARRIENTOS, M., ROMERO, G. 2004. Correlation between desulfovibrio sessile growth and OCP, hydrogen permeation, corrosion products and morphological attack on iron, 1-28. Available from: https://www.researchgate.net/profile/Matilde_De_Romero/publication/241792862_Correlation_between_Desulfovibrio_Sessile_Growth_and_OCP_Hydrogen_Permeation_Corrosion_Products_and_Morphological_Attack_on_Iron/links/59ac60cbaca272f8a15889df/Correlation-between-Desulfovibrio-Sessile-Growth-and-OCP-Hydrogen-Permeation-Corrosion-Products-and- Morphological-Attack-on-Iron.pdf. (Accessed: 23 May 2018).

RP-38. 1965. API Recommended Practice for Biological Analysis of Subsurface Injection Waters. New York: American Petroleum Institute [API].

SCOTT, P.F.B., DAVIES, M. 1989. Microbiologically influenced corrosion of alloy 904L. Materials Performance, 28(25):57-60.

SCOTT, P.J.B., GOLDIE, J. 1991. Ranking alloys for susceptibility to MIC-a preliminary report on high-Mo alloys. Materials Performance, 30(1):55-57, January.

SHIBATA, T., TAKEYAMA, T. 1976. Pitting corrosion as a stochastic process. Nature, (260):315-316, March.

SHIBATA, T., TAKEYAMA, T. 1977. Stochastic theory of pitting corrosion. Corrosion, 30(7):243-251, July.

SHIN, H.D., HAN, Y.S., PARK, T.K., KIM, S.Y., PAIK, N.Y. 2003. Spheroidization of Low Carbon Steel Processed by Equal Channel Angular Pressing. Materials Transactions, 44(8):1630-1635, June.

SIEBERT, O.W., IN: HAYNES, G.S., BABOIN, R. 1985. Laboratory Corrosion Tests and Standards. Philadelphia: ASTM, 65.

SPRUIT, C.J.P., WANKLYN, J.N. 1951. Iron/Sulphide ratios in corrosion by sulphate-reducing bacteria. Nature, 168:951-952, December.

STARKEY, R.L. 1946. Sulphate-reduction and the anaerobic corrosion of iron. Antonie Van Leeuwenhoek, 12(1-4):193-203, March.

STOTT, J.F.D. 1993. What progress in the understanding of microbially induced corrosion has been made in the last 25 years? A personal viewpoint. Corrosion Science, 35(1-4):667-673, June.

SUO, X., ABDOLI, L., LUI, Y., XIA, P., YANG, G., LI, H. 2017. Colonization of Bacteria on the Surfaces of Cold-Sprayed Copper Coatings Alters Their Electrochemical Behaviors. Journal of Thermal Spray Technology, (26), 687-694.

TAN, E.T., HALIM, Z.A. 2015. A novel approach to detect sulphate-reducing bacteria-main contributor of microbiologically influenced corrosion. *American Association for Science and Technology*, 1(4):120-124. Available from: www.aascit.org/author/download?paperId=1317&stateId=8000&fileType=3. (Accessed: 04 April 2015).

TILLER, A.K. 1983. Electrochemical aspects of microbial corrosion: An overview, Proceedings of microbial corrosion. London: The Metals Society.

TRETHEWAY, K.R., CHAMBERLAIN, J. 1995. 2nd Edition. Corrosion for Science and Engineering. United States: Longman, Technology and Engineering.

USHER, K.M., KAKSONEN, A.H., BOUQUET, D., CHENG, K.Y., GESTE, Y., CHAPMAN, P.G., JOHNSTON, C.D. 2015. The role of bacterial communities and carbon dioxide on the corrosion of steel. Corrosion Science, 98:354-365, September.

VEDAGE, H., RAMANARAYANAN, T.A., Mumford, J.D., Smith, S.N. 1993. Electrochemical Growth of Iron Sulfide Films in H_2S Saturated Chloride Media. Corrosion, 49(2):114-121, February.

VENZLAFF, H., ENNING, D., SRINIVASAN, J., MAYRHOFER, K., HASSEL, A.W., WIDDEL, F., STRATMANN, M. 2012. Accelerated cathodic reaction in microbial corrosion of iron due to direct electron uptake by sulphate-reducing bacteria. *Corrosion Science,* 66(2013):88-96. Available from: https://doi.org/10.1016/j.corsci.2012.09.006. (Accessed: 05 June 2017).

VIERA, M.R., GUIAMET, P.S., DE MELE, M.F.L., VIDELA, H.A. 2000. The effect of dissolved ozone on the corrosion behavior of heat exchanger structural materials. Biocidal efficacy on bacterial films. Corrosion reviews, 18(2-3):205-220, May.

VON WOLZOGEN KüHR, C.A.H., VAN DER VLUGT, LS. 1934. The graphitization of cast iron as an electrobiochemical process in anaerobic soil. *Water,* 18(16):147-165. Available from: http://www.dtic.mil/dtic/tr/fulltext/u2/617552.pdf. (Accessed: 04 April 2015).

WADE, S.A., MART, P.L., TRUEMAN, A.R. 2011. Microbiologically influenced corrosion in maritime vessels. *Corrosion Matter*, 36(5):68-79. Available from: https://www.researchgate.net/profile/Scott_Wade/publication/259346181_Microbiologically_influenced_corrosion_in_maritime_vessels/links/0deec52b2420294f0b000000/Microbiologically-influenced-corrosion-in-maritime-vessels.pdf. (Accessed: 04 April 2015).

WAGNER, P., LITTLE, B.J. 1993. Impact of alloying on microbiologically influenced corrosion-a review. *Materials Performance,* 32(9):65–68. Available from: http://www.dtic.mil/dtic/tr/fulltext/u2/a280879.pdf. (Accessed: 04 April 2015).

WANKLYN, J.N., SPRUIT C.J.P. 1952. Influence of sulphate-reducing bacteria on the corrosion potential of iron. Nature, 169:928-929, May.

WHITNEY, W.R. 1903. The corrosion of iron. Journal of American Chemical Society, 25(4):394-406. Available from: https://pubs.acs.org/doi/pdf/10.1021/ja02006a008. (Accessed: 04 April 2015).

WIDDEL, F., FINN, R.K., PRAVE, P., SCHLINGMANN, M., CRUEGER, W., ESSER, K., THAUER, R., WAGNER, F. 1992. Biotechnology focus 3. Germany: Microbial corrosion, 277-318.

XU, C., ZHANG, Y., CHENG., G., ZHU, W. 2006. Corrosion and electrochemical behaviour of 316L stainless steel in sulphate-reducing and iron-reducing bacteria solutions. Chinese Journal of Chemical Engineering, 14(6):829-834, December.

Appendix A: Potentiodynamic data

A1. Data from experiments

The data presented below give the detail of the results from the Autolab potentiostat, PGSTAT 302 machine, note that the C and D SRB corrosion rates were recalculated and is presented in a separate excel spreadsheet. Experiments were carried out at a temperature of at 35 °C and a pH of 8.2 for SRB media and control media using distilled water was at a temperature of 35 °C. The data below can be viewed in the disc provided.

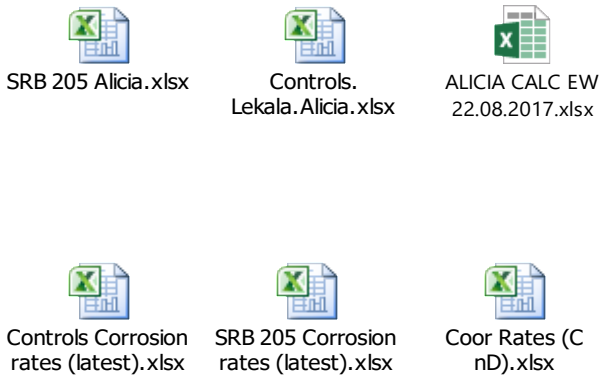

A.2 Mathematical basis of SYMADEC software to produce polarisation curves according to Flitt & Scheinsburg (2005:2126)

This is a basis that was referred to in order to understand the results produced by the program.

According to Flitt & Scheinsberg (2005:2126), the generation of polarisation curves continues to be important in the aqueous corrosion research. The time consuming potentiostatic method has been largely replaced by the potentiodynamic approach where the potential (E) of the corroding metal is automatically varied with time. The current (I) needed to maintain the metal (working electrode (WE)) at each applied potential (E_w) is ascertained and the potential/current data is plotted to give the experimental polarisation curve. In corrosion studies it is common practice for the curve to be displayed with the independent variable (in this case the potential) rather than the dependent variable as ordinate. Further, the logarithm$_{10}$ of the current density ($\log_i$) is plotted in the positive x-direction and cathodic current is negative.

The magnitude of E_w can be regarded as a measure of the oxidizing power of the corrodent (Liening *et al.* 1986:85), with the $\log_i$ axis reflecting the rate of each reaction in the corrosion

process. Depending on the corrosion system under study it follows that from the shape of the experimental curve it may be possible to obtain information on the kinetics of the corrosion reactions, protectiveness of a passive film ability of a compound to act as a corrosion inhibitor, relative corrosivity of process streams and corrosion rate (i_{corr}) of the metal.

Unfortunately, extracting any of the above from the experimental curve may be quite difficult. This is because at each applied potential the recorded current is the sum of the anodic and cathodic components of the corrosion reaction and the experimental curve (e.g., for the simple cases of pure Fe in O_2-free dilute H_2SO_4) will be the sum of the two true polarisation curves, one describing oxidation of Fe to Fe^{2+} and the other reduction of H^+ ion. This means that for potentials not greatly removed from that of the free corroding WE (corrosion potential (E_{corr})) the shape of the anodic and of the cathodic portions of the experimental curve will differ from that exhibited by each true curve. However, for the potentials further from E_{corr} the effect of the cathodic reaction on the anodic reaction and vice-versa is progressively lessened, and the shape of the experimental curve eventually becomes an accurate representation of the kinetics of the anodic and cathodic reactions. Of course, if an alloy is involved or if the corroded contains more than one oxidant (commonly H^+ ion and dissolved O_2) the net experimental curve will be more complex, and correspondingly harder to interpret in terms of its components.

An example where failure to correctly analyze the experimental curve can lead to error is when the curve is employed to evaluate the corrosion rate. The Tafel extrapolation method is well known but it is often forgotten that the metal is required to be uniformly corroding and at the corrosion potential either the anodic or the cathodic reaction needs to be under complete activation control. Further, for the accurate estimation of i_{corr} the identified linear portion of the experimental curve should extend over about one decade on the $\log_i$ axis. Unfortunately, in practice these requirements are not always met: the relevant cathodic reaction may be experiencing both activation and concentration polarisation at E_{corr} and extrapolation of what is perceived as a ‘shortened’ Tafel portion is completely erroneous. Another example pertaining to corrosion rate evaluation is when corrosion-monitoring probes based on the polarisation resistance method are used. The reaction kinetics of the corrosion process must be established before installation as these devices again assume that at E_{corr} the anodic and cathodic corrosion reactions are under activation control. A final example where the experimental curve can be difficult to interpret is when the metal spontaneously passivates/pits in the corroding prior to polarisation. The anodic portion of the experimental curve may now exhibit ‘straight line behavior’ but, because localized corrosion is involved, extrapolation of this portion of the curve does not lead to a ‘corrosion rate’. Also, in this case

the cathodic portion of the experimental curve may exhibit either a confusing 'cathodic loop or dip' negative peak. In practice it is difficult, except for the simplest corrosion systems, to visualize and experimental curve in terms of its anodic and cathodic components. Schematic representations of experimental curves with their schematic 'true' anodic and cathodic curves have been published (Liening *et al*. 1986:85; Siebert *et al*. 1985:65).

The most common cathodic reactions driving the aqueous solution of a metal are:

$2H^+(aq) + 2e^- \rightarrow H_{2(g)}$ (equivalent $2H_2O + 2e^- \rightarrow H_{2(g)} + 2OH^-(aq)$) (A.1)

and

$O_2(g) + 2H_2O + 4e^- \rightarrow 4OH^-(aq)$ (equivalent $O_2\ (g) + 4H^+\ (aq) + 4e^- \rightarrow 2H_2O$) (A.2)

The relationship between the rate of each of the above reactions, expressed as cathodic current density, i_c and high values of the activation over potential, $\eta_{act,c}$ (> approx. -0.03V) at the metal/solution interface is

$$i_c = i_0 \exp(-\alpha n\, \eta_{act,c}/RT) \quad \text{(A.3)}$$

Where:

α = transfer coeficient; n = number of electrons involved in the reaction

F = Faraday's constant; $\eta_{act,c} = E_W - E_{reversible}$; R = 8.314 J.K^{-1}mol^{-1}; T = abs. temp. (K)

Rearranging gives the Tafel equation:

$$\eta_{act,c} = b_c \log(\frac{i_c}{i_0}) \quad \text{(A.4)}$$

Where:

b_c = Tafel slope = $-2.303\ RT/\alpha nF$.

At higher reaction rates concentration polarisation is present (this is most often seen for the oxygen reduction reaction) and the relationship between the cathodic current density and the cathodic concentration over potential, $\eta_{act,c}$ is:

$$i_c = i_L\{1 - \exp(nF\eta_{conc,c}/RT)\} \quad \text{(A.5)}$$

Where:

i_L = limiting current density

Rearranging:

$$\eta_{conc,c} = \left(2.303\frac{RT}{nF}\right) log\{1 - (i_c/i_L)\} \quad \text{(A.6)}$$

Charge transfer and concentration overpotentials are additive, and for a single cathodic process Eqs. (A.4) and (A.6) can be added to give:

$$\eta_{total,c} = -\left(\frac{2.303RT}{\alpha nF}\right)\log\left(\frac{i_c}{i_0}\right) + \left(\frac{2.303RT}{nF}\right)\log(1 - \frac{i_c}{i_L})) \quad \text{(A.7)}$$

It follows (Nesic & Postlethwaite 1996:280) that the approximate value of the total cathodic current density is given by:

$$i_{total,c} = \left[i_0 \exp(-\frac{\alpha nF\eta}{\mathrm{RT}})\right] / \left[1 + \{i_0 \exp(-\frac{\alpha nF\eta}{\mathrm{RT}})\}/i_L\right] \quad \text{(A.8)}$$

Or:

$$i_{total,c} = i_L i_c/(i_L + i_c) \quad \text{(A.9)}$$

Appropriate versions of Equation (A.8) are used to model the curves for H^+ and O_2 reduction. The current densities at each potential are then summed.

The general anodic reaction for active metal dissolution is $M \rightarrow M^{n+} + ne^-$. Consider the corrosion of iron. This process is pH dependent, and reference to the well-known Pourbiax diagram (Pourbaix 1974) for the iron/water system at 25°C (dissolved iron activity$< 10^{-6}M$) shows the following:

1. For $pH < \sim 4.2$ as the potential of the iron (E_w) is made more positive the reaction is

$$Fe\ (s) \rightarrow Fe^{2+}(aq) + 2e^- \text{ (active corrosion)} \quad \text{(A.10)}$$

2. For $pH \sim 4.2\ to\ \sim 9.4$ as E_w is made more positive active corrosion (formation of the Fe^{2+}) is followed by the passivation due to precipitation of the hydrous oxide. $Fe_2O_3.nH_2O$; after dehydration of $Fe(OH)_3$; (Note the precipitate is usually represented as $Fe(OH)_3$.)

3. For $pH \sim 9.4\ to\ \sim 12.2$ as E_w is made more positive iron passivates to form $Fe(OH)_2$ then $Fe(OH)_3$.

4. For $pH \sim 12.2$ as E_w is made more positive iron is transformed to soluble $HFeO_2^-$ ions followed by passivation due to $Fe(OH)_3$.

For active dissolution of a metal, e.g., Fe (Equation A.10) above the Tafel equation is used:

$$i_a = i_0 \exp\ (\{1 - \alpha\}nF\eta_{act,a}/RT) \quad \text{(A.11)}$$

Or

$$\eta_{act,a} = b_a \log\left(\frac{i_a}{i_0}\right) \quad \text{(A.12)}$$

where b_a = Tafel slope = $2.303RT/(1-\alpha)nF$.

In order to model the anodic curve for a transition from active to passive behavior, i.e., from the potential where passivation commences (passivation potential, E_p) to that value where passivation is complete (E_{cp}), Hines (1983:10) assumed that the metal surface consists of two independent regions-one where metal dissolution occurs, as given in the reaction equation below, and the other where a film deposit occurs.

$$M \rightarrow M^{n+} + ne^-$$

Initially, metal dissolution is seen over the entire surface, but as filming starts the area on which the anodic reaction proceeds unimpeded gradually decreases, reaching a minimum when the potential at E_{cp} is reached. Suppose S is the fraction of the metal area on which no film forms and $(1-S)$ is the fraction filmed. The rate of the anodic reaction on the total surface $i_{total,a}$ can now be expressed in terms of the anodic current densities (i) on the filmed and unfilmed regions. Thus

$$i_{total,a} = i_u S + i_f(1-S) \quad \text{(A.13)}$$

where i_u and i_f are the rates on the un-filmed and filmed regions, respectively. S will be equal to unity at E_p and will reach a value of zero at E_{cp}.

Hines (1983:10) suggested two physical models for the dependence of S on the applied potential E. However, Equations (A.16) and (A.17) in his paper do not generate the S curve. The corrected equations and variation of S with the applied potential according to Hines (1983:10) second model is now given by

$$S = 2[\exp(-A(E_W - E_P)^p]/[1 + \exp(-A(E_W - E_P)^p] \quad \text{(A.14)}$$

where p = constant used to shape the passivation peak (2 symmetrical: 2-3 asymmetrical) and A = constant ($10^{-3} - 10^{-4}$) that determines the width of the passivation peak. Both p and A are obtained empirically and appear to have no physical significance (Brook *et al*. 1984:243).

Substitution in (A.13) gives the following for $i_{total,a}$

$$i_{total,a} = i_u\left\{2\frac{[\exp(-A(E_w-E_p)^p]}{[1+\exp(-A(E_w-E_p)^p]}\right\} + i_f\{1-2[\exp(-A(E_w-E_p)^p]/[1+\exp(-A(E_w-E_p)^p)]\} \quad \text{(A.15)}$$

In summary, when $S = 1$ (no film) (A.13) reduces to $i_{total,a} = i_u$ and the Tafel relationship applies. When $S = 0$, $i_{total,a} = i_f = i_{cp}$.

In presence of certain anions (e.g.,Cl^-) the film is attacked and at points where the film is thin metal dissolution may proceed (localised or pitting corrosion). That part of the anodic curve from the point where pitting commences (E_{br}) to the maximum potential reached (E_m) is now modelled. It is assumed that the metal dissolution can be described by a linear logarithmic current density/potential relationship. The following empirical expression is proposed for the dependence of the anodic current density i_a on the potential E_w

$$i_a = i_{cp}\{(i_{cp} + v)/v\} \tag{A.16}$$

where

$$v = exp\{lni_{cp} + (1/(iron\ transpassive\ slope)[E_m - (E_w + E_{br})]\} \tag{A.17}$$

with respect to Equations (A.16) and (A.17), the following applies:

(1) When E_w is equal to or less than $|E_{br}|v$, becomes large and $i_a = i_{cp}$;

(2) When $E_w < |E_{br}|v$ is small and $i_a >> i_{cp}$.

At higher positive potentials film breakdown (in the absence of aggressive anions) and oxygen evolution may be possibilities. Currently these aspects have not been factored into the SYAMDEC program.

Resistance polarisation due to the presence of the passive film will also be present and the recorded anodic potentials must be corrected for the IR drop. Sometimes and ionically conducting but non-passive porous film (e.g., graphitic carbon) may form on a metal and the IR drop across this film must also be considered. If a current *I* is passed across a film whose resistance is R_Ω there will be a potential drop given by $\eta_\Omega = IR_\Omega$. Resistance polarisation has the effect of making the electrode potential (E_w) for a corrosion system larger than the 'true' value (E_{true}). Thus

$$E_{true} = E_w - IR \tag{A.18}$$

This type of polarisation can be responsible for the anodic portion of an experimental curve (e.g., for mild steel in oxygen-free 0.5 M sulphuric acid) exhibiting curvature instead of the expected straight-line indicative of Tafel behaviour. SYMADEC allows for the insertion of different values of film resistance and subsequent calculation of the true potential.

In (Flitt & Scheinsburg 2005:2142) a case with low-alloy steel corroding in oxygen-containing, simulated steam turbine condensate (active corrosion, induced passivation and pitting):

The experimental curve given in Figure A.1 was recorded potentiodynamically by Otieno-Alego *et al*. (1993:103) for A-470 turbine rotor disc steel with composition ($0.24\%\ \mathrm{C}, 1.8\%\ \mathrm{Cr}, 3.68\%\ \mathrm{Ni}, 0.46\%\ \mathrm{Mo}, 0.3\%\ \mathrm{Mn}, 0.12\%\ \mathrm{V}, 0.0004\%\ S, 0.0004\%\ \mathrm{P}, 0.05\%\ \mathrm{Si}$) immersed in a synthetic steam turbine condensate containing 2 ppm NaCl, 2 ppm Na_2SO_4, 2 ppm $NaOH$ and 5 ppm $SiO2$. A single compartment Perspex cell (800 cm^3) fitted with a Perspex lid was used. The WE (10 mm dia.) and Pt counter electrode (1 cm^2) were mounted in chemical resistant epoxy resin and immersed in the test solution using a Perspex holder. A saturated calomel electrode (SCE) connected to a Luggin capillary was used as the reference electrode. The temperature was 30°C and the solution pH = 9.0. Bottled nitrogen gas (containing traces of oxygen) was passed continuously through the corrodent and this resulted in a dissolved oxygen level of approximately 0.01 mg L^{-1}. The WE was abraded with 1200 grade SiC paper, degreased with AR grade acetone, inserted in the solution and then immediately pre-polarised at - 756 mV (SHE) for 10 min to remove any air-formed oxide film. After reaching a steady E_{corr} (approximately 1 h) the corroding WE was polarised cathodically. This was followed by anodic polarisation when E_{corr} had returned to within ± 5 mV of the previous value. The polarisation scan rate was 10 mV min^{-1}. In this case there are two oxidants (H^+ ion and small amount of O_2) driving corrosion. E_{corr} was - 539 mV (Standard Hydrogen Electrode-SHE). Although low-alloy steel is corroding, the material is approximately 93% Fe, and the Pourbaix diagram for pure iron is a reasonable guide to corrosion behaviour and subsequent anodic polarisation. The diagram shows that at pH = 9.0 and for an E_{corr} ~ - 539 mV (SHE) pure iron is actively corroding to form Fe^{2+} ions. Further, if the WE is made more positive iron passivates with the formation of precipitated $Fe_2O_3 . nH_2O$ (or $Fe(OH)_3$). The shape of the experimental polarisation curve shown in Figure A.1 supports the use of the iron Pourbaix diagram to predict corrosion behaviour. The curve suggests active corrosion at E_{corr} and indicates that polarisation in the positive direction (by means of the potentiostat) results in a classical active/passive transition. This is followed at more positive potentials by a rapid increase in current density suggesting in the presence of Cl^- pitting corrosion. Otieno-Alego *et al*. (1993:103) reported that pits were observed on the WE after anodic polarisation.

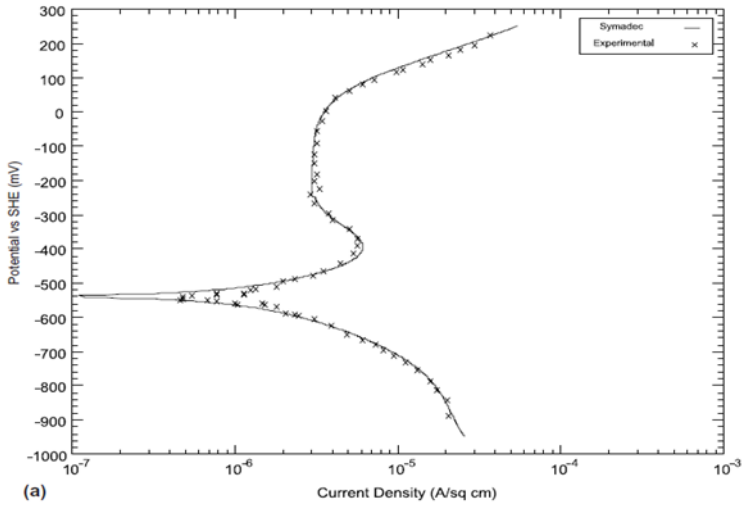

Figure A.1: Experimental and synthesised polarisation curves for low-alloy steel in synthetic condensate at 30 °C (0.01 mg L^{-1} O_2) (Flitt & Scheinsberg 2005:2143).

Appendix B: Methods of preparation and growth

B.1 Metals after exposure to SRB

Figure B.1 shows the specimens that were exposed to SRB media, a bright corrosion product and biofilm can be seen. The white arrows indicate the exposed areas.

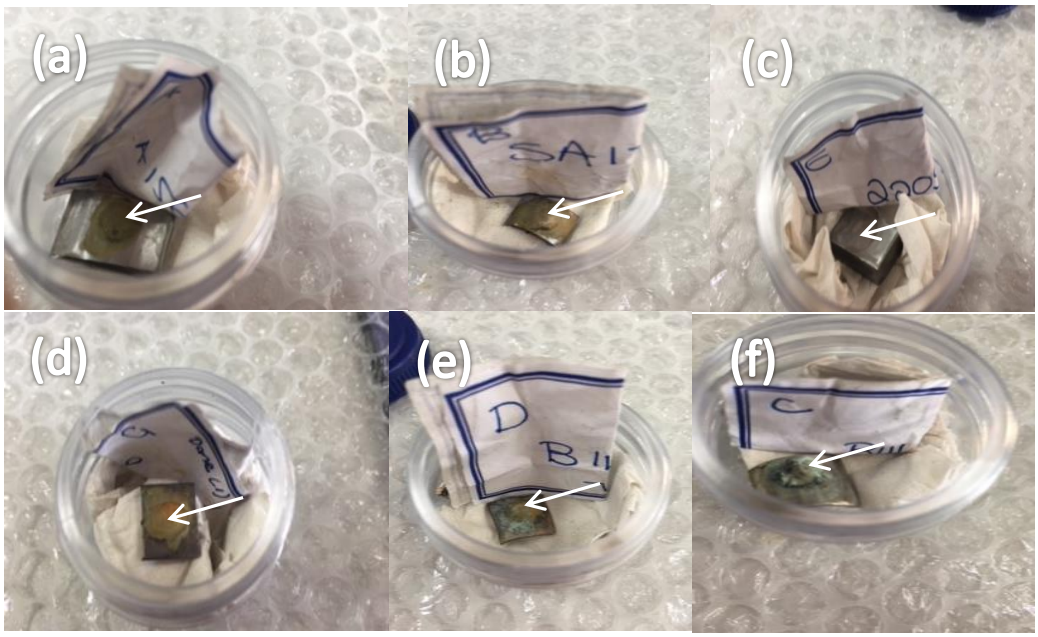

Figure B.1: Shows biofilm/bright corrosion product formed on the 10 × 10 mm specimens exposed to SRB at 35°C at pH 8.2, white arrows show exposed area, (a) ASTM A516-70, tube, (b) ASTM A179, tube, (c) 2205 Duplex stainless steel, plate, (d) ASTM A106-B, plate, (e) B111 grade C70600 (90-10), tube, (f) B111 grade C71500 (70-30), tube.

B.2 Potentiodynamic polarisation under different corrosion conditions

Results presented are from the works of Liu *et al*. (2015:485). Electrochemical parameters fitted from the potentiodynamic polarisation under different corrosion conditions after 15 day incubation.

Table B.1: Electrochemical parameters fitted from the potentiodynamic polarisation under different corrosion conditions after 15 day incubation (Liu *et al*. 2015:485)

	βa (V/dec)	βc (V/dec)	E_{corr} (V vs. SCE)	I_{corr} (A/cm^2)
Control	0.145	-0.092	-0.810	8.00×10^{-6}
Aerobic iron-oxidizing bacteria (IOB)	0.039	-0.362	-0.762	1.28×10^{-5}
Anaerobic sulphate-reducing bacteria (SRB)	0.430	-0.053	-0.729	2.77×10^{-5}
SRB + IOB	0.311	-0.175	-0.678	2.52×10^{-5}

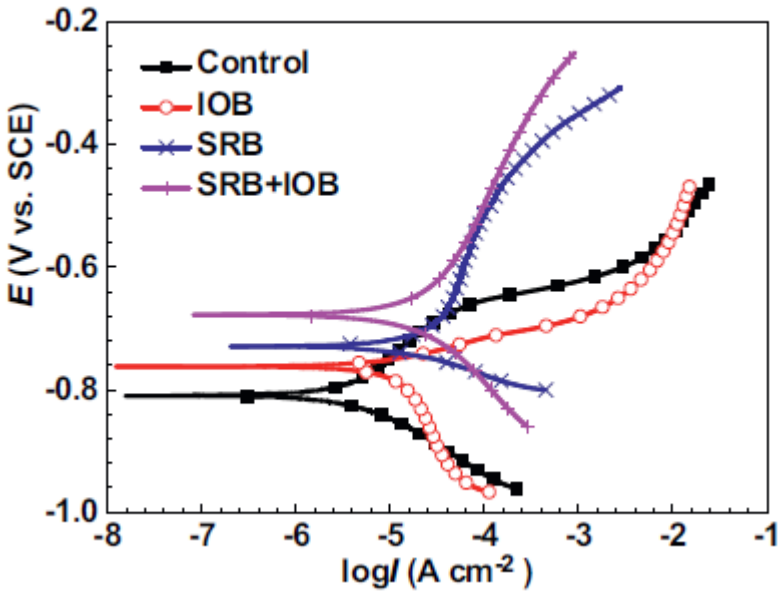

Figure B.2: Potentiodynamic polarisation curves of coupons under different corrosion conditions after 15 day incubation (Liu *et al*. 2015:485).